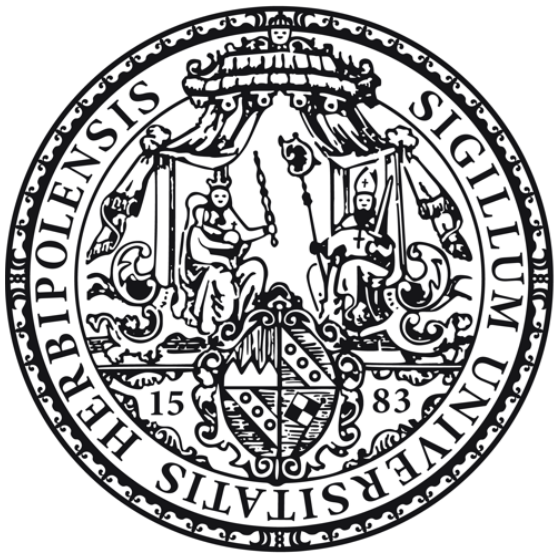

The role of BRCA1 and DCP1A in the coordination of transcription and replication in neuroblastoma

Die Rolle von BRCA1 und DCP1A in der Koordination von Transkription und Replikation im Neuroblastom

Doctoral thesis for a doctoral degree
at the Graduate School of Life Sciences,
Julius-Maximilians-Universität Würzburg,
Section Biomedicine

submitted by

Jacqueline Kalb

from

Saarbrücken

Würzburg, 2021

Submitted on: 28th May 2021

Members of the Thesis Committee

Chairperson: Prof. Dr. Alexander Buchberger

Primary Supervisor: Prof. Dr. Martin Eilers

Second Supervisor: Prof. Dr. Matthias Dobbelstein

Third Supervisor: Prof. Dr. Stefan Gaubatz

Date of Public Defense:

Date of Receipt of Certificates:

Meiner Mutter

Substantial parts of this thesis were published in the following articles:

Büchel*, Carstensen*, Mak*, Roeschert, Leen, Sumara, Hofstetter, Herold, **Kalb**, Baluapuri, Poon, Kwok, Chesler, Maric, Rickman, Wolf, Bayliss, Walz, Eilers. *These authors contributed equally. (2017) Association with Aurora-A Controls N-MYC-Dependent Promoter Escape and Pause Release of RNA Polymerase II during the Cell Cycle. *Cell Reports* 21, 3483-3497

Herold*, **Kalb***, Büchel*, Ade, Baluapuri, Xu, Koster, Solvie, Carstensen, Klotz, Rodewald, Schülein-Völk, Dobbelstein, Wolf, Molenaar, Versteeg, Walz, Eilers. *These authors contributed equally. (2019) **Recruitment of BRCA1 limits MYCN-driven accumulation of stalled RNA polymerase.** *Nature* 567, 545-549

Papadopoulos, **Kalb**, Solvie, Baluapuri, Herold, Endres, Giansanti, Schülein-Völk, Ade, Schneider, Fischer, Dobbelstein, Wolf, Eilers. **The MYCN oncoprotein resolves conflicts of stalling RNA Polymerase with the replication fork.** *In Revision.*

Table of contents

Summary

The deregulation of the MYC oncoprotein family plays a major role in tumorigenesis and tumour maintenance of many human tumours. Because of their structure and nuclear localisation, they are defined as undruggable targets which makes it difficult to find direct therapeutic approaches. An alternative approach for targeting *MYC*-driven tumours is the identification and targeting of partner proteins which score as essential in a synthetic lethality screen.

Neuroblastoma, an aggressive entity of *MYCN*-driven tumours coming along with a bad prognosis, are dependent on the tumour suppressor protein BRCA1 as synthetic lethal data showed. BRCA1 is recruited to promoter regions in a MYCN-dependent manner. The aim of this study was to characterise the role of BRCA1 in neuroblastoma with molecular biological methods.

BRCA1 prevents the accumulation of RNA Polymerase II (RNAPII) at the promoter region. Its absence results in the formation of DNA/RNA-hybrids, so called R-loops, and DNA damage. To prevent the accumulation of RNAPII, the cell uses DCP1A, a decapping factor known for its cytoplasmatic and nuclear role in mRNA decay. It is the priming factor in the removal of the protective 5'CAP of mRNA, which leads to degradation by exonucleases. BRCA1 is necessary for the chromatin recruitment of DCP1A and its proximity to RNAPII. Cells showed upon acute activation of MYCN a higher dependency on DCP1A. Its activity prevents the deregulation of transcription and leads to proper coordination of transcription and replication. The deregulation of transcription in the absence of DCP1A results in replication fork stalling and leads to activation of the Ataxia telangiectasia and Rad3 related (ATR) kinase. The result is a disturbed cell proliferation to the point of increased apoptosis. The activation of the ATR kinase pathway in the situation where DCP1A is knocked down and MYCN is activated, makes those cells more vulnerable for the treatment with ATR inhibitors.

In summary, the tumour suppressor protein BRCA1 and the decapping factor DCP1A, mainly known for its function in the cytoplasm, have a new nuclear role in a MYCN-dependent context. This study shows their essentiality in the coordination of transcription and replication which leads to an unrestrained growth of tumour cells if uncontrolled.

Zusammenfassung

Die MYC Onkoproteine spielen in einer Vielzahl humaner Tumore eine entscheidende Rolle und sind in fast allen Fällen dereguliert. Aufgrund ihrer Struktur und Lokalisation im Zellkern gelten sie für die Arzneimittelentwicklung als therapeutisch schwer angreifbar. Der Ansatz der synthetischen Lethalität ist es, Partnerproteine zu finden, die gerade für MYC-getriebene Tumore essenziell sind und diese zu inhibieren.

Neuroblastome, die in einer besonders aggressiven Entität durch eine *MYCN*-Amplifikation getrieben sind und damit mit einer schlechten Prognose einhergehen, sind abhängig vom Tumorsupressor BRCA1, wie Daten zur synthetischen Lethalität zeigten. BRCA1 wird in Abhängigkeit von MYCN zu Promotoren rekrutiert. Diese Arbeit diente daher der Charakterisierung der Funktionalität von BRCA1 im Neuroblastom.

BRCA1 verhindert die Akkumulation von RNA Polymerase II (RNAPII) in der Promoterregion. Ist BRCA1 nicht präsent, führt dies zur Bildung von DNA/RNA-Hybriden, sogenannten R-loops, und zu DNA Schäden. Um die Akkumulation von RNAPII zu verhindern, nutzt die Zelle DCP1A, einen Decapping Faktor, der sowohl im Cytoplasma als auch im Nukleus eine Rolle im mRNA Abbau spielt. DCP1A entfernt den schützenden 5'CAP der mRNA, wodurch diese von Exonukleasen abgebaut wird. BRCA1 ist notwendig für die Chromatin Bindung von DCP1A und die Rekrutierung zu RNAPII. Zellen mit einer akuten Aktivierung des MYCN Onkoproteins zeigen eine erhöhte Abhängigkeit von DCP1A. DCP1A verhindert eine Deregulation der Transkription, um Transkription mit Replikation erfolgreich zu koordinieren. Andernfalls führt dies beim Verlust von DCP1A zur Blockierung von Replikationsgabeln und der Aktivierung der Ataxia telangiectasia and Rad3 related (ATR) Kinase führt. In der Folge ist das Zellwachstum gestört und Zellen gehen vermehrt in Apoptose. Die Aktivierung des ATR Signalweges beim Verlust von DCP1A und MYCN Aktivierung verhindert vorerst den Zelltod, wodurch diese Zellen jedoch sensitiver auf die Inhibition von ATR reagieren.

Zusammenfassend lässt sich sagen, dass BRCA1 als Tumorsupressor und DCP1A als Decapping Faktor, hauptsächlich beschrieben als cytoplasmatisches Protein, eine entscheidende nukleäre Rolle in der Situation einer akuten Aktivierung von MYCN spielen. Dort sind sie essenziell um Transkription mit Replikation zu koordinieren und damit zu einem ungebremsten Wachstum der Tumorzellen beizutragen.

1 Introduction

1.1 The MYC oncoprotein family

MYC proteins are a family of oncoproteins which consist of three paralogues, namely MYC, MYCN and MYCL. Their expression is necessary for cellular development and tightly controlled in normal cell proliferation. However, a deregulation of them plays a major role in the tumorigenesis and tumour maintenance of most human tumours. Deregulation can either be caused by direct genetic alterations, such as amplifications of the genetic locus, or by indirect influence of upstream players regulating their stability, like APC (Dang, 2012).

The three MYC paralogues share high similarities (Figure 1.1), like their structural composition of different MYC boxes, their target gene regulation, their heterodimerisation with MAX through the helix-loop-helix leucine zipper domain which promotes gene expression, and their binding to other proteins (Baluapuri et al., 2020).

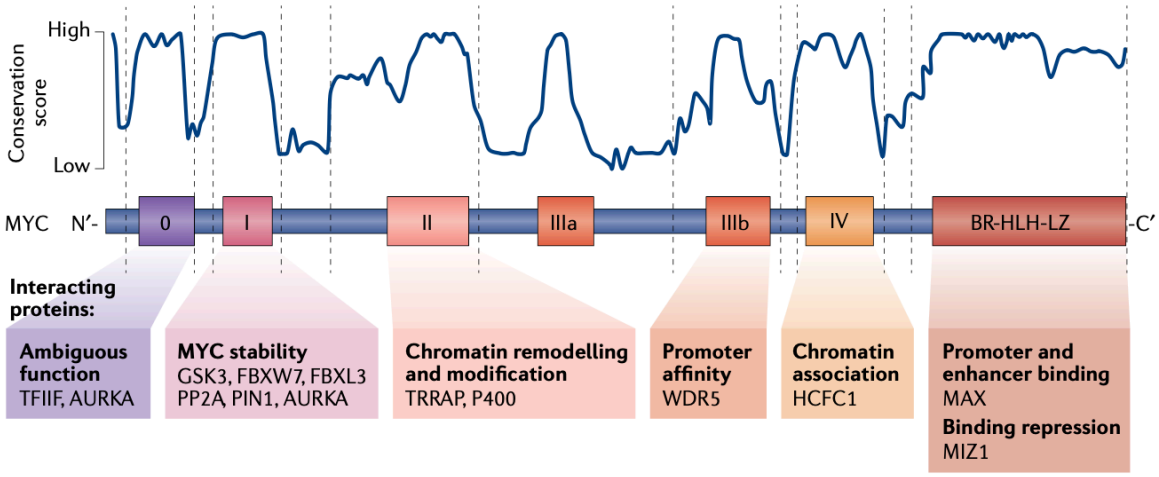

Figure 1.1 Schematic overview of MYC protein domains and their canonical function (Baluapuri et al., 2020) Top: The amino acid sequence reveales the conservation score between the three MYC paralogues. Bottom: Examples for proteins interacting with MYC proteins at different MYC boxes.

Since this study focuses on MYC and MYCN, these two will be discussed further. One major difference between them is their affinity to MIZ1, which leads in *MYC*-driven tumours to repression of genes (Walz et al., 2014; Wolf et al., 2013). MYCN, however, binds much weaker to MIZ1 (Vo et al., 2016). Therefore, the exact mechanism of gene repression by MYCN is currently unknown.

MYCN is expressed in the early development of neuronal cells and almost absent in adult tissue (Figure 1.2). Deregulated expression affects the sympathetic nervous system causing tumorigenesis of neuroendocrine tumours, such as neuroblastoma, the most common

extracranial solid tumour in childhood (Rickman et al., 2018). Amplification of the *MYCN* locus correlates with a very poor prognosis. Treating options for high risk neuroblastoma patients include high doses of chemotherapy causing severe side effects (Mosse et al., 2019). Therefore, the understanding of MYCN's biology could help to improve these therapeutic options.

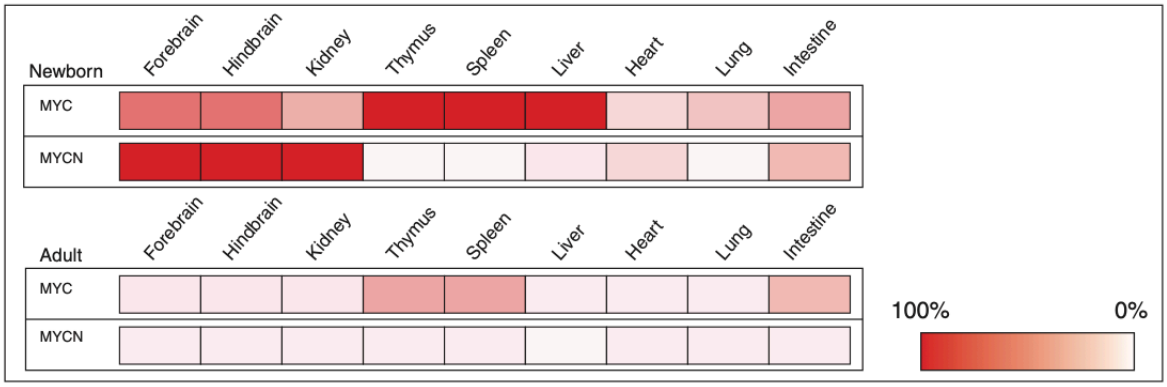

Figure 1.2 Expression levels of MYC and MYCN in newborn and adult tissue (Huang and Weiss, 2013)

1.1.1 The transcription process

Transcription *per se* consists of different steps in which all of the MYC proteins are involved (1.1.2): The opening of DNA and the recruitment of RNAPII as initiation, the promoter proximal pausing, the productive elongation which is accompanied by splicing events and the regular termination process at the transcriptional end sites (TES) (Figure 1.3). The different steps can be characterised by modifications of the unstructured carboxy-terminal domain (CTD) of RNA Polymerase II (RNAPII) (Harlen and Churchman, 2017). Unphosphorylated RNAPII is initially recruited to promoters where it associates with the pre-initiation complex (Lu et al., 1991). The opening of the promoter DNA region happens through the XPB DNA translocase as subunit of the general transcription factor TFIIH (Egly and Coin, 2011; Holstege et al., 1996; Kim et al., 2000). Phosphorylation of the Ser5 residue by CDK7 in the TFIIH complex (Akhtar et al., 2009) mediates the promoter escape of RNAPII (Jeronimo and Robert, 2014; Wong et al., 2014). RNAPII pauses about 20-100 bp downstream of the transcriptional start site of most genes. Not all promoters show the same pausing of RNAPII, but high GC content and lacking of a TATA box at promoters are features more associated with pausing of RNAPII (Core et al., 2008; Day et al., 2016). Promoter proximal pausing is mediated through binding of DRB sensitivity-inducing factor (DSIF) and negative elongation factor (NELF) to RNAPII (Adelman and Lis, 2012; Wu et al., 2003), which prevents the binding of transcription elongation factor TFIIS (Vos et al., 2018b).

TFIIS is not only involved in transcriptional elongation at the pause site, it also rescues backtracked RNAPII, e.g. at the +1 nucleosome, resulting in a restart of RNAPII (Kireeva et al., 2005). The +1 nucleosome is a highly regulated and well-positioned packaging unit of eukaryotic chromatin downstream of the TSS (Lai and Pugh, 2017). As a natural barrier, the +1 nucleosome can additionally modulate RNAPII pausing (Jimeno-Gonzalez et al., 2015) and acts as a second pausing step since it is the cause for global stopping of RNAPII upon acute depletion of NELF. The study describes NELF's acting – besides its pause release function – also in early elongation by recruiting the cap binding complex (CBC) which results in stabilisation of nascent transcripts (Aoi et al., 2020).

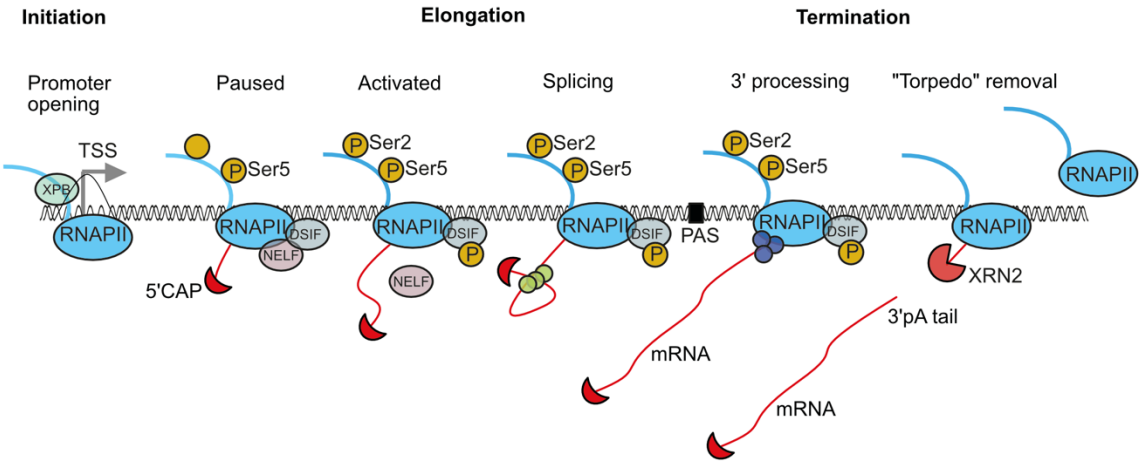

Figure 1.3 Stepwise illustration of the transcription cycle through initiation, elongation and termination of RNAPII (adapted from Cramer, 2019)

Promoter proximal pausing regulates gene expression (Core and Adelman, 2019). A restart of promoter proximal paused RNAPII is mediated by the CDK9 kinase of the positive transcription elongation factor b (PTEFb) via phosphorylation of the DRB sensitivity inducing factor (DSIF) and the Ser2 residue of the RNAPII CTD. This causes NELF's dissociation and turns DSIF into a positive elongation factor (Marshall et al., 1996; Ni et al., 2008; Peterlin and Price, 2006). Furthermore, RNA Polymerase II associated factor (PAF1) displaces NELF from RNAPII promoting active transcription (Vos et al., 2018a).

The status of the CTD is not only an associated hallmark of transcription but also a signal for co-transcriptional processes such as 5'capping of nascent transcripts (Schroeder et al., 2000) or co-transcriptional splicing during productive elongation (Bentley, 2014). For termination, RNAPII passes a polyadenylation signal (PAS) which dictates termination. The AAUAAA motif of the PAS is recognised by cleavage and polyadenylation (CPA) factors that lead to the cleavage of the transcript and its polyadenylation (Chan et al., 2011). There are two models

discussed for the dissociation of RNAPII from chromatin: The allosteric model postulates that the simple RNAPII transition through the PAS leads to dissociation of factors associated with RNAPII and its conformational change which results in the dissociation of RNAPII from chromatin (Eaton and West, 2020). The torpedo model predicts first the cleavage of the mRNA, then the activity of a 5' → 3' exonuclease to degrade the RNA left attached to RNAPII. Since RNAPII slows down after PAS, the faster acting exonuclease hits RNAPII (i.e. like a 'torpedo') and RNAPII gets dissociated from chromatin (Eaton et al., 2020). One exonuclease widely accepted to function as a 'torpedo' is XRN2, since its knockdown leads to termination defects (West et al., 2004).

Just a minority of paused RNAPII is going into productive elongation (Steurer et al., 2018), whereas the majority is getting turned over rapidly (Erickson et al., 2018). So called premature termination (Figure 1.4) is an important process for gene regulation (Kamieniarz-Gdula and Proudfoot, 2019). Factors involved in general terminationat the TES – as described above – can also act throughout the gene body, such as cleavage and polyadenylation factor PCF11 (Kamieniarz-Gdula et al., 2019) or the 'torpedo' exonuclease XRN2 together with decapping factors (Brannan et al., 2012), which showed increased chromatin binding at promoter regions.

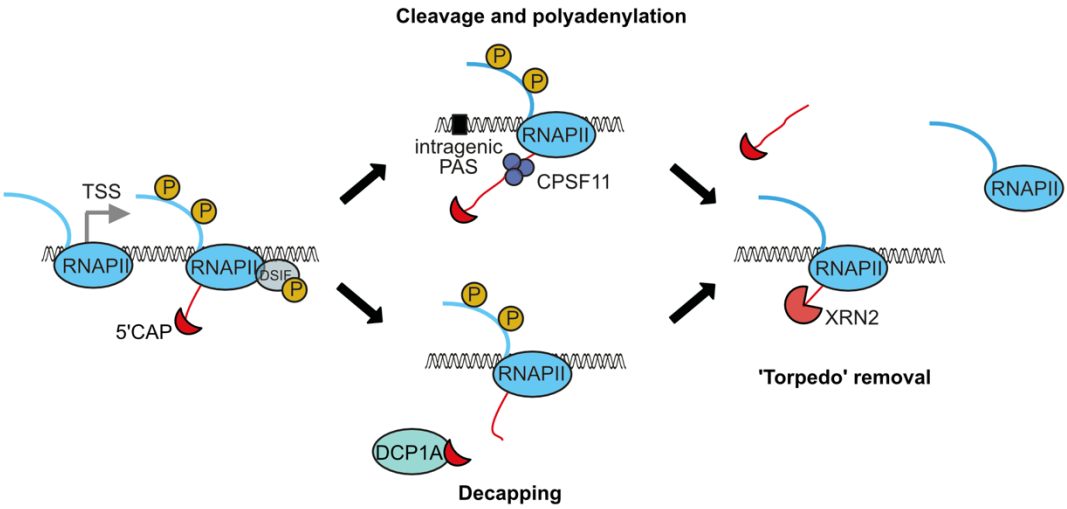

Figure 1.4 Premature termination pathways
This can either happen through cleavage and polyadenylation through an intragenic polyadenylation signal (PAS) or decapping of nascent transcripts. Both cases result in the 'torpedo' removal of RNAPII (adapted from Eaton and West, 2020).

1.1.2 Transcriptional regulation by MYC oncoproteins

The oncogenic potential of the MYC proteins is well documented but their oncogenic activity is only partially understood. MYC proteins are transcription factors that bind to thousands of

promoters and enhancers (Walz et al., 2014). Whether and how this binding results in MYC's oncogenic potential is currently controversial. There is on the one hand the hypothesis that MYC promotes a gene expression profile which results from up- and downregulation of specific genes (Walz et al., 2014). On the other hand, since it has thousands of binding sites, MYC was suggested to be a 'global amplifier' which drives a global gene overexpression under mitogenic conditions (Lin et al., 2012; Nie et al., 2012). Another model is based on the affinity to promoters as a regulation for the oncogenic gene expression profile: so called 'high affinity genes' – which perform physiological functions – are already occupied by MYC when expressed at physiological levels. Only supraphysiological levels of MYC lead to the expression of 'low affinity genes' – involved in oncogenesis – that were not bound before, while the expression of 'high affinity genes' remains (Lorenzin et al., 2016).

MYC and its paralogues are involved in all of the described transcriptional processes (1.1.1) and affect the overall chromatin occupancy of RNAPII. MYC proteins increase promoter recruitment of RNAPII (de Pretis et al., 2017), promoter escape of it (Buchel et al., 2017) and the capping of nascent transcripts leading to target gene stabilisation (Lombardi et al., 2016). Furthermore, they promote the promoter proximal pause release of RNAPII (Herold et al., 2019; Rahl et al., 2010; Walz et al., 2014). This controlled pause release mechanism regulates gene expression (Core and Adelman, 2019). MYC proteins can also enhance the processivity of RNAPII during the elongation process (Baluapuri et al., 2019). Data about the interplay between the transcription elongation factor polymerase associated factor 1 complex (PAF1C) and MYC and MYC's turnover via ubiquitination showed the necessity for productive elongation of RNAPII (Jaenicke et al., 2016). It could recently be shown that the E3 Ligase HUWE1 drives the transfer of PAF1C from MYC to RNAPII. Downstream of the transfer, the mechanism results in ubiquitin-mediated histone modifications, chromatin remodelling and the recruitment of the repair machinery coupling transcription elongation with double strand break repair (Endres et al., 2021). This argues for a new role of MYC in tumorigenesis by maintaining genomic stability in situations of transcriptional deregulation, independent of effects on target gene expression. Through interaction with complexes involved in DNA repair, here the PAF1C, MYC delivers repair factors to active promoters thereby preventing double strand break accumulation. This mechanism is regulated through ubiquitylation and de-ubiquitylation of MYC.

1.1.3 Targeting of MYC proteins

Considering the prevalent role of MYC proteins in tumours, their targeting would open a wide therapeutic window. MYC genetic interference employing the dominant negative allele *Omomyc* in mouse models has provided proof-of-principle evidence of the benefits of MYC targeting (Jung et al., 2017; Soucek et al., 2002). Nevertheless, MYC proteins have highly unstructured regions which makes drug design with a direct protein inhibition challenging. A number of indirect approaches have been investigated (Wolf and Eilers, 2020). Among them were the inhibition of CDK7 to block transcriptional initiation (Chipumuro et al., 2014), the inhibition of the bromodomain and extraterminal (BET) protein BRD4 (Henssen et al., 2016) or of the histone chaperone complex FACT (Carter et al., 2015), both leading to downregulation of transcription elongation. In neuroblastoma, MYCN is stabilised through the interaction with Aurora-A in S-phase (Buchel et al., 2017; Otto et al., 2009). The destabilisation of MYCN through high doses of Aurora-A inhibitors showed beneficial results for the overall survival in animal experiments (Brockmann et al., 2013), but showed severe side effects and a low response rate in patients (Mosse et al., 2019). A new approach is the targeting of Aurora-A with a PROTAC, leading to its precise degradation and apoptotic cell death in cell culture experiments (Adhikari et al., 2020). Additionally, also the combinational treatment of Aurora-A and ATR inhibitors significantly prolonged the survival of mice with neuroblastic tumours (Roeschert et al., 2021).

1.2 The DNA damage response and its role in transcription regulation

1.2.1 DNA damage pathways

The genome is regularly exposed to DNA damage due to environmental, e.g. UV rays, or metabolic processes, e.g. reactive oxygen species (ROS), which can result in genomic instability (Tubbs and Nussenzweig, 2017). Among dozens of kinases being involved in DNA damage responses, there are three main kinases described in literature regulating DNA damage pathways: Ataxia-telangiectasia and Rad3 related (ATR), Ataxia-telangiectasia mutated (ATM) and DNA-dependent protein kinase (DNA-PK) (Blackford and Jackson, 2017). A target of all three proteins is the phosphorylation of the histone variant H2A.x (γH2A.x) (McManus and Hendzel, 2005; Wang et al., 2005; Ward and Chen, 2001), which can be used as a measurable output for DNA damage (Kuo and Yang, 2008). Even though all three kinases sense and signal DNA damage in some way, their activation is restricted to certain cellular events, which will be discussed in the following paragraphs.

ATR mediates replication stress responses in genotoxic situations, e.g. the formation of ssDNA regions which can result from helicase-polymerase uncoupling at stalled replication forks (Byun et al., 2005) (Figure 1.5). Replication protein A (RPA), a heterotrimer that decorates exposed single-stranded DNA and the ATR partner protein ATRIP mediate the recruitment of ATR to ssDNA (Zou and Elledge, 2003). ATR is activated through the interplay with TOPBP1 (Mordes et al., 2008) leading downstream to phosphorylation of checkpoint kinase 1 (CHK1) (Guo et al., 2000). Furthermore, TOPBP1 binds to the RAD9-RAD1-HUS1 (9-1-1) complex (Delacroix et al., 2007), which is loaded on DNA in exchange to the sliding clamp proliferating cell nuclear antigen (PCNA) at damaged sites (Eichinger and Jentsch, 2011). One mechanism by which ATR stabilises stalled replication forks (i.e. prepare for a restart of replication) and prevents fork collapse (i.e. stop in replication, degradation of replication proteins and DNA damage) is the repression of origin (ORI) firing. This prevents RPA exhaustion (i.e. when the amount of exposed ssDNA exceeds the available RPA molecules), replication catastrophe and ultimately apoptosis (Toledo et al., 2013). The ATR kinase is responsible for BRCA1 phosphorylation upon genotoxic stress (Tibbetts et al., 2000). So does ATM, which will be discussed as follows.

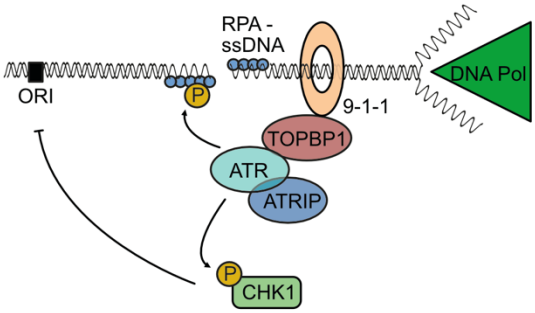

Figure 1.5 ATR signalling (adapted from Blackford and Jackson, 2017)
ATR gets recruited to ssDNA via the signalling of RPA and through its partner protein ATRIP. The interaction with TOPBP1 leads to phosphorylation of the downstream target CHK1 and the repression of ORI firing. This results in replication fork stabilisation and prevents RPA exhaustion.

ATM and DNA-PK kinases mediate the response to double strand breaks (DSB) by homologous recombination (HR) and non-homologous end-joining (NHEJ), respectively (Brandsma and Gent, 2012).

ATM activates the DSB repair cascade (Blackford and Jackson, 2017), either via error-free HR in S- and G2/M-phase (Hustedt and Durocher, 2017) or via NHEJ throughout the cell cycle (Escribano-Diaz et al., 2013). The binding of ATM to its cofactor NBS1 as part of the MRN complex is required for the recruitment to DSB sites (Falck et al., 2005) (Figure 1.6). ATM has

hundreds of substrates (Matsuoka et al., 2007), including the well-known checkpoint kinase 2 (CHK2) (Ahn et al., 2000). The tumour suppressor protein BRCA1 is a downstream target of CHK2 (Stolz et al., 2010). Subsequently, BRCA1 in a complex with CtIP leads to dephosphorylation and therefore replacement of 53BP1. The replacement of 53BP1, the key component of NHEJ, leads to repression of NHEJ and the recruitment of BRCA2 and RAD51 resulting in HR with the sister chromatid that serves as a repair template (Daley and Sung, 2014; Kowalczykowski, 2015; Venkitaraman, 2014). Besides the activation of HR, ATM activates also NHEJ by phosphorylation of 53BP1 to repair DSB. This happens throughout the cell cycle, but most prominently in G1-phase when no sister chromatid for HR is available (Escribano-Diaz et al., 2013).

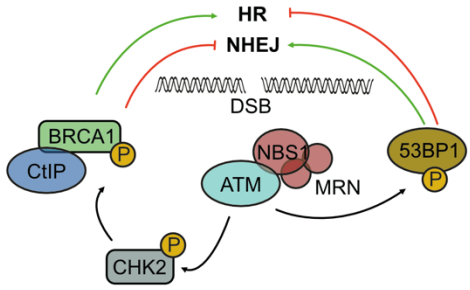

Figure 1.6 ATM signalling (adapted from Blackford and Jackson, 2017)
ATM cofactor NBS1 leads to recruitment of ATM to DSB. ATM either phosphorylates 53BP1 which leads to NHEJ or CHK2 which phosphorylates in turn BRCA1 and results in HR with the sister chromatid.

DNA-PK is activated through the interplay with Ku80 (Gell and Jackson, 1999; Singleton et al., 1999) (Figure 1.7). Also DNA-PK senses DSB and induces the repair via NHEJ (Jette and Lees-Miller, 2015). Several proteins such as XRCC4 (Li et al., 1995), XLF (Ahnesorg et al., 2006) and DNA ligase IV (LIG4) (Critchlow et al., 1997) are involved in the repair of two broken DNA ends through ligation without a repair template. Physiologically, NHEJ is needed for immunoglobulin class switching and V(D)J for generating immune-receptor diversities (Alt et al., 2013).

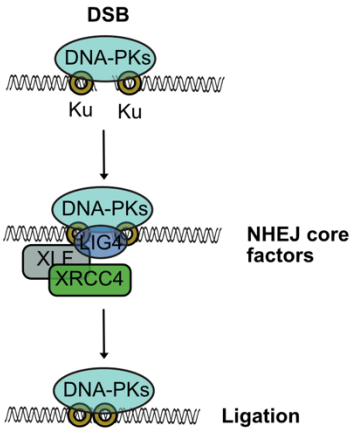

Figure 1.7 DNA-PK signalling (adapted from Blackford and Jackson, 2017)
The interplay with Ku80 activates DNA-PKs at DSB. Subsequently, several proteins such as XLF, XRCC4 and DNA ligase LIG4 lead as NHEJ core factors to repair of broken DNA ends through ligation and without a repair template.

1.2.2 The tumour suppressor protein BRCA1

BRCA1 is a tumour suppressor protein through its involvement in HR as downstream target of ATM (Gatei et al., 2000). BRCA1 and BRCA2 are large proteins with unstructured regions. These can serve as 'hubs' for different macromolecular complexes that coordinate and perform distinct biological functions, depending on the interacting proteins (Venkitaraman, 2014). One example is the BRCA1-BARD1 heterodimer complex which acts as an E3-ligase (Hashizume et al., 2001). BRCA1 promotes the ubiquitination of PCNA in response to replication blockade (Tian et al., 2013) and, furthermore, the isomerisation of BRCA1 and BARD1 is necessary for replication fork protection (Daza-Martin et al., 2019). It also marks stalled RNAPII at damaged sites (Kleiman et al., 2005). The evidence of BRCA1 interacting with RNAPII (Anderson et al., 1998; Scully et al., 1997) and the association with the hyperphosphorylated form (Krum et al., 2003) suggests the existence of further functions of BRCA1 in transcription regulation and gene expression.

MYCN-driven neuroblastoma show high dependencies on the tumour suppressor protein BRCA1 (Herold et al., 2019). Patient data revealed a worse overall survival if BRCA1 expression is high (Figure 1.8 a). Consistently, patients suffering from high-risk neuroblastoma often show a hypomethylation of the *BRCA1* locus (Figure 1.8 b), in keeping with a higher expression of the BRCA1 gene.

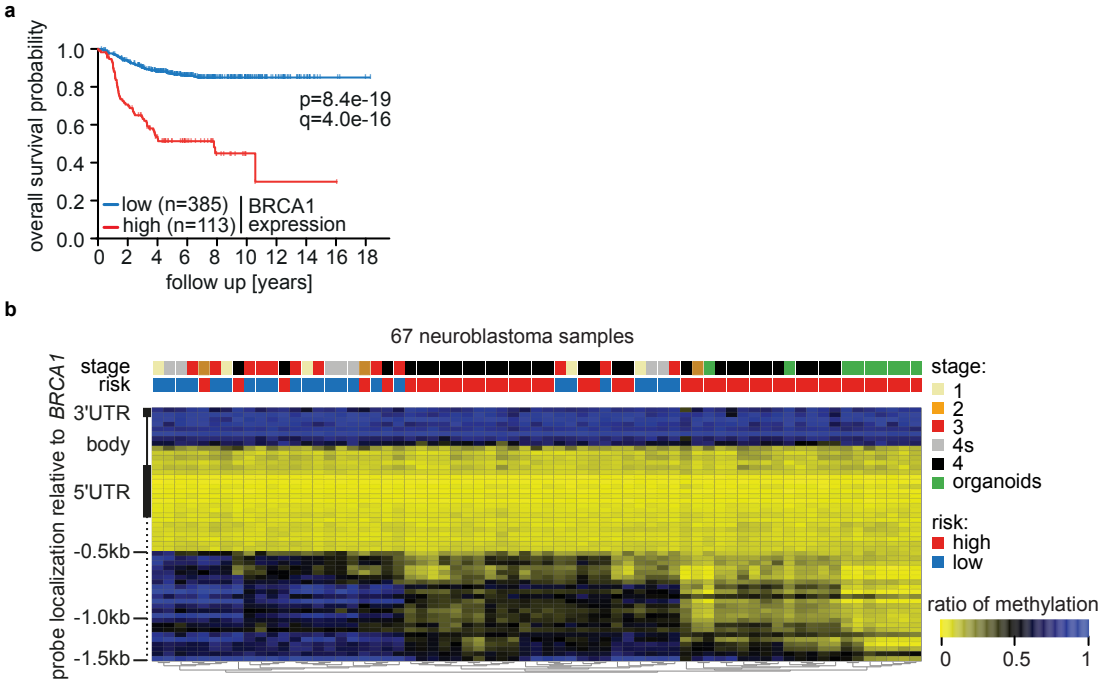

Figure 1.8 BRCA1 expression correlates with *MYCN*-status in neuroblastoma (Herold et al., 2019)
a Kaplan-Meyer curve showing the survival of neuroblastoma patients stratified for *BRCA1* expression.
b Average Methylation status of the *BRCA1* genomic region of primary neuroblastoma and organoids. UTR, untranslated region.

1.2.3 Transcriptional regulation by the DNA damage response

The involvement of the DNA damage response in transcriptional regulation is suggested by a number of evidences, including the finding that RNAPII occupancy at actively transcribed genes is more downregulated the closer to a DSB (Iannelli et al., 2017). This can be critical for the control of early replicating fragile sites (ERFSs), that are prone to damage upon replication stress and are present at clusters of high gene expression (Barlow et al., 2013). Promoters are inherently fragile since promoter proximal DSB occur frequently through torsional stress of transcription itself (Kouzine et al., 2013) or if transcription is stimulated rapidly (Haffner et al., 2010; Madabhushi et al., 2015). Mechanistically, different and also opposing models have been proposed to explain the role of DNA damage response – and specifically ATM – in coupling transcription and DSB repair (Burger et al., 2019):

ATM leads to ubiquitination of histone variant H2A through RNF8 and RNF168 (Shanbhag et al., 2010) and ENL1, through the interaction with the Polycomb Repressive Complex 1 (PRC1) resulting in repression of transcription and repair of chromatin by NHEJ (Ui et al., 2015). Also BRCA1 - as an ATM target - acts as an E3 ligase for H2A (Kalb et al., 2014b) which promotes H3 methylation and polycomb repression (Kalb et al., 2014a). H2B ubiquitination correlates with transcription elongation rate due to chromatin decompaction (Fuchs et al., 2014). This

allows the accessibility for repair factors and timely repair of DNA damage through HR or NHEJ mediated by ATM (Moyal et al., 2011).

MYC as a transcription factor is not only regulating different steps of transcription measured as changes in RNAPII chromatin occupancy and gene expression, it also coordinates transcription elongation with replication at promoter proximal DSB. The rapid transfer of elongation factor PAF1C onto RNAPII and the ubiquitination of H2B by HUWE1 make chromatin accessible for repair factors and keep transcription levels high (Endres et al., 2021). Furthermore, relief of torsional stress and DNA break-induced signalling is required for transcriptional elongation (Bunch et al., 2015) and to sustain oncogenic programs (Bacon et al., 2020).

1.3 Transcription associated events resulting in DNA damage

1.3.1 Transcription-replication conflicts

Replication is the central cellular mechanism by which an identical duplicate of the cell's DNA is produced to prepare for cell division. Originated from the origin of replication (ORI), the replication machinery is working bidirectionally (Sclafani and Holzen, 2007). As transcription and replication use both DNA as template leading to potential clashes of transcription and replication machineries. While transcription of genes takes place throughout the cell cycle, replication is mainly restricted to S-phase. Therefore, these two processes need to be coordinated especially in S-phase to avoid transcription-replication conflicts. The mechanisms of regulating and coordinating transcription with replication were studied extensively during the last years:

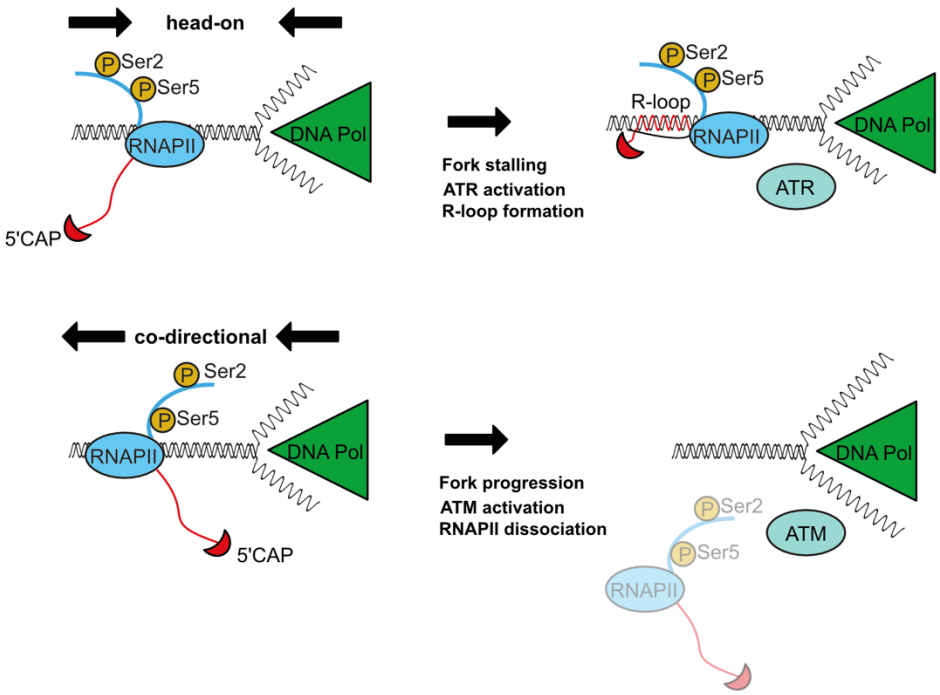

Figure 1.9 Signalling pathways for head-on and co-directional conflicts (adapted from Hamperl et al., 2017) Head-on conflicts of RNAPII and replication machinery result in fork stalling, R-loop formation and ATR activation. Co-directional conflicts result in replication fork progression, ATM activation and RNAPII dissociation.

The clashes can either be head-on or co-directional collisions (Figure 1.9). The nature of collisions determines which DNA damage pathway is getting activated. Head-on conflicts lead to replication fork and RNAPII stalling, the activation of the ATR pathway and the increase of DNA/RNA-hybrids named R-loops (1.3.2) (Hamperl et al., 2017). The ATR kinase is further proposed to be a coordinator of transcription with replication because it regulates origin firing, stabilises replication forks and promotes their repair and restart (Hamperl and Cimprich, 2016). Co-directional conflicts, however, lead to fork progression, the activation of the ATM kinase and a decrease of R-loops, since RNAPII dissociates from chromatin eventually through ubiquitination and subsequent degradation (Hamperl and Cimprich, 2016; Noe Gonzalez et al., 2021). Head-on conflicts lead to stalled forks and genomic alterations (Garcia-Muse and Aguilera, 2016), but also co-directional collisions can be dangerous for genome integrity, as they cause DSB when the replication fork crashes into a stalled or backtracked RNAPII (Dutta et al., 2011).

Eukaryotes evolved different mechanisms to prevent transcription-replication conflicts. One is the temporal and spatial regulation of these processes, such as compartmentalisation of transcription and replication within the nucleus (Marchal et al., 2019; Rivera-Mulia and Gilbert,

2016; Wei et al., 1998). Another mechanism is the general avoidance of obstacles for the replisome such as stalled and backtracked RNAPII, p.e. through transcription restart by TFIIS (Kireeva et al., 2005). Stalled RNAPII can be the cause or the consequence of R-loop formation, which will be discussed in the following paragraph.

1.3.2 DNA/RNA-hybrids (R-loops)

DNA/RNA hybrids, so called R-loops, are a naturally occurring chromatin associated phenomenon studied since 1976 (Thomas et al., 1976). They are three stranded structures consisting of nascent RNA protruding from RNAPII that hybridised to the template DNA stand, displacing the other non-template DNA strand. R-loops build a structure with a remarkable stability, higher than double stranded DNA (dsDNA) (Lesnik and Freier, 1995). R-loops form naturally within the transcription bubble, but are then just about a few base pairs long. The conformation of the RNAPII and the exit channels for RNA and DNA generally avoid R-loop formation (Westover et al., 2004). However, wherever RNAPII slows down or stalls, p.e. because of an obstacle (i.e. nucleosome, replication machinery, DSB), at the promoter proximal pause site or after the PAS, the backfolding of nascent RNA and the formation of R-loops is favoured. Every process that circumvent stalling of RNAPII and results in proper mRNA processing during transcription prevents the formation of R-loops: deficiencies in mRNA export occurring from THO complex defects trigger genomic instability and R-loop formation in yeast (Huertas and Aguilera, 2003). Furthermore, supercoiling of DNA resulting from the transcriptional process favours the formation of R-loops suggesting the importance of topoisomerases in preventing this scenario (Phoenix et al., 1997). Splicing factor defects result also in increased formation of R-loops (Cossa et al., 2020), replication stress and the activation of the ATR kinase (Chen et al., 2018; Cossa et al., 2020). Also transcriptional elongation factors, such as PAF1C, are recruited to promoter proximal paused RNAPII to promote pause release and prevent R-loops (Shivji et al., 2018).

R-loop formation is generally favoured by the increased window of opportunities by RNAPII slowing or stalling and can form all over the gene, but genome-wide sequencing revealed their tendency for promoter proximal regions with a high GC content (Chen et al., 2017; Ginno et al., 2013; Ginno et al., 2012; Sanz et al., 2016) which are associated with increased promoter proximal pausing of RNAPII as described above (1.1.1). R-loops form also at TES (Hatchi et al., 2015), where RNAPII slows down before transcription termination. Furthermore, nutrient deprivation leads to R-loop formation within gene bodies, where RNAPII stalls suddenly (Dejure et al., 2017).

On the one hand, R-loops are viewed as a source for DNA damage and a threat to genome stability (Aguilera and Garcia-Muse, 2012). The DNA damage response can prevent R-loop formation, but is even more important for their resolution (Barroso et al., 2019). On the other hand, R-loops are beneficial and necessary for immunoglobulin class switching in B-cells (Roy et al., 2008) and regulate transcription by influencing chromatin remodelling through different cofactors (Niehrs and Luke, 2020).

Recent work about the interactome of R-loops shed some light in R-loop biology (Cristini et al., 2018). Several factors have been proposed to promote R-loop resolution, mainly helicases that lead to the resolution of the hybrids and make them accessible for degradation factors. Examples are BRCA1 together with the DNA/RNA-helicase Senataxin (SETX) that resolve R-loops specifically at TES (Hatchi et al., 2015), the DEAD box helicase DDX5 that resolves R-loops at DSBs (Yu et al., 2020), and another DEAD box helicase, DDX21, that lead to R-loop resolution together with SIRT7 to protect the genome from damage (Song et al., 2017).

Since R-loops are byproducts of active transcription, their indirect targeting through the interactome could sensitise aggressive tumours for cancer therapy (Boros-Olah et al., 2019). However, whether R-loops are ‘good’, p.e. for cellular processes such as immunoglobulin class switching, or ‘bad’, p.e. because of increased risk of DNA damage, is still a matter of debate and context dependent.

1.4 The nuclear role of premature termination and decapping factors

1.4.1 Premature termination and DNA damage

Besides XRN2’s function in the ‘torpedo’ model in normal termination, it is also involved in premature termination. XRN2 interacts with the decapping complex that removes the protective 5’CAP of mRNA and acts as an exonuclease downstream of it. This leads to promoter proximal premature termination (Brannan et al., 2012, Figure 1.4).

The DNA/RNA helicase SETX does not only resolve R-loops through its helicase function as described above, XRN2 acts downstream of it and promotes subsequently transcription termination (Skourti-Stathaki et al., 2011). This is also a mechanism for the resolution of R-loops at DSB to prevent translocations (Cohen et al., 2018). Strikingly, XRN2 colocalises with 53BP1 upon DNA damage and resolves R-loops (Morales et al., 2016) to ensure chromatin accessibility for DNA damage repair factors (Dang and Morales, 2020).

These findings argue for a direct interplay of DNA damage pathways and premature termination to mediate proper DNA damage repair.

1.4.2 Decapping factors involved in premature termination

The role of decapping factors in mRNA-decay is well described in cytoplasmic processing bodies (P-bodies) (Luo et al., 2018). For the decapping of mRNA in P-bodies, EDC4 acts as a scaffold protein for the binding of the catalytic protein DCP2 and activating protein DCP1 (Chang et al., 2014). DCP1, a heterodimer of DCP1A and DCP1B, activates DCP2 to remove the 5'CAP of the mRNA (Tritschler et al., 2009; Tritschler et al., 2007).

Besides their cytoplasmatic role, decapping factors are also involved in nuclear processes. EDC4 acts in a complex with TOPBP1 and BARD1 to promote end resection at DSB, similarly to BRCA1's role in homologous recombination (Hernandez et al., 2018), suggesting a decapping independent function. Additionally, several termination factors, p.e. DCP1A and DCP2, interact with the exonuclease XRN2 and promote decapping of nascent transcripts, their degradation by XRN2 and premature termination to limit bidirectional transcription (Brannan et al., 2012).

1.4.3 Premature termination and gene regulation

Premature termination is not only necessary at DNA damage sites, but is also an important process in gene regulation (Kamieniarz-Gdula and Proudfoot, 2019). Antisense oligonucleotides trigger the cleavage of nascent transcripts, resulting in premature termination by XRN2 and downregulation of mRNA levels (Lee and Mendell, 2020). Moreover, DCP1A is involved in gene regulation: SMIF, a synonym of DCP1A, is a SMAD4 interacting protein that acts as a co-activator of the immune pathway of TGFβ and the interaction is responsible for the nuclear shuttling of DCP1A (Bai et al., 2002). Furthermore, EDC4 and DCP1A assembly in P-bodies is essential for the posttranscriptional regulation of IL-6 as a component of the immune regulation (Seto et al., 2015). EDC4 was previously identified to be post-translationally modified or rather phosphorylated in response to DNA damage in a proteomic screen, although the dependence on ATM or ATR remained unclear (Elia et al., 2015; Matsuoka et al., 2007). The post-translational phosphorylation of DCP1A is also documented in a signalling pathway that is active during neuronal development (Blumenthal et al., 2009). Moreover, the IκB kinase (IKK) – the key regulator for NF-κB activation and nuclear

translocation – interacts with and phosphorylates EDC4 which gives the stimulus for P-body formation and influences mRNA stability indirectly (Mikuda et al., 2018).

Overall, decapping factors have multiple roles in different cellular compartments but are also involved in transcriptional (Brannan et al., 2012) and gene regulation (Bai et al., 2002) which makes them to potential partner proteins of MYC-driven transcription.

1.5 The aim of this study

MYCN-driven neuroblastoma is an aggressive type of neuroendocrine tumour with a very poor prognosis for patients. The current treatment, which includes aggressive chemotherapy, has severe side effects (Mosse et al., 2019). The further characterisation of MYCN as an oncogenic driver might result in the identification of vulnerable targets for cancer therapy.

MYCN-driven neuroblastoma cells are highly dependent on BRCA1 (Herold et al., 2019). Besides its role as a tumour suppressor (Venkitaraman, 2014), BRCA1 is also connected to transcription and RNAPII itself (Anderson et al., 1998; Scully et al., 1997). The identification of BRCA1's role in neuroblastoma was the aim of this study. In particular, how BRCA1 influences the DNA damage response upon acute activation of MYCN, whether BRCA1 is involved in MYCN-driven transcription, and if so how it influences RNAPII chromatin occupancy and gene expression. The identification of BRCA1 partner and downstream acting proteins could potentially serve as therapeutic targets.

2 Materials

2.1 Bacterial strains and cell lines

2.1.1 Bacterial strains

XL1-Blue

Escherichia coli strain, used for plasmid amplification and protein expression with the following genotype: *recA1, endA1, gyrA96, thi-1, hsdR17, supE44,relA1, lac [F´ proAB lacIqZΔM15 Tn10 (Tetr)]*

2.1.2 Mammalian Cell lines

Table 2.1: Mammalian cell lines used in this study

HEK293TN	Human embryonic kidney cell line (ATCC)
SH-EP	Human neuroblastoma cell line, *MYCN* non-amplified
SH-EP MYCN-ER	Human neuroblastoma cell line, *MYCN* non-amplified, stably transfected with the MYCN-ER chimera (Hygromycin and G418 resistance)
SH-SY5Y	Human neuroblastoma cell line, *MYCN* non-amplified
NB69	Human neuroblastoma cell line, *MYCN* non-amplified
SK-N-AS	Human neuroblastoma cell line, *MYCN* non-amplified, derived from bone marrow metastasis
Kelly	Human neuroblastoma cell line, *MYCN*-amplified
IMR5	Human neuroblastoma cell line, *MYCN*-amplified
SMS-KCN	Human neuroblastoma cell line, *MYCN*-amplified
NGP	Human neuroblastoma cell line, *MYCN*-amplified, derived from a lung metastasis
NIH/3T3	Mouse embryonic fibroblast cell line

2.2 Cultivation media and supplements

2.2.1 Media and antibiotics for bacterial cell culture

LB medium

10% Bacto tryptone

0.5% Yeast extract

1% NaCl

LB agar

LB medium

1.2% Bacto-Agar

Autoclaved, heated in a microwave oven, cooled to 50°C before adding specific antibiotics, approximately 10ml filled into 10 cm dishes.

Antibiotics

100 µg/ml ampicillin was added to the medium to select successfully transformed bacteria.

2.2.2 Media for mammalian cell culture

For cultivation of the mammalian cells named above, Roswell Park Memorial Institute (RPMI) 1640 medium containing 300 mg/ml L-glutamine from Thermo Fisher Scientific and Dulbecco's Modified Eagle's Medium (DMEM) containing 580 mg/ml L-glutamine were used. Fetal bovine serum (FBS, Capricorn Scientific GmbH) was heat-inactivated for 30min at 56°C.

Basal medium: RPMI/DMEM, 10% FBS, 1% penicillin/streptomycin (Sigma)

Freezing medium: 60% Basal medium, 30% FBS, 10% DMSO

Transfection medium: DMEM, 2% FBS

2.2.3 Antibiotics for mammalian cell culture

Penicillin/streptomycin (100,000 U/ml, Sigma) was added to cultivation media to avoid bacterial contaminations. For the selection of transfected or infected mammalian cells, 2 µg/ml puromycin (stock 10 mg/ml, InvivoGen) or 100 µg/ml hygromycin B gold (stock 100 mg/ml, InvivoGen) was added to the medium. Doxycycline at a concentration of 1 µg/ml (stock 1 mg/ml, Sigma) was added for the induction of the tetracycline inducible shRNA system.

2.2.4 Other compounds for mammalian cell culture

For infection of mammalian cells, 4 µg/ml Polybrene (Sigma-Aldrich) in sterile water was used. Doxycycline was used for induction of the shRNAs of the tetracycline inducible vector system with a final concentration of 1 µg/ml. For the activation of the MYCN-ER transgene, SH-EP MYCN-ER cells were treated with 100-200 nM 4-Hydroxytamoxifen (4-OHT).

2.3 Nucleic acids

2.3.1 Primers

The primers and oligonucleotides used in this study were designed with Primer3 and purchased from Sigma-Aldrich. qRT-PCR primers are designed as intron spanning to avoid false positive signals from genomic DNA. Oligonucleotides for shRNAs were based on the mirE design described in Fellmann et al., 2013.

Table 2.2: Oligonucleotides used for cloning
for=forward, rev=reverse

Name	Application	Sequence (5' to 3')
mirE_cloning_XhoI_PCR_for (EW880)	mirE-shRNA generation	TACAATACTCGAGAAGGTATA TTGCTGTTGACAGTGAGCG
mirE_cloning_EcoRI_PCR_rev (EW881)	mirE-shRNA generation	TTAGATGAATTCTAGCCCCT TGAAGTCCGAGGCAGTAGGCA
shSCR control	Non-targeting control	ctcgagAAGGTATATTGCTGTTG ACAGTGAGCGCAGGAATTAT AATGCTTATCTATAGTGAAG CCACAGATGTATAGATAAGC ATTATAATTCCTATGCCTACT GCCTCGGACTTCAAGGGGCTAgaattc
Luciferase_control_#20	Luciferase control	TGC TGT TGA CAG TGA GCG CCT ACG TGC AAG TGA TGA TTT ATA GTG AAG CCA CAG ATG TAT AAA TCA TCA CTT GCA CGT AGA TGC CTA CTG CCT CGG A
BRCA1_shRNA_#3 (this study and Herold et al. = #1)	BRCA1 knockdown	TGC TGT TGA CAG TGA GCG ACA GAT AGT TCT ACC AGT AAA ATA GTG AAG CCA CAG ATG TAT TTT ACT GGT AGA ACT ATC TGC TGC CTA CTG CCT CGG A
BRCA1_shRNA_#5 (this study and Herold et al. = #2)	BRCA1 knockdown	TGC TGT TGA CAG TGA GCG ATA CAA GAA AGT ACG AGA TTT ATA GTG AAG CCA CAG ATG TAT AAA TCT CGT ACT TTC TTG TAG TGC CTA CTG CCT CGG A
DCP1A_shRNA_#4	DCP1A knockdown	TGC TGT TGA CAG TGA GCG ATG GGA GAA GAC TGA TAT AGA ATA GTG AAG CCA CAG ATG TAT TCT ATA TCA GTC TTC TCC CAC TGC CTA CTG CCT CGG A

Table 2.3: Primers used for qPCR

Name	Application	Sequence (5' to 3') Forward primer	Sequence (5' to 3') Reverse primer
B2M	qPCR	GTGCTCGCGCTACTCTCTC	GTCAACTTCAATGTCGGAT
BRCA1 (BH_hBRCA1_#1)	qPCR	AGTGACATTTTAACCACTCAGCAG	TGATGGAAGGGTAGCTGTTAGAA
DCP1A (*JK35_36*)	qPCR	CAGGCCAGAATGAATCCCTA	CTCCATCTCGGTGTCCATTT
PLD6 (LJ345_346)	qPCR	CTCAACGGCTCGCAAATC	GCCTGGGTCTTGATCGTG
TFAP4 (LJ391_392)	qPCR	ACGGAGAGAAGCTCAGCAAG	TGAAGCGCTTGAGCTGTGT
TAF4B (LJ389_390)	qPCR	GGTAACCACTGTTCCGAAGC	ACTGTGACGACACTGGTTGG
TAF4B (LJ451_452)	ChIP	AAGGTCGTCGCTCACAC	GCGTGGCTATATAAACATGGCT
PLD6 (LJ424_425)	ChIP	TGTGGGTCCCGGATTAG	CTCCAGAGTCAGAGCCA
TFAP4 (LJ430_431)	ChIP	CCGGGCGCTGTTTACTA	CAGGACACGGAGAACTACAG
NME1 (*GB05_06*)	ChIP	GGGGTGGAGAGAAGAAAGCA	TGGGAGTAGGCAGTCATTCT
NPM1 (*GB89_90*)	ChIP	TTCACCGGGAAGCATGG	CACGCGAGGTAAGTCTACG
Intergenic (*EW09_10*)	ChIP	TTTTCTCACATTGCCCCTGT	TCAATGCTGTACCAGGCAAA
ACTB promoter (Hatchi et al., 2015)	ChIP	GAGGGGAGAGGGGGTAAA	AGCCATAAAAGGCAACTTTCG
ACTB intron 1 (Hatchi et al., 2015)	ChIP	CGGGGTCTTTGTCTGAGC	CAGTTAGCGCCCAAAGGAC
ACTB intron 3 (Hatchi et al., 2015)	ChIP	TAACACTGGCTCGTGTGACAA	AAGTGCAAAGAACACGGCTAA
ACTB 5'pause (Hatchi et al., 2015)	ChIP	TTACCCAGAGTGCAGGTGTG	CCCCAATAAGCAGGAACAGA
ACTB pause site (Hatchi et al., 2015)	ChIP	GGGACTATTTGGGGGTGTCT	TCCCATAGGTGAAGGCAAAG
EIF3B (GB279_298)	DRIP	TGGGTGTGCTGTGAGTGTAG	ATGGACAATTCTGAGGGGCA
RPL5 (GB313_314)	DRIP	TTTTCTTGCCCGTATGCCAG	CGCACTCAGGCTGTCTACTA
IRF2BP1 (GB291_292)	DRIP	AGTACCCTCGTTTGCACTCA	ACACCCCACTTCCTGATCTG

GBA (GB451_452)	DRIP	AGCCCTTCCTCAAGTCTCAT	ACTGTGGGAATTCAATCGCC
RAN (GB287_288)	DRIP	CCGTGACTCTGGGATCTTGA	CAAGGTGGCTGAAACGGAAA
PTPN23 (GB329_330)	DRIP	CCAGTCTCCGGTCAGTGATT	CGTATTGTCAAGAGCCGTGG
DRG2 (JK25_26)	DRIP	CGTGGGCCAGTACAGCAT	CCGGAAGCCAAAGAGAACAG
RPS16 (GB325_326)	DRIP	CCGAGCGTGGACTAGACAA	GTTAGCCGCAACAGAAGCC
POLG (GB331_332)	DRIP	CTTCTCAAGGAGCAGGTGGA	CTTCTCAAGGAGCAGGTGGA
NOLC1 (GB333_334)	DRIP	CAATGACGTAACACAGGCCC	GAGAGTTGGTTATCGCGCAG

Primers used from the oligocollection of the Eilers Laboratory are listed with original numbering written in italic.

2.3.2 Plasmids

The following plasmids were used in this study and were already available in the Eilers Laboratory.

Table 2.4 Empty vectors used in this study

Vector (Brand)	Description
pGIPZ (Dharmacon)	Lentiviral shRNA expression vector; consitutive, puromycin resistance; eGFP
pLT3_GEPIR	Lentiviral shRNA expression vector; Tet-on all in one system; puromycine resistance; PGK promoter; eGFP (inducible)

Table 2.5 Packaging plasmids used for lentivirus production

Name (Brand)	Description
psPAX.2 (Addgene)	Plasmid for lentivirus production, encoding for virion packaging system
pMD2.G (Addgene)	Plasmid for lentivirus production, encoding for virion envelope

Table 2.6: Plasmids generated for this study

Name	Description
pGIPZ shSCR	Lentiviral expression vector constitutively expressing non-targeting shRNA
pGIPZ shBRCA1#3 (this study and Herold et al. = #1)	Lentiviral expression vector constitutively expressing shRNA#3 against BRCA1 mRNA
pGIPZ shBRCA1#5 (this study and Herold et al. = #2)	Lentiviral expression vector constitutively expressing shRNA#5 against BRCA1 mRNA
pLT3 shDCP1A#4	Dox-inducible lentiviral expression vector with shRNA#4 against DCP1A mRNA

2.4 Antibodies

2.4.1 Primary antibodies

Table 2.7: List of antibodies used in this study

Protein	Order Number	Supplier	Application
ACTIN	A5441	Sigma-Aldrich	WB
BRCA1	07-434	EMD Millipore	WB
BRCA1	A300-000A	Bethyl Laboratories	ChIP
Rat α-BrdU	OBT0030	AbD Serotec / Bio-Rad	Fiber Assays
Mouse α-BrdU	347580	BD Biosciences	Fiber Assays
BrdU-FITC	BLD-364104	Biozol / BioLegend	FACS
CHK1	sc-7898	Santa Cruz Biotechnology	WB
pCHK1 (S345)	2348	Cell Signaling	WB, IF
CHK2	sc-17747	Santa Cruz Biotechnology	WB
pCHK2 (Thr68)	2661	Cell Signaling	WB
DCP1A	sc-100706	Santa Cruz Biotechnology	ChIP-seq, WB
DCP1A	ab47811	Abcam	PLA
DCP2	A302-597A-T	Bethyl Laboratories	WB, PLA
EDC4	ab72408	Abcam	WB, ChIP-seq
ER alpha	sc-8002	Santa Cruz Biotechnology	WB
phosphor H2A.x (γH2A.x)	2577	Cell Signaling	WB, IF

KAP1	A300-274A	Bethyl Laboratories	WB
pKAP1 (S824)	ab70369	Abcam	WB
MYC	ab32072	Abcam	WB
MYCN	sc-791	Santa Cruz Biotechnology	WB
MYCN	sc-53993	Santa Cruz Biotechnology	ChIP-seq, IP
NPM	ab10530	Abcam	WB
PCNA	ab92552	Abcam	PLA
RAD1	sc-22783	Santa Cruz Biotechnology	PLA
RAD9	sc-8324	Santa Cruz Biotechnology	PLA
RNAPII	sc-55492	Santa Cruz Biotechnology	PLA
RNAPII	sc-56767	Santa Cruz Biotechnology	PLA, ChIP-seq
RNAPII	sc-17798	Santa Cruz Biotechnology	Total RNAPII ChIP-seq
RNAPII	sc-899 X	Santa Cruz Biotechnology	Total RNAPII ChIP-seq
pSer2-RNAPII	ab5095	Abcam	ChIP-seq
pSer2-RNAPII	920204	BioLegend	PLA
pSer5-RNAPII	904001	BioLegend	PLA, ChIP-seq
pSer5-RNAPII	MMS-128P	Covance	WB
total RPA32	sc-53496	Santa Cruz Biotechnology	WB
pRPA32 (S33)	A300-246A	Bethyl Laboratories	WB, IF
pRPA32 (S4/8)	A300-245A	Bethyl Laboratories	WB
S9.6 (DNA/RNA-hybrids)	ENH001	Kerafast	DRIP
VINCULIN	V9131	Sigma-Aldrich	WB

2.4.2 Secondary antibodies

Table 2.8: List fo secondary antibodies used in this study

Name	Order Number	Supplier	Application
Anti-Mouse IgG HRP conjugated (Mouse TrueBlot® ULTRA)	18-8817-33	Rockland/Biomol	WB

Anti-Rabbit IgG HRP conjugated (Rabbit TrueBlot®)	18-8816-33	Rockland/Biomol	WB
Alexa Fluor® 568 Goat Anti-Mouse IgG (H+L) Antibody	A-11004	Thermo Fisher Scientific	IF
Alexa Fluor® 568 Goat Anti-Rabbit IgG (H+L) Antibody	A-11036	Thermo Fisher Scientific	IF
SuperBoost™ Goat Anti-Rabbit Poly HRP	B40962	Thermo Fisher Scientific	WB
SuperBoost™ Goat Anti-Mouse Poly HRP	B40961	Thermo Fisher Scientific	WB
Alexa Fluor® 488 Goat Anti-Mouse Antibody	A-11001	Molecular probes / Thermo Fisher Scientific	Fiber assays
Alexa Fluor® 555 Goat Anti-Rat Antibody	A-21434	Molecular probes / Thermo Fisher Scientific	Fiber assays

2.5 Chemicals

All chemicals and solutions were purchased from Applichem, Calbiochem, Invitrogen, Merck, Roth and Sigma-Aldrich. If not specified otherwise, buffers were prepared with ddH_2O.

2.6 Buffers and solutions

AnnexinV-binding buffer

10 mM HEPES pH 7.4

140 mM NaCl

2.5 mM $CaCl_2$

Bradford reagent

0.01% Coomassie Brilliant Blue G250

8.5% phosphoric acid

4.75% EtOH

Solution was filtered and stored at 4 °C in the dark

Biotin labelling buffer

25 mM Tris (pH 7.4)

2.5 mM EDTA

Biotin-HPDP-DMF stock

EZ-Link Biotin HPDP (Pierce)

0.2 mg/ml dimethylformamide

3.5x Bis-Tris buffer

1.25 M Bis-Tris

Adjust to pH 6.7 with HCl

Bis-Tris stacking gel

4% acrylamide

1x Bis-Tris

0.03% APS

0.05% TEMED

Bis-Tris separating gel

8-15% acrylamide

1x Bis-Tris

0.03% APS

0.05% TEMED

BLISS lysis buffer I

10 mM Tris-HCl (pH 8)

10 mM NaCl

1 mM EDTA

0.2% Triton X-100

BLISS lysis buffer II

10 mM Tris-HCl (pH 8)

150 mM NaCl

1 mM EDTA

0.3% SDS

BLISS high-salt wash buffer

10 mM Tris-HCl (pH 8)

2 M NaCl

2 mM EDTA

0.5% Triton X-100

BLISS DNA extraction buffer

1% SDS

100 mM NaCl

50 mM EDTA

10 mM Tris-HCl (pH 8)

Blocking solution for PVDF membranes

5% BSA in TBS-T

Blocking solution for Dynabeads

5 mg/ml BSA in PBS

ChIP elutionbuffer

50 mM Tris (pH 7.5)

1 mM EDTA (pH 8.0)

1% SDS

ChIP lysis buffer I (PIPES)

5 mM PIPES pH 8.0

85 mM KCl

0.5% NP-40

ChIP lysis buffer II (RIPA)

50 mM HEPES (pH 7.9)

140 mM NaCl

1 mM EDTA

0.1% SDS

1% Triton-X-100

0.1% Deoxycholic acid sodium salt

ChIP wash Buffer I

20 mM Tris-HCl (pH 8.1)

150 mM NaCl

2 mM EDTA

0.1% SDS

1% Triton-X-100

ChIP wash buffer II

20 mM Tris-HCl (pH 8.1)

500 mM NaCl

2 mM EDTA

0.1% SDS

1% Triton-X-100

ChIP wash buffer III

10 mM Tris-HCl (pH 8.1)

250 mM LiCl

1 mM EDTA

1 % NP-40

1 % Deoxycholic acid sodium salt

Crystal violet solution

0.1% Crystal Violet

20% Ethanol

DNA loading buffer (6x)

10 mM EDTA (pH 8.0)

0.2% Orange G

40% sucrose

Doxycycline

1 mg/ml doxycycline hyclate (Sigma) diluted in EtOH

DRIP binding buffer (10x)

10 mM $NaPO_4$ (pH 7.0)

140 mM NaCl

0.05% Triton X-100

DRIP elution buffer

50 mM Tris-HCl (pH 8.0)

10 mM EDTA

0.5% SDS

Dynabeads wash Buffer A

100 mM NaOH

50 mM NaCl

Dynabeads wash Buffer B

100 mM NaCl

Dynabeads wash Buffer (2x)

1 M NaCl

10 mM Tris (pH 7.5)

1 mM EDTA

0.1% Tween-20

Hoechst 33342

5 mg/ml Hoechst 33342 (Sigma) diluted in ddH_2O

4-Hydroxytamoxifen (4-OHT)

1 mM 4-Hydroxytamoxifen (Sigma) diluted in EtOH

Mini buffer I (Resuspensionbuffer)

50 mM Tris-HCl (pH 8.0)

10 mM EDTA

10 µg/ml RNaseA

Mini buffer II (Lysisbuffer)

20 mM NaOH

1% SDS

Mini buffer III (Precipitationbuffer)

3.1 M Potassiumacetate (pH 5.5 adjusted with conc HCl)

MOPS running buffer (20x)

1 M MOPS

1 M Tris base

20 mM EDTA

2% SDS

MOPS running buffer (ready to use)

1x MOPS running buffer

5 mM Sodium bisulfit

Nuclear extraction buffer (HEPES buffer)

20 mM HEPES (pH 7.9)

150 mM NaCl

0.2% NP-40

0.5 mM EDTA

10% glycerol

2 mM $MgCl_2$

NuPAGE transfer buffer (20x)

500 mM Bis-Tris

500 mM Bicine

20.5 mM EDTA

5.36 mM chlorobutanol

1x NuPAGE transfer buffer (ready to use)

1x NuPAGE Transferbuffer

20% Methanol

PBS (autoclaved)

137 mM NaCl

2.7 mM KCl

10.1 mM Na_2HPO_4

1.76 mM KH_2PO_4

PEI

450 µl PEI (10 % solution)

150 µl HCl (2N)

49.5 ml ddH_2O

Phenol-Chloroform-Isoamylalcohol

25 ml Phenol

24 ml Chloroform

1 ml Isoamylalcohol

Phenylmethylsulfonylfluoride (PMSF)

150 mM PMSF (Roth) in isopropanol

Phosphatase inhibitor

Ser/Thr phosphatase inhibitor (Sigma, P0044), Tyr phosphatase inhibitor (Sigma, P5726), used 1:1,000

Protease inhibitor

Protease inhibitor cocktail (Sigma, P8340), used 1:1,000

Proteinase K

10 mg/ml Proteinase K (Roth) in ddH_2O

Sample buffer (6x) (Lämmli)

1.2 g SDS

6 mg bromphenol blue

4.7% glycerol

1.2 ml 0.5 M Tris (pH 6.8)

2.1 ml ddH_2O

The solution was heated up,

0.93 g DTT was dissolved,

solution was aliquoted and stored at -20 °C

Stripping buffer

62.5% Tris (pH 6.8)

2% SDS

100 mM β-mercaptoethanol

TAE (50x)

2 M Tris base

1 M acidic acid

50 mM EDTA (pH 8.0)

TBS (20x)

50 mM Tris base

450 mM Tris HCl

2.8 M NaCl

TBS-T

1x TBS (20x)

0.2% Tween-20

TE

10 mM Tris (pH 8.0)

1 mM EDTA (pH 8.0)

TNN

50 mM Tris-HCl (pH7.4)

120 mM NaCl

5 mM EDTA

0.5% NP-40

Trypsin solution

0.25% Trypsin

5 mM EDTA

22.3 mM Tris (pH 7.4)

125 mM NaCl

2.7 Enzymes, standards and kits

2.7.1 Enzymes

Benzonase nuclease purity >99% (Merck/Millipore)

DNase I, RNase-free (Thermo Fisher Scientific)

M-MLV Reverse Transcriptase (Promega)

Proteinase K (Roth)

Restriction enzymes: AsiSi, BsrGI, EcoRI, HindIII, SSpI, XbaI XhoI (New England Biolabs)

Recombinant Ribonuclease Inhibitor (Thermo Fisher Scientific)

RNase A (Roth)

RNaseH1 (New England Biolabs)

T4 DNA Ligase (New England Biolabs)

T4 RNA Ligase 2 (New England Biolabs)

2.7.2 Standards

1 kb DNA Ladder (New England Biolabs)

HiMark pre-stained HMW STD (Thermo Fisher Scientific)

HS NGS Fragment DNA Ladder (Agilent)

PageRuler™ Prestained Protein Ladder (Thermo Fisher Scientific)

2.7.3 Kits

Agencourt AMPure® XP Beads (Beckman Coulter)

Agencourt RNAClean XP Beads (Beckman Coulter)

Click-iT™ EdU Cell Proliferation Kit for Imaging, Alexa Fluor™ 647 dye (Thermo Fisher Scientific)

Duolink® In Situ PLA® Probe Anti-Rabbit PLUS (Sigma)

Duolink® In Situ PLA® Probe Anti-Mouse MINUS (Sigma)

Duolink® In Situ Detection Reagents Red (Sigma)

Dynabeads® Protein A (Thermo Fisher Scientific)

Dynabeads® Protein G (Thermo Fisher Scientific)

Dynabeads™ MyOne™ streptavidin T1 beads (Invitrogen)

Immobilon Western Substrate (Millipore)

MAXtract high-density tubes (Qiagen)

MEGAscript™ T7 Transcription Kit (Thermo Fisher Scientific)

MinElute PCR Purification Kit (Qiagen)

miRNeasy Mini Kit (Qiagen)

NEBNext® rRNA Depletion Kit (New England Biolabs)

NEBNext® Ultra II Directional RNA Library Prep Kit for Illumina (New England Biolabs)

NEBNext® Ultra™ RNA Librar Prep Kit for Illumina® (New England Biolabs)

NEBNext® Multiplex Oligos for Illumina® (New England Biolabs)

NEBNext® RNA Sample Purification Beads (New England Biolabs)

NEBNext® Sample Purification Beads (New England Biolabs)

NEBNext® Ultra II DNA Library Prep Kit for Illumina (New England Biolabs)

NEBNext® ChIP-Seq Library Prep Master Mix Set for Illumina® (New England Biolabs)

NEBNext® Oligo $d(T)_{25}$ Magnetic Beads (New England Biolabs)

NEBNext® High-Fidelity 2X PCR Master Mix (New England Biolabs)

NextSeq® 500/550 High Output Kit v2.5 (75 cycles) (Illumina)

NGS Fragment High Sensitivity Analysis Kit, 1-6,000 bp, 500 samples (Agilent)

PowerUp™ SYBR® Green Master Mix (Thermo Fisher Scientific)

PureLink® HiPure Plasmid Maxiprep Kit (Life Technologies)

QIAquick PCR Purification Kit (Qiagen)

QIAquick Gel Extraction Kit (Qiagen)

QIAzol Lysis Reagent (Qiagen)

Quant-iT PicoGreen dsDNA assay (Thermo Fisher Scientific)

Quant-iT™ RiboGreen® RNA Assay Kit (Thermo Fisher Scientific)

Quick Blunting Kit (New England Biolabs)

Random Primer (Sigma/Roche)

RNeasy Mini Kit (Qiagen)

RNeasy MinElute Cleanup Kit (Qiagen)

SuperScript III Reverase Transcriptase Kit (Thermo Fisher Scientific)

Standard Sensitivity RNA Analysis Kit (15nt), 500 samples (Agilent)

2.8 Consumables and equipment

Consumables such as reaction tubes, cell culture dishes and other plastic products were used from Applied Biosystems, B. Braun, Eppendorf, Greiner, Kimberly-Clark, Millipore, PerkinElmer, Nunc, Sarsted, Schleicher, Schuell and VWR international.

2.8.1 Equipment

Table 2.9: Equipment used in this study

Automated capillary electrophoresis	Fragment Analyzer™ (Agilent) Experion™ (Bio-Rad)
Chemiluminescence imaging	LAS-4000 mini (Fujifilm)
Cell culture incubator	BBD 6220 (Heraeus)
Cell Counter	Casy® cell counter (Innovatis) Countess™ (Thermo Fisher Scientific)
Centrifuges	Centrifuge 5417 R (Eppendorf) Centrifuge 5424 (Eppendorf) Heraeus Multifuge 1S-R (Thermo Fisher Scientific) Heraeus Megafuge 40R (Thermo Fisher Scientific)
Deep Sequencer	NextSeq 500 (Illumina)
Flow cytometer	BD FACS Canto™ II (BD Biosciences)
Fluorescence readers	Infinite 200 PRO Microplate Reader (Tecan)
Heating block	Dry Bath System (Starlab)
High-Content Imaging	Operetta® High-Content Imaging System (PerkinElmer)

	Operetta® CLS High-Content Analysis System (PerkinElmer)
Immunoblot transfer chamber	PerfectBlue Tank Electro Blotter Web S (Peqlab)
Incubator shaker	Model G25 (New Brunswick Scientific)
Microscopes	Axiovert 40 CFL (Zeiss)
PCR thermal cycler	Mastercycler pro S (Eppendorf)
Photometer	Ultrospec™ 3100 pro UV/Visible (Amersham Biosciences) NanoDrop 1000 (Thermo Fisher Scientific)
Power Supply	Power Pac (Bio-Rad)
PVDF transfer membrane	Immobilon-P transfer membrane (Millipore)
Quantitative RT-PCR machine	StepOne™ Realtime Cycler (Applied Biosystems)
SDS-PAGE system	Mini-PROTEAN Tetra Cell (Bio-Rad)
Sterile bench	HeraSafe (Heraeus)
Thermoshaker	Thermomixer® comfort (Eppendorf)
Ultrasonifier	Digital Sonifier® W-250 D (Branson) M220 Focused Ultrasonicatior (Covaris)
UV fluorescent table	Maxi UV fluorescent table (Peqlab)
Vortex Mixer	Vortex-Genie 2 (Scientific Industries)
Whatman filter paper	Gel Blotting Paper (Schleicher and Schuell)

2.9 Software

ApE v2.0.50b3

Adobe Acrobat Reader DC v2020

Affinity Photo

Affinity Designer

BD FACSDiva Software v6.1.2

BEDtools v2.26.0

Bowtie v1.2

Bowtie v2.3.2

CASAVA v1.7

DeepTools v2.3.5

EdgeR

FASTQC v0.11.3

Genomic Alignments

GraphPad Prism 8

GSEA v2.2.0

Harmony High Content Imaging Analysis Software (PerkinElmer)

Integrated Genome Browser v9.1.4

Illumina's FASTQ Generation software v.1.0.0

ImageJ v.1.50j

MacOS Catalina

MACS v1.4.1

MEME Suite v4.10.1

Microsoft Office 365

MultiGauge software v3.0

NGSplot v2.61

R v3.3.3

RStudio v1.3.1056

SAMtools v1.3

skewR

StepOne Software v2.3

TopHat v2.1.0

UMI tools (Smith et al., 2017)

ZEN2 (Zeiss), blue edition

2.10 Online tools and databases

DAVID

Galaxy

GEO

MSigDB v5.2

Primer3

Pubmed

UCSC

3 Methods

All the methods listed below are well established in the laboratory of Professor Eilers and were described in former theses and publications.

3.1 Cell biology methods

3.1.1 Cultivation of cells

All cell lines were cultivated in standard medium with 10% FBS and 1% penicillin/streptomycin in a cell incubator at 37 °C, 5% CO_2 and 95% relative humidity. Cells in culture were routinely tested for mycoplasma contaminations.

3.1.1.1 Passaging of cells

Adherent cells were passaged every third day for maintenance. Therefore, medium was removed, cells were washed with PBS and detached with trypsin/EDTA from the cell culture plate. Trypsin/EDTA was inhibited by the addition of full serum-containing medium and cells were resuspended. A portion of the cell suspension was plated onto a new cell culture dish with fresh medium, while the rest was discarded. For seeding a defined number of cells, the cell number was determined using either a Casy® cell counter or the Countess™ Automated Cell Counter according to manufacturer's recommendation.

3.1.1.2 Freezing of cells

For the storage of cells in liquid nitrogen, the medium of a 70% confluent cell culture dish was removed, cells were washed, trypsinised and harvested as described above. The cell suspension was transferred to a 15 ml tube and centrifuged at 1,000 rpm for 5 min. After discarding the supernatant, cells were resuspended in freezing medium and transferred to cryo vials. After freezing the vials in a MrFROSTY freezing container at -80 °C over night, to ensure a slow freezing process (1 °C per min), cells were transferred to the liquid nitrogen storage tanks.

3.1.1.3 Thawing of cells

Frozen cells were thawed quickly in the 37 °C water bath and resuspended in full medium. The solution was transferred to a 15 ml tube and centrifuged for 5 min at 1,000 rpm. After removal of the supernatant, the cells were resuspended in fresh medium and plated onto a new cell culture dish.

3.1.2 Synchronisation with Double Thymidine Block

For the analysis of a certain cell cycle phase, cells were synchronised using a double-thymidine block. Thymidine, as a pyrimidine deoxynucleoside, blocks DNA synthesis at the border of G1/S-phase (Chen and Deng, 2018). Therefore, cells were plated in full medium, and, after attachment, blocked with 2 mM thymidine for 16 h. For the release, medium was removed, cells were washed with PBS and full medium was added for 8 h, followed by another block for 16 h with 2 mM thymidine. After the second block, cells were released after washing with PBS, and addition of full medium. After 4 h (S-phase), 8 h (G2/M-phase) and 12 h (G1-phase) cells were harvested for following experiments.

3.1.3 Flow cytometry analysis (FACS)

All subsequent FACS experiment were performed on the BD FACS Canto^{TM} II Flow Cytometer and analysed with the BD FACSDiva software.

3.1.3.1 AnnexinV / Propidiumiodide (PI)-FACS

For the analysis of apoptotic cells, two different markers were used: AnnexinV recognises phosphatidylserine as an apoptotic marker when it is on the outer plasma membrane and Propidiumiodide (PI) as an intercalator into DNA that cannot dye living and pro-apoptotic cells with an intact cell membrane. AnnexinV negative and PI negative cells are healthy, whereas AnnexinV positive but PI negative populations are pro-apoptotic and both markers positive suggests necrotic cell populations.

For the analysis, cell culture supernatant with floating cells of the respective cell culture dish was pooled together with the trypsinised cells. After centrifugation for 5 min at 1,500 rpm, cells were washed with cold PBS and centrifuged again. The cell pellets were resuspended in 100 µl AnnexinV binding buffer and 2 µl AnnexinV/Pacific-Blue Dye and incubated for 15 min in the dark at room temperature. Afterwards, 400 µl binding buffer was added together with 54 µM propidiumiodide and solutions were stored on ice in the dark until further analysis.

3.1.3.2 PI FACS

Propidium iodide as an intercalator dye can be used to determine the DNA content and therefore the cell cycle distribution of the cell population. The DNA content as a basis for the analysis gives rise whether a cell is in G1/G0-phase (DNA content 2N), S-phase (DNA content >2N, <4N) or G2/M-phase (4N).

Cells were trypsinised, resuspended in full medium and centrifuged at 1,500 rpm for 5 min. After a washing step with ice cold PBS, cells were fixed in 80% EtOH overnight at -20 °C. On the following day, cells were centrifuged for 10 min at 1,500 rpm, washed with ice cold PBS and centrifuged again. The cell pellet was resuspended in 400 µl PBS, 54 µM propidium iodide and 2 µg/ml RNaseA and incubated for 30 min at 37 °C in the dark. Tubes were stored on ice in the dark until further analysis.

3.1.3.3 BrdU/PI FACS

Bromodeoxyuridin (BrdU) is a thymidine analogue, that is incorporated into DNA during S-phase. Together with a PI co-staining, cells that are actively replicating can be identified more precisely. Cells were labelled for 1 h with 10 µM BrdU (Sigma-Aldrich), harvested and fixed according to the PI protocol listed in 3.1.3.2. After the washing step, cells were resuspended in 1 ml 2 M HCl / 0.5% Triton X-100 and incubated for 30 min at room temperature for permeabilisation. After pelleting through centrifugation, cells were resuspended in 1 ml 0.1 M $Na_2B_4O_7$ (pH 8.5) for neutralisation. Afterwards samples were centrifuged and resuspended in 100 µl 1% BSA in PBS-T (0.5% Tween-20 in PBS) and 5 µl anti-BrdU-FITC antibody. The mixture was incubated for 30 min at room temperature in the dark. Subsequently, cells were centrifuged, washed with 200 µl 1% BSA in PBS-T, and pellets were resuspended in 400 µl 38 mM sodium citrate with 24 µg/ml RNaseA and 54 µM PI. After the incubation at 37 °C in the dark for 30 min, cells were stored on ice and dark until measurement.

3.1.4 Production of lentivirus

The day before transfection, 4-5x10^6 HEK293TN cells were seeded that they reach a confluency of about 60-70 % the day of transfection. On the following day, prior to transfection, cells were starved in 6 ml medium containing just 2% FCS prior to transfection. For lentivirus production, 2.6 µg packaging plasmid psPAX2, 1.4 µg virion envelope plasmid pMD2G, and 11.1 µg lentiviral expression plasmid were mixed in 700 µl Opti-MEM™. In a second tube, 700 µl Opti-MEM™ medium was mixed with 30 µl PEI (stock 1 µg/ml) solution. After 5 min incubation at room temperature, the two reactions were mixed and incubated for 15 more minutes at room temperature, before adding it dropwise to the cells. 6 h post-transfection, medium was removed and 6 ml fresh full medium was added to the cells. The virus containing supernatant was harvested 48 h and 72 h post-transfection, pooled and filtered through a 0.45 µm filter. Virus was either used directly or aliquoted in cryo vials and stored at -80 °C.

3.1.5 Lentiviral infection of cells

For the infection of cells cultivated onto a 10 cm cell culture dish, 4 ml full medium together with 1 ml filtered lentiviral supernatant and 5 µl polybrene infection/transfection reagent (4 µg/ml, Sigma-Aldrich) was added. 24 h after infection, medium was changed. From the following day on, cells were selected with 0.5 to 2 µg/ml puromycin depending on the cell line. Non-infected cells were used as control and selected in parallel.

3.1.6 Colony formation assay (crystal violet staining)

Whether a treatment has certain effects on cell proliferation, colonies can be visualised by crystal violet dye. Cells were therefore plated with the same cell number in 6-well plates and treated as indicated. Afterwards, they were fixed by the addition of 1% formaldehyde to the medium and incubated for 20 min at room temperature. After removal of the supernatant, cells were dried and afterwards dyed with the crystal violet solution for 2 h. Abundant dye was washed off with ddH_2O and plates were air dried overnight at room temperature.

3.1.7 Proximity Ligation Assay (PLA)

To determine a close proximity of two proteins, Proximity Ligation Assays (PLA) were performed. PLAs were routinely performed in a 384 well plate, seeding between 200 and 2,000 SH-EP MYCN-ER cells depending on treatment and duration. Cells were treated as indicated and fixed with 4% paraformaldehyde for 10 min. After washing with PBS, fixed cells were permeabilised either with 0.1 % Triton X-100 for 10 min at room temperature or methanol for 20 minutes at -20 °C, depending on the used antibodies. 5% BSA in PBS was used as blocking reagent for 1 h after another washing step. The primary antibodies against two different proteins raised in two different species were diluted accordingly in 5% BSA in PBS and incubated overnight at 4 °C. Single primary antibodies in the same concentrations were used as controls. Cells were treated for 1 h at 37 °C with the plus and minus probes recognising rabbit and mouse antibodies, and ligated afterwards for 30 min at 37 °C. The *in situ* PCR amplification was performed with the Alexa568-conjugated oligonucleotides for 2 h at 37 °C in the dark. Counterstaining with 2.5 µg/ml Hoechst33342 was included into the last washing step. Operetta CLS High-Content Imaging System with 40x magnification and Harmony High Content Imaging and Analysis Software was used for image acquisiton, which was performed in the High Content Microscopy Core Unit by Christina Schülein-Völk and Ursula Eilers.

3.1.8 Immunofluorescence

To visualise protein abundance within a cell, immunofluorescence (IF) can be used. IF was performed in 96-well plate that can be used in the Operetta® CLS High-Content Analysis System run by the High Content Microscopy Core Unit named above. Prior to fixation of the cells with 4% paraformaldehyde, cells were treated as indicated. Permeabilisation was performed with 0.2% Triton X-100 for 10 min at room temperature, followed by washing with PBS and blocking in 5% BSA in PBS for 1 h at room temperature. Primary antibodies were diluted accordingly in 5% BSA in PBS and cells were incubated at 4 °C overnight. Secondary fluorescently labelled antibodies Alexa488 or Alexa568 were also diluted in 5% BSA in PBS and cells were incubated for 1 h at room temperature in the dark. After washing, cells were counterstained with 2.5 µg/ml Hoechst33342 for 10 min at room temperature and incubated cold and dark until further analysis.

3.1.9 Cell Cycle Proximity Ligation Assay and Immunofluorescence

With the aim of stratifying the results from PLAs and IF to specific cell cycle stages, cells were pulsed with 10 µM 5-ethynyl-2-deoxyuridin (EdU), also a thymidine analogue that is incorporated into DNA in S-phase, for 30 minutes prior to fixation. DNA, which was newly synthesised, was visualised by performing a copper(I)catalysed azide-alkyne cycloaddition, a click-chemistry reaction allowing the binding of a fluorescent dye to incorporated EdU. Therefore, cells were incubated with 100 mM Tris pH 8.5, 4 mM $CuSO_4$, 10 mM AFDye 647 Azide, 10 mM L-Ascorbic Acid for 30 min at room temperature in the dark just before incubation with the primary antibodies. Afterwards, staining for PLA or IF was performed as described in 3.1.7 and 3.1.8. Images were taken with the Operetta® High-Content Imaging or CLS High-Content Imaging System at 40x magnification and analysed using the Harmony High Content Imaging and Analysis Software and R. Cells were grouped according to Hoechst and EdU staining in the control condition.

3.1.10 Fiber Assays

To determine the impact of a certain treatment on replication, precisely on the replication fork progression, DNA fiber assays were used. These experiments were carried out in collaboration with Sabrina Rodewald and Celeste Giansanti in the laboratory of Professor Matthias Dobbelstein in Göttingen according to the protocol described previously (Klusmann et al., 2016). Cells were treated as indicated and afterwards first labelled for 20 min with 5-chloro-2-deoxyuridine (CldU, 25 µM) followed by one hour incubation with 5-iodo-2-deoxyuridine

(IdU, 25 µM). Fibers were spread on glass slides and acid treated. The labelled tracks were afterwards incubated at 20 °C for one hour with rat anti-BrdU antibody (detects BrdU and CldU) and mouse anti-BrdU antibody (detects BrdU and IdU). Slides were fixed with 4% paraformaldehyde and incubated for 2 h at 20 °C with Alexa Fluor 555-conjugated goat anti-rat antibody and Alexa Fluor 488-conjugated goat anti-mouse antibody. Fiber images were acquired by fluorescence microscopy using the Axio Scope A1 running with the microscope software ZEN (Zeiss) for image acquisition and processing. ImageJ was used for analysis of the fibers.

3.2 Molecular biology methods

3.2.1 RNA isolation

To isolate total RNA from cultured cells, medium was removed and 1 ml TriFast™ lysis reagent (Peqlab) was added directly to the cell culture dish. The suspension was homogenised and transferred into a fresh 1.5 ml reaction tubes. After adding 200 µl chloroform, samples were vortexed thoroughly and incubated at room temperature for 5 min. The samples were centrifuged for 5 min at 14,000 rpm and the upper phase containing the RNA was transferred to a new tube containing 1 volume isopropanol for precipitation. After incubation at -20 °C for 15 min, tubes were centrifuged for 10 min at 14,000 rpm and 4 °C, followed by a wash with 70% EtOH and another centrifugation. The RNA pellet was air-dried and resuspended in 30 µl of ddH_2O. The concentration of RNA was determined by NanoDrop (3.2.9.1) for subsequent experiments and afterwards stored at -80 °C.

3.2.2 cDNA synthesis

Total RNA was reverse transcribed into complementary DNA (cDNA). Up to 1 µg of RNA was diluted in 10 µl ddH_2O and incubated for 1 min at 65 °C. The reaction was cooled down on ice and the following mixture was added:

10 µl 5x RT buffer (Promega)

1 µl M-MLV Reverse transcriptase (200 U/ml, Promega)

0.2 µl Ribolock (Fermentas)

1.25 µl dNTPs (10mM, Roth)

2 µl Random primer (2 mg/ml, Roche)

25.55 µl ddH_2O

Reverse transcription was performed in a thermocycler for 10 min at 25 °C, 50 min at 37 °C and 15 min at 70 °C before getting stored at 4 °C until further analysis by qPCR.

3.2.3 Polymerase chain reaction

3.2.3.1 Quantitative polymerase chain reaction (qPCR)

Quantitative polymerase chain reaction (qPCR) was used for quantification of mRNA expression levels after cDNA synthesis (3.2.2) or recovered DNA from Chromatin-Immunoprecipitation (3.3.8.) to measure chromatin enrichment of a certain protein pull down. The DNA can be quantified in real time since a fluorescence dye intercalates into the freshly synthesised double stranded DNA, which can be monitored in every cycle after the end of the elongation step. The reaction was set up as follows:

10 µl cDNA (diluted 1:5 beforehand) / Chromatin from ChIP

5 µl SYBR Green Mix (Thermo Fisher Scientific)

4 µl ddH_2O

1 µl primer forward + reverse (stock 10 µM)

The measurement was carried out on the StepOne™ Realtime Cycler with the following thermal cycling profile:

Table 3.1: qPCR program

Temperature	Time	Cycles
50 °C	2 min	1x
95 °C	2 min	1x
95 °C	3 sec	40x
60 °C	30 sec	

For the calculation of relative expression or DNA enrichment the ΔΔ-CT method (Livak and Schmittgen, 2001) was used. Relative expression of mRNA was normalised to the housekeeping gene β2-Microglobulin (B2M), and ChIP samples were normalised to the input sample, respectively.

3.2.3.2 PCR to amplify cDNA for cloning

To generate vectors expressing shRNAs, the sequences of interest including restriction sites were amplified. The protocol for the mirE-design based method was adapted from Fellmann et al., 2013.

The PCR mixture was set up and ran with the cycling profile as follows:

10 ng Oligo template

10 µl 5x Phusion High-Fidelity Buffer (Thermo Fisher Scientific)

2.5 µl DMSO (5% of reaction volume)

1 µl dNTPs (10mM, Roth)

2.5 ul mirE XhoI forward primer (stock 10 µM)

2.5 µl mirE EcoRI forward primer (stock 10 µM)

0.5 µl Phusion Hot Start II High-Fidelity DNA Polymerase (Thermo Fisher Scientific)

ad 50 µl ddH_2O

Table 3.2: PCR program run for cloning

Cycle step	Temperature	Time	Cycles
Initial template denaturation	98 °C	2 min	1x
Denaturation	98 °C	25 sec	20x
Annealing	62 °C	25 sec	
Extension	72 °C	20 sec	
Final extension	72 °C	5 min	1x

The PCR product was cleaned up using the QIAquick Gel Extraction Kit (Qiagen) according to manufactuer's protocol and eluted in 20 µl ddH_2O.

3.2.4 Preparation of DNA with restriction digest

Restriction endonucleases were used for sequence specific hydrolysis of DNA. The PCR product and the empty vector were incubated with the restriction enzymes XhoI and EcoRI. The digestion was performed for 2 h at 37°C and set up as follows:

3 µg vector DNA / 20 µl PCR product

1 µl XhoI (New England Biolabs)

1 µl EcoRI (New England Biolabs)

5 µl CutSmart buffer (New England Biolabs)

ad 50 µl ddH_2O

3.2.5 Ligation of DNA encoding shRNA into plasmids

The ligation of DNA fragments and the vector DNA after digestion with specific endonucleases was performed with the T4 DNA Ligase (New England Biolabs).

Ligation mixture: 1 µl vector DNA
7 µl PCR product
1 µl 10x ligation buffer
1 µl T4 DNA Ligase

The mixture was incubated for 1 h at room temperature before transformation into competent bacteria.

3.2.6 Transformation

XL-1 blue, chemically competent bacteria, were thawed on ice and mixed either with 1 µg of DNA or with the ligation mix. They were incubated for 30 min on ice, followed by a heat shock for two minutes at 42 °C and a cool down on ice. Samples were mixed with 1 ml LB medium without antibiotics and incubated for 30 min at 37 °C in a thermoshaker (200 rpm) before plating on LB-agar plates containing the appropriate antibiotics. The bacterial suspension was centrifuged shortly, resuspended in 50 µl LB medium and the complete reaction was plated. LB-agar plates were incubated at 37 °C overnight. The following day, single colonies were picked and incubated in 3 ml LB medium containing the appropriate antibiotics in a shaking incubator with the set temperature fitting to the used vector.

3.2.7 Bacterial plasmid DNA preparation for analysis (Miniprep)

Alkaline lysis was performed for analytical preparation of plasmid DNA. 1.5 ml overnight culture were centrifuged and the bacteria were resuspended in 200 µl Mini Buffer I containing 100 µg/ml RNaseA. Lysis was performed in Mini Buffer II and incubated for 3 min at room temperature. Lysis was stopped by precipitation after addition of Mini Buffer III. The samples were centrifuged for 5 min at 14,000 rpm at room temperature. The supernatant was mixed with 500 µl isopropanol in a fresh 1.5 ml reaction tube, and incubated for 15 min at -20 °C. The plasmid DNA was pelleted by centrifugation at 14,000 rpm at 4 °C, washed with 70% EtOH, air-dried and resuspended in 20 µl ddH_2O. Further analysis by restriction digest was performed.

3.2.8 Isolation of plasmid DNA (Maxiprep)

200 ml overnight culture, consisting of LB medium with appropriate antibiotics and the rest of the overnight pre-culture that was not used for analytics, was processed with the PureLink® HiPure Plasmid Maxiprep Kit according to manufacturer's protocol. The purified plasmid DNA was resuspended in TE buffer, measured at the NanoDrop and adjusted to a concentration of 1 mg/ml (3.2.9.1).

3.2.9 Nucleic acid quantification

3.2.9.1 Absorbance based analysis (NanoDrop)

RNA and DNA concentration were routinely determined by the NanoDrop 1000 (Peqlab). Absorbance was measured at 260 nm and for the purity of the nucleic acid solution, the ratio of absorbance at 260 and 280 nm was determined. A ratio of ~ 2.1 for pure RNA and ~ 1.8 for pure DNA determines a successful isolation.

3.2.9.2 Fluorescence based analysis

3.2.9.2.1 RiboGreen

The concentration of biotinylated RNA for 4sU-sequencing (3.4.3) was determined using the Quant-iT™ RiboGreen® RNA Assay Kit (Thermo Fisher Scientific) according to manufacturer's protocol. The RiboGreen reagent binds to RNA and the fluorescence can be measured by Excitation at 480 nm and Emission at 520 nm. With the help of the provided rRNA standard, the RNA concentration in the sample can be determined according to a standard curve.

3.2.9.2.2 PicoGreen

The concentration of double-stranded DNA (dsDNA) was determined prior to ChIP-sequencing library preparation by using the Quant-iT™ PicoGreen® dsDNA Assay Kit (Thermo Fisher Scientific) according to manufacturer's protocol. PicoGreen intercalates into dsDNA, this leads to fluorescently labelled DNA which can be measured at a wavelength of 485/535 nm. With the help of the provided DNA standard, the DNA concentration can be determined according to a standard curve.

3.2.9.3 Automated gel based analysis (Bioanalyzer)

The quality of RNA used for sequencing as well as the post-PCR DNA libraries resulting from all sequencing methods described in section 3.4 were routinely measured either on the

Experion™ Automated Electrophoresis System (Biorad) or the Fragment Analyzer (Agilent) according to manufacturer's protocols provided with the kits.

3.2.10 Agarose gel electrophoresis

DNA fragment size was determined with agarose gel electrophoresis. Depending on the expected DNA size, a solution of 1-2% agarose in 1x TAE buffer was prepared. The solution was boiled, shortly cooled down and 0.3 µg/ml ethidium bromide (Sigma-Aldrich) was added. Afterwards the solution was poured to gel chambers with combs for polymerisation. The samples were mixed with DNA loading buffer (6x stock) and loaded onto the polymerised gel. 10 µl of 1 kb DNA ladder (New England Biolabs) were used as a reference next to the samples. The gel was run at a voltage of 150 V for 45 min and DNA bands were visualised using the UV transilluminator.

3.3 Biochemical methods

3.3.1 Preparation of whole cell protein extracts

For whole cell protein extracts, cells were washed once with ice cold PBS and scraped directly in RIPA lysis buffer that contained protease and phosphatase inhibitor cocktails. The suspension was transferred into a 1.5 ml reaction tube and cells were lysed on ice for 20 min. Afterwards, the tubes were centrifuged for 20 min at 14,000 rpm and 4 °C. The supernatant was transferred into a fresh 1.5 ml reaction tube. After protein concentration was determined by Bradford assay (3.3.3), lysates were stored at -80 °C.

3.3.2 Fractionation of cell extracts

To investigate distribution of proteins within different cell compartments, cell extracts were fractionated into cytoplasmic and nuclear / chromatin bound fractions. Therefore, cells were washed once with ice cold PBS, scraped in PBS and pelleted via centrifugation. The pellet was resuspended in ChIP lysis buffer I containing protease and phosphatase inhibitor cocktails. The suspension was incubated for 10 min on ice, before nuclei were pelleted via centrifugation for 10 min at 1,500 rpm and 4° C. The supernatant containing the cytoplasmic fraction was transferred into a fresh 1.5 ml reaction tube and the nuclei pellet was resuspended in HEPES benzonase compatible buffer. The suspension, containing the nuclear / chromatin bound fraction, was sonicated 4x for 10 sec with 45 sec pause in between and an amplitude of 20% with the ultrasonifier before 50 U/ml benzonase were added and incubated for 1 h at 4 °C on a

rotating wheel. All lysates, chromatin and pooled nuclear / chromatin bound fractions were centrifuged at 14,000 rpm for 20 min at 4 °C and the protein content in the supernatants, which were transferred to a fresh 1.5 ml reaction tube, was determined by Bradford assay (3.3.3)

3.3.3 Total protein quantification with Bradford assay

The protein concentration in lysates was determined according to the Bradford method (Bradford, 1976). 1 ml Bradford reagent was mixed together with 2 µl of lysate in cuvettes. The solution was mixed by vortexing and measured at 595 nm against a cuvette just containing Bradford reagent. The concentration was calculated according to the absorbance of a previously calculated standard curve.

3.3.4 Electrophoresis

Bis-Tris gels were used for gel electrophoresis to separate proteins in cell lysates according to their molecular weight. The gels can be used in different percentages depending on the molecular weight of the proteins of interest. After adding 1x Laemmli buffer to the samples, they were boiled for 8 min at 95 °C. Equal amounts were then loaded next to the HiMark pre-stained HMW STD (Thermo Fisher Scientific) or PageRuler^{TM} Prestained Protein Ladder (Thermo Fisher Scientific) as reference to asses protein size. Gels were run in 1x MOPS running buffer in a SDS-PAGE chamber (Bio-Rad) at a voltage between 80-120 V until the migration front was run out of gel.

3.3.5 Immunoblot

After separation of proteins with a Bis-Tris gel, they were transferred onto a PVDF membrane. Therefore, a PVDF membrane was activated by incubation in methanol (1 min), followed by water (2 min) and transfer buffer. The gel was layered above the PVDF membrane between Whatman papers and fixed in a tank blot transfer chamber that was filled with 1x transfer buffer. The transfer was performed in the cold room at 4 °C with an amperage of 330 mA for 2-3 h depending on the size of the separated proteins. Afterwards, the membrane was blocked in 5% BSA in TBS-T for 1 h to decrease unspecific antibody binding before getting cut and incubated overnight at 4 °C with the primary antibody diluted in blocking solution. The following day, membranes were washed three times with TBS-T and incubated for 1 h at room temperature with secondary antibody, followed by three times washing with TBS-T. Chemiluminescence generated by horseradish peroxidase reaction coupled to the secondary antibody was performed

with the Immobilon Western Substrate Kit (Millipore) according to manufacturer's protocol to visualise the antibodies on the LAS-4000 imager (Fujifilm).

3.3.6 Stripping of PVDF membranes

To remove antibodies from PVDF membranes, the membranes were incubated for 30 min at 50 °C in stripping buffer, followed by several washing steps with TBS-T and incubated in blocking solution for 1 h again. The antibody incubation and visualisation were performed as described in 3.3.5.

3.3.7 Immunoprecipitation of proteins

The identification of protein-protein interactions can be performed with immunoprecipitation. Therefore, cell culture dishes were harvested and pooled for the same treatment and cells were either fractionated as described in 3.3.2 or directly lysed in TNN buffer for 30 min on ice. Afterwards, samples were sonicated for 20 sec at an amplitude of 20 % and cleared by centrifugation.

After determination of protein concentration with the Bradford assay (3.3.3), 0.5-2 mg protein were mixed with 1-2 µg of antibody and incubated at 4 °C for six hours on a rotator. In the meantime, 10 µl of Dynabeads A were mixed with 10 µl of Dynabeads G per immunoprecipitation and washed three times with 5 mg/ml BSA in PBS, before equal amounts of beads were added to the protein-antibody mixture and incubated overnight at 4 °C on a rotator. The following day, beads were washed three times with the HEPES or TNN buffer and once with TNN high salt buffer (80 mM NaCl added to TNN buffer). Afterwards, beads were resuspended in 1x Laemmli buffer, boiled and immunoblot analysis was performed (3.3.5).

3.3.8 Chromatin-immunoprecipitation (ChIP)

To detect protein-DNA interactions, Chromatin-Immunoprecipitation (ChIP) was used. Therefore, proteins were crosslinked on DNA, chromatin was isolated and fragmented and the protein of interest together with the binding DNA was precipitated using specific antibodies. The enrichment of DNA was then detected using quantitative real-time PCR for primers that bind to a certain DNA sequence.

3.3.8.1 Protein-DNA crosslinking with formaldehyde fixation and chromatin isolation

For ChIP, cells were grown on 15 cm cell culture dishes and per IP about $1.2x10^7$ cells were used. Cells were treated as indicated and then fixed with 1% formaldehyde for 10 min at room temperature slowly shaking. Fixation was stopped by the addition of 1 M glycine for 5 min at room temperature.

The cells were washed twice with ice cold PBS and then scaped on ice in PBS containing protease and phosphatase inhibitor cocktails and 1 mM PMSF. The suspension was centrifuged and the pellet was either frozen in liquid nitrogen and stored at -80°C or used for further experimental procedure. The pellet was resuspended in 3 ml ChIP lysis buffer 1 containing protease and phosphatase inhibitor cocktails to disrupt the cell membrane. After 20 min incubation on ice, nuclei were pelleted by centrifugation for 5 min at 1,500 rpm and 4 °C. The supernatant was discarded and the nuclei were resuspended in 2 ml ChIP RIPA lysis buffer II containing protease and phosphatase inhibitor cocktails. The suspension was then proceeded to sonication to obtain DNA fragments of a size between 200 and 300 bp. The sonication condition depended on the cells used for ChIP. For SH-EP MYCN-ER cells, sonication was performed for 20 min with an amplitude of 20 %, a pulse of 10 sec and a pause of 30 sec.

3.3.8.2 Size control of fragmented DNA

The size of the fragmented DNA was then determined with agarose gel electrophoresis. Therefore, 25 µl of chromatin were diluted in 475 µl TE buffer together with 160 mM NaCl and 20 µg/ml RNaseA. The samples were decrosslinked by incubation for 1 h at 37 °C followed by 65 °C overnight in a thermoshaker (800 rpm). The next day, 200 µg/ml Proteinase K was added for protein digestion at 45 °C for 2 h. DNA was isolated using a phenol/chloroform extraction. DNA was precipitated in 100 % EtOH with 3 M sodiumacetate at -20 °C for 30 min and washed twice with 75 % EtOH. After the DNA was air-dried at room temperature, it was resuspended in 20 µl ddH_2O and after the addition of 6x DNA-loading buffer loaded on a 2% agarose gel for electrophoresis. DNA size between 200 and 300 bp was aimed. Afterwards, chromatin was centrifuged for 20 min 14,000 rpm and 4 °C and the supernatant with the soluble chromatin was transferred to a fresh 1.5 ml reaction tubes.

3.3.8.3 Coupling of antibodies to Dynabeads A and G

To immunoprecipitate the protein of interest bound to DNA, Dynabeads A and G were coupled to the antibody raised against the protein of interest or IgG as a control. Per IP, 30 µl of

Dynabeads (A and G equally mixed) were washed three times with blocking solution, resuspended in 1 ml of blocking solution and 3 µg of antibody. The beads-antibody suspension was incubated on a rotator overnight at 4 °C before getting washed three times with blocking solution and resuspended in 30 µl of blocking solution per IP.

3.3.8.4 Immunoprecipitation

As a reference, 1% of the soluble chromatin was stored at 4 °C while 30 µl of Dynabeads-antibody solution were added to the rest of the chromatin solution and incubated at 4 °C for 6 h on a rotator.

Afterwards, beads were washed three times with ChIP washing buffer I, followed by three times high salt ChIP washing buffer II and three times LiCl ChIP washing buffer III and one time with TE. After each step, Dynabeads were separated with a magnetic rack, the buffer was removed and fresh buffer, which was stored at 4°C, was added.

3.3.8.5 Elution

The precipitated DNA was eluted from the beads twice with 250 µl elution buffer by incubating the mixture for 15 min each at room temperature on a rotating wheel. The beads were then sedimented with a magnetic rack, and the eluted DNA was pooled from both elution steps into a fresh 1.5 ml reaction tube. The input samples were also filled up with equal amounts of elution buffer. To decrosslink protein and DNA, 160 mM NaCl together with 20 µg/ml RNaseA were added to the solution and incubated first for 1 h at 37 °C and then overnight at 65 °C in a thermo shaker (800 rpm). The following day, 200 µg/ml Proteinase K was added and samples were incubated for 2 h at 45 °C in a thermo shaker before the DNA was purified with a phenol/chloroform extraction. DNA was precipitated in 100 % EtOH with 3 M sodiumacetate for 30 min at -20 °C. After centrifugation, the pellet was washed twice with 75 % EtOH before it was air-dried and resuspended in 300 µl ddH_2O. For quantitative real-time PCR, 10 µl of chromatin was used for reaction.

3.3.9 DNA-RNA-immunoprecipitation (DRIP)

To detect DNA-RNA hybrids, so called R-loops, DNA-RNA-immunoprecipitation was used. The method was performed as described previously (Ginno et al., 2012) and similar to ChIP (3.3.8). Briefly, cells grown on several 15 cm dishes were washed twice and then scraped in PBS. After centrifugation for 5 min at 1,500 rpm, cells were digested in TE buffer with 0.5%

SDS and Proteinase K overnight. DNA was purified with phenol/chloroform extraction and precipitated in 100 % EtOH with 3 M sodiumacetate for 30 min at -20 °C. After centrifugation, the pellet was washed twice with 75 % EtOH before it was air-dried and resuspended in 500 µl ddH_2O. DNA was fragmented by restriction enzymatic digestion (BsrGI, EcoRI, HindIII, SSpI, XhoI, 60 U each) overnight at 37 °C upon rotating. For the negative control, 60 U RNaseH1 were additionally added to the appropriate sample. After phenol/chloroform purification as described above and resuspension of the pellet in 500 µl ddH_2O, chromatin size was determined on a 2% agarose gel.

To immunoprecipitate R-loops, Dynabeads A and G were coupled to the S9.6 antibody (Boguslawski et al., 1986) or IgG as a control. Per IP, 30 µl of Dynabeads (A and G equally mixed) were washed three times with blocking solution and then resuspended in 1 ml of blocking solution and 4 µg of antibody. The beads-antibody suspension was incubated on a rotator overnight at 4 °C before getting washed three times with blocking solution and resuspended in 30 µl of blocking solution per IP.

As a reference for the precipitation, 1% of purified genomic DNA was stored at 4°C, while the rest of the solution was incubated with 30 µl of Dynabeads-antibody solution and incubated rotating at 4°C overnight. Afterwards, beads were washed three times with ChIP washing buffer I, followed by three times high salt ChIP washing buffer II and three times LiCl ChIP washing buffer III and one time with TE. After each step, Dynabeads were separated with a magnetic rack, the buffer was removed and fresh buffer, which was stored at 4°C, was added. The precipitated R-loops were eluted in 150 µl DRIP elution buffer for 15 min at room temperature for each of the two elution runs. 200 µg/ml Proteinase K was added for 2 h at 45 °C followed by another phenol/chloroform extraction and ethanol precipitation with 3 M sodiumacetate for 30 min at -20 °C. After centrifugation, the pellet was washed twice with 75 % EtOH before it was air-dried and resuspended in 300 µl ddH_2O. For quantitative real-time PCR, 10 µl of chromatin was used for reaction.

3.4 Next-generation sequencing

All sequencing methods were performed on an Illumina NextSeq 500 sequencing machine by Carsten Ade according to manufacturer's protocol.

3.4.1 ChIP-sequencing

Samples for ChIP-sequencing were prepared as described in 3.3.8. For deep-sequencing, cell number, amount of antibody and beads was approximately three times increased. Fragmentation of cells was adjusted accordingly. Cell number was determined on a separated cell culture dish using Casy® cell counter. According to the amount of cells, 10% mouse cells were used for spike-in and added prior to the lysis in ChIP lysis buffer I. Precipitated DNA was eluted in 50 µl ddH_2O and quantified using the Quant-IT^{TM} PicoGreen® dsDNA Assay Kit (Thermo Fisher Scientific).

ChIP-sequencing libraries regarding the influence of BRCA1 knockdown were prepared with 1-2 ng of purified DNA and according to the NEBNext® ChIP-Seq Library Prep Master Mix Set for Illumina. Libraries were size selected on an agarose gel and purified by gel extraction (Qiagen). The amplification reached 15-18 cycles and the PCR product was cleaned up using the QIAquick PCR Purification Kit (Qiagen).

The library preparation for the ChIP-sequencing with the shRNA against DCP1A were performed with at least 1 ng of purified DNA according to the protocol for NEBNext® Ultra II DNA Library Prep Kit for Illumina. Libraries were size selected and purified using NEBNext® Sample Purification beads. The PCR amplification was done with 18 cycles and the PCR product was cleaned up by using NEBNext® Sample Purification beads.

The concentration and the quality of the final post-PCR library was determined using the Fragment Analyzer (Agilent).

3.4.2 mRNA-sequencing

Cells for total mRNA-sequencing were lysed and mRNA was extracted using the RNeasy Mini Kit (Qiagen) with an on column DNaseI digestion step according to the manufacturer's protocol. RNA quality indicator (RQN) was determined using the Fragment Analyzer. The RQN for RNA used for sequencing was at least 9. This parameter can range from 1 (degraded RNA) to 10 (intact RNA). After quality analysis, 1 µg of RNA was used for the pull down of mRNA using the NEBNext® Oligo $d(T)_{25}$ beads according to the NEBNext® Poly(A) mRNA magnetic isolation module and library preparation was carried out using the NEBNext® Ultra RNA Library Prep Kit for Illumina following the manufacturer's protocol. Libraries were size selected and purified with Agencourt AMPure® XP Beads and the PCR amplification was carried out with 12 cycles. The PCR product was purified using Agencourt AMPure® XP

Beads. The quality and the concentration of the resulted library was determined on a Bio-Rad Experion Automated Electrophoresis system.

3.4.3 4sU-sequencing

The 4sU-sequencing method was adapted from Fuchs et al., 2015.

For 4sU-sequencing, cells were pre-treated as indicated. Cell number for spike-in was counted on a separate cell culture dish by Countess™ Automated Cell Counter (Thermo Fisher Scientific). 20 min prior to harvest, cells were pulsed with 500 µM 4-thiouridine (4sU) and afterwards lysed in 2.1 ml QIAzol lysis solution. The 10% spike-in of mouse T-cells was done according to cell number. Total RNA was isolated using the Qiagen miRNeasy kit according to manufacturer's protocol together with an on-column DNaseI digestion. The quality of RNA was determined by Fragment Analyzer according to manufacturer's protocol. RNA used for 4sU-RNA enrichment had a RQN of at least 9. After quality analysis, 20-35 µg of RNA measured by NanoDrop were used for biotinylation. The RNA was diluted in biotin labelling buffer and incubated with biotin-HPDP-DMF stock solution for 2 h on a shaking mixer. After chloroform/isoamylalcohol (24:1) extraction using MAXtract columns (Qiagen), RNA was precipitated in isopropanol. For the pulldown, streptavidin-coupled Dynabeads (Invitrogen) were washed with Dynabeads wash buffer A and B and then resuspended with biotinylated RNA in washing buffer and incubated for 15 min at room temperature on a rotating wheel. Afterwards, beads were washed with washing buffer accordingly and the RNA was eluted with 100 mM freshly prepared DTT. The pulled down RNA was cleaned up with the RNeasy MinElute kit (Qiagen).

Quant-IT RiboGreen® RNA assay (Thermo Fisher Scientific) was used according to manufacturer's protocol to determine the amount of pulled down RNA. The library preparation was performed with 20 ng of 4sU-labelled RNA according to the NEBNext® Ultra II directional RNA protocol from Illumina. PCR amplification reached 12-14 cycles. Libraries were size selected and purified with Agencourt AMPure® XP Beads.

The concentration of post-PCR library was determined using the Fragment Analyzer according to the manufacturer's DNA protocol.

3.4.4 Breaks labelling in situ and sequencing (BLISS8)

To map DNA breaks genome-wide, breaks were labelled in situ and sequenced (BLISS-sequencing method). The experimental preparation of the library for sequencing was performed by Theresa Endres and the subsequent bioinformatic analysis was done by Daniel Solvie. The original protocol (Yan et al., 2017) was adapted, modified and published already in (Endres et al., 2021) in the following way: cells were treated as indicated in a 24-well plate in triplicates and fixed with 4% paraformaldehyde for 20 min, washed with PBS and stored at 4 °C in PBS. Cells were lysed in BLISS lysis buffer I for 1 h at 4 °C, washed with PBS and incubated in BLISS lysis buffer II for 1 h at 37 °C. After washing with PBS, the cells were incubated in CutSmart buffer (New England Biolabs) prior to restriction enzymatic digestion by AsiSI according to manufacturer's protocol. After another washing step with PBS, cells were again equilibrated in CutSmart buffer and blunting was performed using the Quick Blunting Kit (New England Biolabs) according to manufacturer's protocol. Adapters and oligos were custom synthesised and Unique Molecular Identifiers (UMIs) generated by random incorporation of the four standard dNTPs using the 'Machine mixing' option. Sense and antisense adapters were annealed by incubating them for 5 min at 95 °C in a thermo cycler, followed by ramping down to 25 °C over a period of 45 min. Annealed adapters were mixed with T4 DNA Ligase (New England Biolabs) in CutSmart and T4 Ligase buffer and cells were incubated with the mixture at 16 °C for 16 h. Excessive adapters were washed away with BLISS high-salt washing buffer. Genomic DNA was extracted in BLISS DNA extraction buffer, together with Proteinase K (1mg/ml) for 16 h at 55 °C in a thermo shaker. DNA was cleared with phenol/chloroform extraction and precipitated in isopropanol, resuspended in TE buffer and shared to a size of 300-500 bp with the Covaris Focused Ultrasonicator M220 for one to two minutes. DNA fragment size was determined by Fragment Analyzer and afterwards concentrated using Agencourt AMPure® CP Beads, transcribed into RNA together with a DNA digest using the MEGAscript™ T7 Transcription Kit according to manufacturer's protocol. RNA was cleaned-up in a two-sided way with a 0.4x followed by a 0.2x ratio using the Agencourt RNAClean® XP Beads. RNA concentration was determined on the Fragment Analyzer running the Standard Sensitivity RNA Analysis Kit. Library preparation was performed by ligation of RA3 adapter to the sample with a T4 RNA Ligase 2 mixed with recombinant Ribonuclease Inhibitor (Thermo Fisher Scientific). Samples were reverse transcribed with the Super Script III Reverse Transcriptase Kit and library indexing and amplification performed using the NEBNext High-Fidelity 2X PCR Master Mix with RP1 and desired RPI-primers. The amplification reached 17

cycles. The post PCR library was cleaned up with Agencourt AMPure® XP Beads and quality and quantity were determined on the Fragment Analyzer.

3.4.5 Sequencing Data Analysis

Bioinformatic analysis for deep-sequencing data and single-cell immunostaining were performed by Susanne Walz (ChIP-sequencing, mRNA-Sequencing), Florian Röhrig (ChIP-sequencing), Apoorva Baluapuri (ChIP-sequencing, 4sU-sequencing) and Daniel Solvie (BLISS8, EdU incorporation with quantitative immunofluorescence and PLA).

Base calling for generating FASTQ-Files for deep-sequencing data was performed with Illumina's FASTQ Generation software and sequencing quality was tested using the FastQC script. The FASTQ files were normalised either to reads or spike-in, and therefore first aligned to the mouse genome mm10 and subsequently to the human genome hg19. Bedgraph files for ChIP-sequencing were generated using the genomecov function from BEDtools. Further analyses were performed in R or RStudio.

For mRNA-sequencing, reads were mapped to hg19 using TopHat2 and Bowtie2 and normalised to the number of reads of the smallest sample. Reads per gene were counted using the 'summarizeOverlaps' function from R package 'GenomicAlignments' using the 'union' mode and Ensembl genes. Non- and weakly expressed genes were removed (mean count <1 over all samples). Differentialy expressed genes were called with edgeR and p-values were adjusted for multiple testing using the Benjamini-Hochberg procedure. Gene set enrichment analysis were done with the 'Hallmark', 'C2' and 'C5' databases from MSigDB, 1,000 permutations and default settings.

For 4sU-sequencing, the same procedure as for mRNA-sequencing was applied, except that reads falling into exons were removed.

Also the BLISS8 bioinformatical analysis was already published in (Endres et al., 2021) and was performed in the following way: BLISS8 samples were demultiplexed based on their condition-specific barcodes using UMI-tools, allowing one mismatch in the barcode, and were mapped to the human genome hg19 using Bowtie2 with default parameters. The respective samples of biological triplicates were merged and also mapped and processed collectively. Samples were filtered against an ENCODE Blacklist file using bedtools intersect to remove regions of high variance in mappability, frequently found in telomeric, centromeric and satellite repeats. To allow absolute quantification of double-strand breaks and remove PCR-introduced

artefacts, duplicated reads were identified based on their UMI, grouped and deduplicated using UMI-tools with default parameters. For normalisation, deduplicated reads in AsiSI specific restriction sites were counted using ‘countBamInGRanges’ from the R package ‘exomeCopy’. The sample with the smallest number of AsiSI specific reads was divided by the total amount of deduplicated reads and samples randomly subsampled to the calculated number of reads. AsiSI specific restriction sites were generated by in silico digestion of the hg19 genome. From the 1,123 predicted restriction sites, sites without mapped reads across all conditions in the respective experiment were dropped. Annotation of reads to genomic features was performed using ‘annotatePeak’ from the R package ‘ChIPseeker’. Gene sets were defined as described according to mRNA-sequencing in Herold et al., 2019.

Detailed scripts can be found within the person’s own records.

4 Results

4.1 Characterisation of the DNA damage response pathway in neuroblastoma

4.1.1 Characterisation of the SH-EP MYCN-ER cell system

In order to understand the differences between MYC and MYCN in neuroblastoma, neuroblastoma cells (SH-EP) expressing only endogenous MYC were stably transfected with the MYCN-ER chimera. This cell system is well established and was documented before (Herold et al., 2019). But as control, protein levels of endogenous MYC, chromatin binding of MYCN and target gene enrichment in RT-qPCR were always investigated routinely. The addition of 4-Hydroxytamoxifen (4-OHT) led to a downregulation of endogenous MYC levels (Figure 4.1 a). Chromatin-immunoprecipitation followed by deep-sequencing (ChIP-sequencing) showed the chromatin binding of MYCN (Figure 4.1 b) after the addition of 4-OHT, suggesting that the hormone dependent binding to MAX and the chromatin recruitment took place. The activation of MYCN had profound effects on gene expression as seen before (Herold et al., 2019): known MYC target genes were upregulated upon 4-OHT treatment in RT-qPCR (Figure 4.1 c).

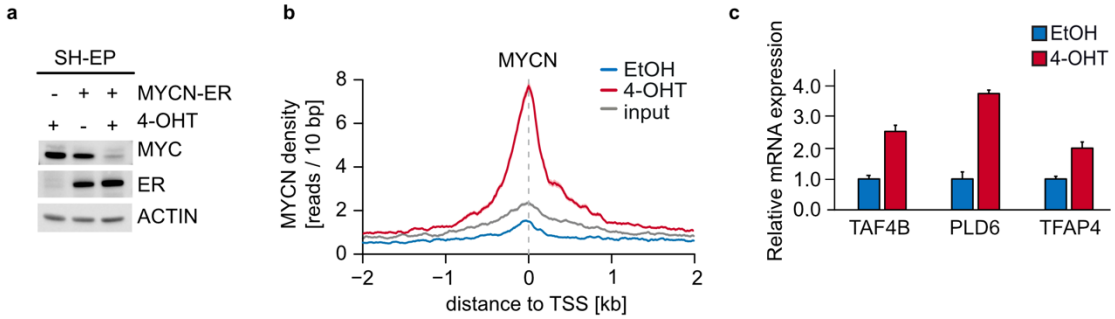

Figure 4.1 Characterisation of the SH-EP MYCN-ER cell system
a Immunoblot of SH-EP WT cells and SH-EP MYCN-ER cells, treated for 4 h with 200 nM 4-Hydroxytamoxifen (4-OHT) or ethanol (EtOH). Vinculin was used as loading control.
b Density plot of MYCN occupancy after 4-OHT or EtOH treatment (3 h) around the transcription start site.
c Relative mRNA expression upon MYCN activation (200 nM 4-OHT, 4 h). Expression was normalised to B2M. Relative mRNA expression was set in reference to the EtOH condition. Shown is one representative experiments (n=3). In all subsequent legends, *n* indicates the number of independent biological replicates. Data are mean and SD of technical triplicates.

The switch of MYC proteins is advantageous to study their initial driving events and certain vulnerabilities in cells that are suddenly acutely driven by a different oncoprotein, namely MYCN.

4.1.2 BRCA1 knockdown and MYCN activation is synthetic lethal

The former PhD student of Professor Eilers, Jiajia Xu, studied the dependencies of *MYCN*-driven tumours employing in SH-EP MYCN-ER cells. She therefore performed a genome wide shRNA screen looking for synthetic lethality with MYCN-ER expression. One hit out of her screen was the tumour suppressor protein BRCA1. As described in the introduction, *MYCN*-driven neuroblastoma cells have higher BRCA1 protein levels and patient data revealed a hypomethylation of the BRCA1 promoter (Herold et al., 2019). To characterise the role of BRCA1 in neuroblastoma, two independent shRNAs targeting BRCA1 were cloned into the pGIPZ vector, which allows a constitutive expression of the constructs. After infection of SH-EP MYCN-ER cells and selection, the knockdown was determined by RT-qPCR for mRNA-levels (Figure 4.2 a) and immunoblot (Figure 4.2 b) for protein levels. SH-EP cells themselves had lower BRCA1 levels as compared to the *MYCN*-amplified IMR5 cells (Figure 4.2 b, (Herold et al., 2019). BRCA1 was mainly localised in the nucleus and protein levels were targeted efficiently, also proved by immunofluorescence (Figure 4.2 c). Both shRNAs had a knockdown efficiency up to 85% on mRNA and protein levels.

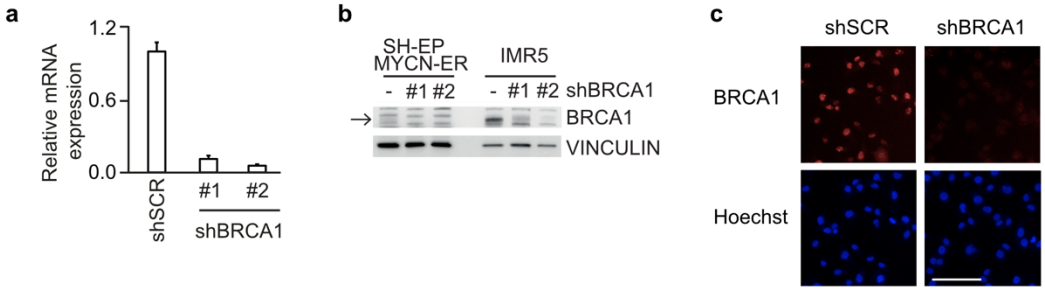

Figure 4.2 Validation of BRCA1 knockdown efficiency
a qRT-PCR data of BRCA1 mRNA levels in control or BRCA1-depleted SH-EP MYCN-ER cells. Data are mean and SD of technical triplicates, normalised to B2M expression (n=3).
b Immunoblot of SH-EP MYCN-ER cells or *MYCN*-amplified IMR5 cells documenting the knockdown of BRCA1 with two different shRNAs. Vinculin was used as loading control. The arrow points to the BRCA1 band, asterisks denote unspecific band. This experiment was performed by Steffi Herold.
c Immunofluorescence staining of BRCA1 in SH-EP MYCN-ER cells expressing either control shRNA, which is named 'shSCR' in all subsequent figures and legends, or shBRCA1#2. Nuclei were counterstained with Hoechst. Scale bar shows 100 µm (n=3).

The synthetic lethal effect of the BRCA1 knockdown together with MYCN activation was also validated with the new shRNA sequences based on the mirE design described in (Fellmann et al., 2013). The knockdown of BRCA1 itself had already a strong effect on the fitness of the cells, but the activation of MYCN over several days showed the synthetic lethality that was originally described by Jiajia Xu (Figure 4.3).

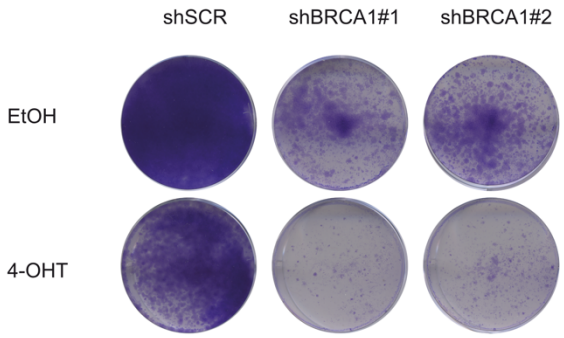

Figure 4.3 Synthetic lethality of BRCA1 knockdown and MYCN activation
Colony formation assays in SH-EP MYCN-ER cells expressing either shSCR or shBRCA1#1 and #2 treated for 6 d with 200 nM 4-OHT or EtOH. Colonies were stained with crystal violet (n=3).

4.1.3 BRCA1 regulates DNA damage in neuroblastoma

The activation of MYCN upon BRCA1 knockdown showed an apoptotic outcome. To look further into the cellular effects of BRCA1 loss, the cell cycle distribution was investigated by BrdU/PI FACS and subsequent quantification. Control cells proceeded normally through all cell cycle phases, while the knockdown of BRCA1 led them accumulate in G1-phase. This was already seen at the first day after selection (Figure 4.4 a) but more prominently after four days of BRCA1 loss (Figure 4.4 b). The activation of MYCN for six hours had just a mild effect on the cell cycle distribution in the situation when BRCA1 was knocked down (Figure 4.4 a). However, MYCN overexpression for 48 hours forced the cells over the G1/S-checkpoint into S-phase (Figure 4.4 b).

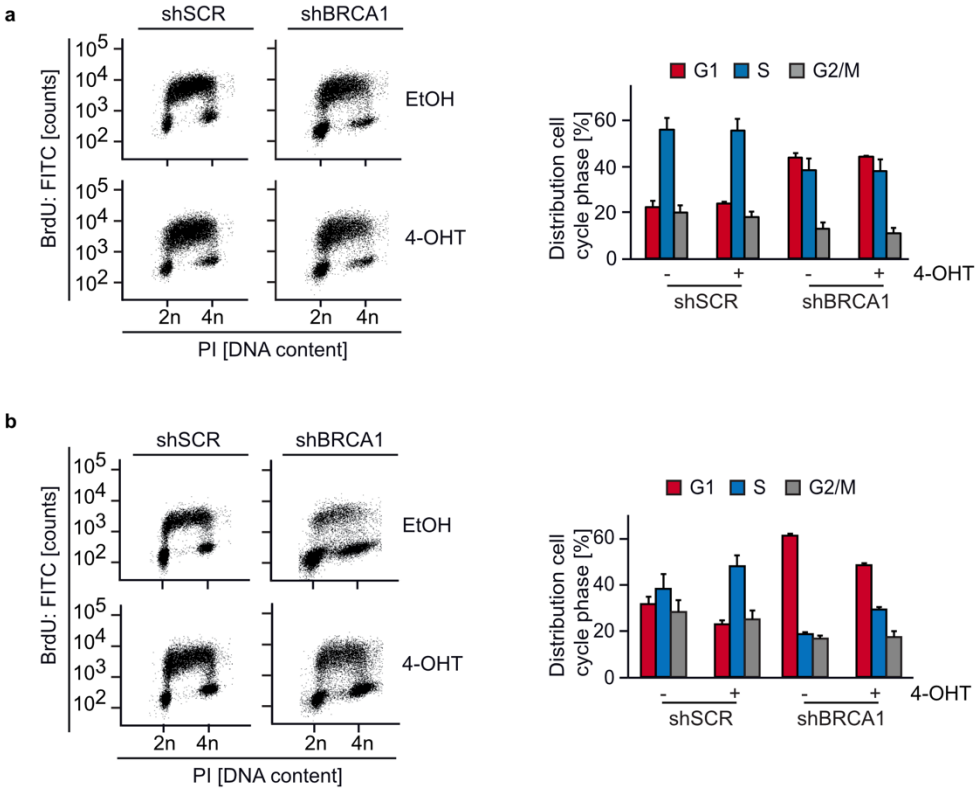

Figure 4.4 Cell cycle distribution upon BRCA1 knockdown and MYCN activation
Representative Bromodeoxyurdine (BrdU) – Propidiumiodide (PI) FACS profiles (left) and quantification (right) of the PI staining of SH-EP MYCN-ER control or BRCA1-deficient cells (shBRCA1#2) treated for 6 h (**a**) and 48 h (**b**) with 200 nM 4-OHT or EtOH. Data represents mean with SD of biological triplicates.

Upon the time when they accumulated in G1 phase, their apoptosis level was even lower compared to control cells, indicating a growth deficit first (Figure 4.5 a). The cells lacking BRCA1 showed an increase of γH2A.x and 53BP1 foci, markers for DNA damage, and this effect was even more pronounced when MYCN was activated (Figure 4.5 b). Before the cells went into apoptosis and showed the synthetic lethal phenotype of BRCA1 knockdown and MYCN activation, they showed defects in cell cycle progression and increased DNA damage.

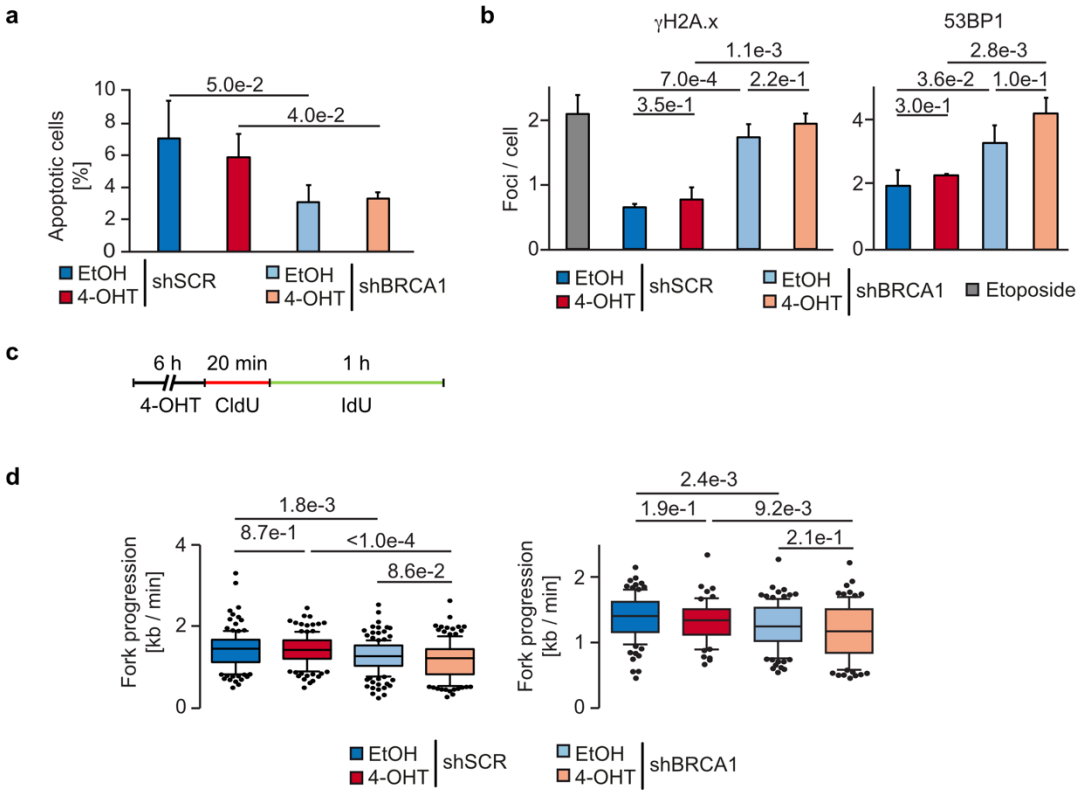

Figure 4.5 Elucidating the role of BRCA1 in neuroblastoma
a Quantification of apoptotic cells defined as AnnexinV and PI positive measured in a AnnexinV/PI FACS in SH-EP MYCN-ER cells expressing either control shRNA or shRNA targeting BRCA1 (#2). Cells were treated for 48 h with 200 nM 4-OHT. Data represent mean with SD of biological triplicates.
b Quantitative immunofluorescence staining of γH2A.x (left) and 53BP1 (right) foci in control or BRCA1-deficient (shBRCA1#2) SH-EP MYCN-ER cells treated additionally for 24 h with 200 nM 4-OHT or EtOH. Etoposide was used as positive control (25 µM, 2 h). Nuclei were counterstained with Hoechst. Shown is one representative experiment (n=3). Data represent mean and SD of biological triplicates.
c Scheme of experimental setup for the DNA fiber assays that were carried out by Sabrina Rodewald, Laboratory of Prof. Dobbelstein, Göttingen.
d Box plots showing the fork progression measured during both labels in SH-EP MYCN-ER cells, expressing either a shSCR or shBRCA1#1 (left) or shBRCA1#2 (right). Cells were treated with 4-OHT or EtOH (6 h, 200 nM). Shown is one representative experiment (n=3). *P* values were calculated using a two-tailed, unpaired *t*-test with additional Welch's correlation. The central line within the boxes reflects the median, the borders show the lower and upper quartile of the plotted data, with 10^{th}-90^{th}-percentile whiskers and outliers are shown as dots. Number of DNA fibers that were analysed, Left: shSCR EtOH (n = 130), 4-OHT (n = 131); shBRCA1#1: EtOH (n = 161), 4-OHT (n = 139). Right: shSCR EtOH (n = 95), 4-OHT (n = 69); shBRCA1#2: EtOH (n = 109), 4-OHT (n=90).

BRCA1 has its main role in homologous recombination to repair DNA damage in S-phase (Venkitaraman, 2014). To measure its effect on replication fork progression, the driver of DNA synthesis in S-phase, DNA fiber assays were carried out. For the experimental outline, freshly synthesised DNA is marked with two different fluorescently labelled pyrimidine analogues and analysed via microscopy. Due to different labelling, conclusion to the origin of replication (ORI) firing can additionally be drawn. In this case, just the fiber length upon different treatments was analysed. The loss of BRCA1 – resulting from both shRNAs – showed a

decrease in fiber length and replication slowed even more down upon the addition of 4-OHT (Figure 4.5 c, d).

4.1.4 BRCA1 recruitment is cell cycle dependent

The results presented so far indicated that BRCA1 as a tumour suppressor had a major role in the DNA damage response, the cell cycle progression and ongoing replication upon MYCN overexpression. While MYCN contributed to the increase of cellular stress, these features did not explain completely the dependency on BRCA1 of *MYCN*-driven neuroblastoma. Interestingly, MYCN overexpression induces the promoter recruitment of BRCA1 (Herold et al., 2019), suggesting an influence on transcriptional start sites.

The recruitment of BRCA1 to core promoters did not result from a direct interaction demonstrated by co-immunoprecipitates, where BRCA1 and MYCN did not interact (Figure 4.6 a), and indicated also by mass spectrometry analysis previously performed in the Eilers laboratory (Buchel et al., 2017). Interestingly, cells synchronised by a double thymidine block and then released for different time-points representative of specific cell cycle phases (Figure 4.6 b) showed a differential ChIP enrichment for BRCA1 (Figure 4.6 c). In detail, while MYCN overexpression always induced BRCA1 promoter enrichment, this happened mostly in S- and G2/M-phase.

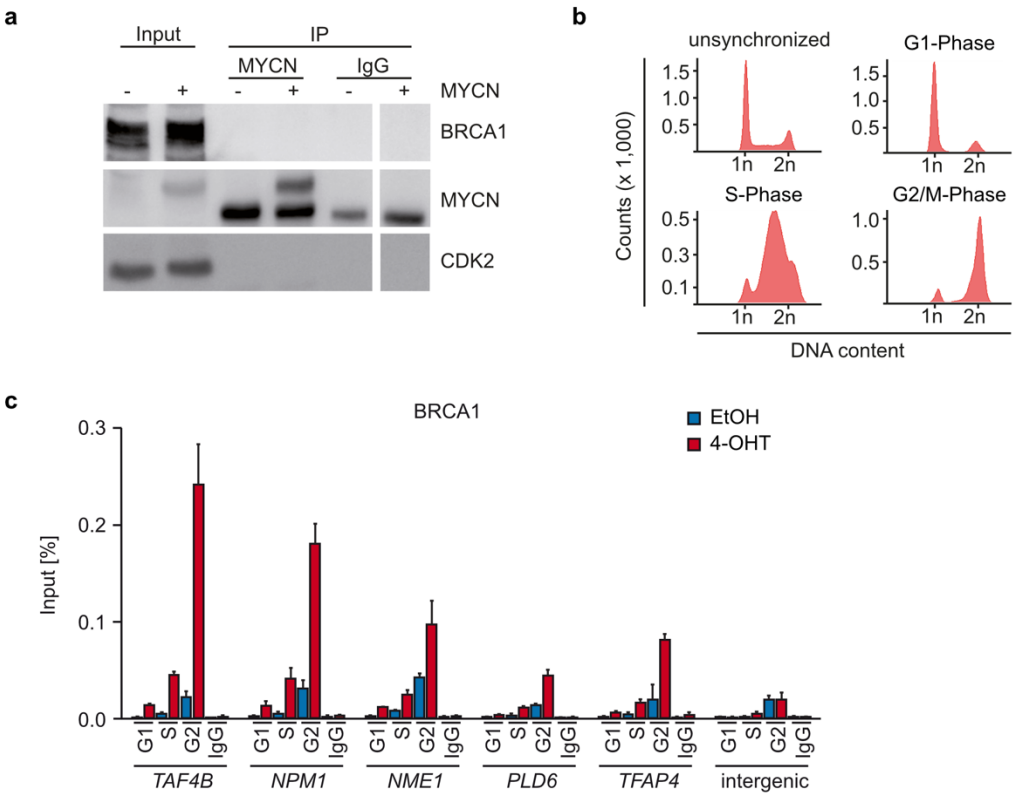

Figure 4.6 MYCN recruits BRCA1 in a cell-cycle dependent manner
a Immunoblot of anti-MYCN immunoprecipitates from SH-EP WT cells and SH-EP cells stably expressing MYCN and blotted for BRCA1. Shown is 5% input. CDK2 was used as loading control (n=3).
b PI FACS profiles of SH-EP MYCN-ER cells either non-synchronised or synchronised by a double thymidine block and released for 4 h (S-phase), 8 h (G2/M-phase) and 12 h (G1-phase).
c Chromatin-immunoprecipitation (ChIP) of BRCA1 in SH-EP MYCN-ER cells synchronised and released for the indicated cell cycle phase as described in b, treated for the last 4 h prior to harvest with 4-OHT or EtOH. IgG was used as pull-down control. Data represents mean with SD of technical triplicates (n=1).

4.2 The role of BRCA1 in MYCN-driven transcription

4.2.1 BRCA1 recruitment happens before CDK7 mediated RNAPII phosphorylation

It is conceivable that a MYCN-influenced pathway led to the recruitment of BRCA1. To shed further light on this, the connection of BRCA1 to transcription was studied, considering the predominantly discussed function of MYC proteins in literature as transcription factors changing RNAPII chromatin occupancy and gene expression profiles. Also BRCA1 – beyond its role in DNA damage response – influences transcription (Monteiro, 2000) and is even interacting with the RNAPII (Anderson et al., 1998; Scully et al., 1997).

To investigate at which step of the transcription cycle BRCA1 is recruited and whether active transcription is needed for the recruitment, different CDK inhibitors mediating transcription initiation (CDK7) or pause release (CDK9), were used. THZ1, a CDK7 inhibitor, showed a decreased phosphorylation of Ser5- and Ser2-RNAPII in immunoblots indicating indeed the

inhibition of CDK7, the block of RNAPII release from the promoter and subsequently the block of further transcription (Figure 4.7 a). However, BRCA1 was still recruited to a similar extent to promoter proximal sites, even though CDK7 was inhibited (Figure 4.7 b). Because THZ1 just inhibits the CDK7 kinase activity, the MYCN mediated BRCA1 recruitment to core promoters happened already before Ser5 phosphorylation of the CTD and therefore pausing of RNAPII. Furthermore, transcriptional activity *per se* does not seem to be relevant for BRCA1 recruitment since RNAPII proceeding in the transcriptional cycle was blocked by THZ1.

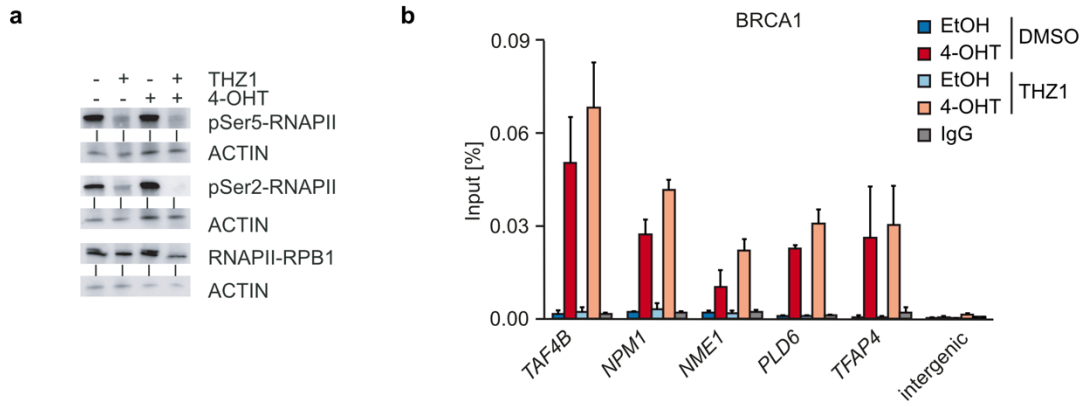

Figure 4.7 BRCA1 recruitment happens before CDK7 mediated CTD phosphorylation
a Immunoblot showing total RNAPII, pSer5-RNAPII and pSer2-RNAPII in SH-EP MYCN-ER cells. Cells were treated with CDK7 inhibitor THZ1 (200 nM, 4 h) or DMSO as control together with 4-OHT or EtOH (200 nM) treatment. Actin was used as loading control (n=1).
b ChIP of BRCA1 at the indicated loci in SH-EP MYCN-ER cells treated as described in a. Data show mean and SD of technical triplicates (n=1).

Interestingly, inhibition of CDK9, the kinase that regulates pause release of RNAPII, by flavopiridol increased the recruitment of BRCA1 to promoter proximal sites and BRCA1 showed a higher proximity to Ser5-phosphorylated RNAPII (Herold et al., 2019). Since promoter proximal pausing regulates gene expression (Core and Adelman, 2019), the impact of BRCA1 on transcriptional activity and RNAPII chromatin occupancy were analysed.

4.2.2 Loss of BRCA1 results in accumulation of RNAPII

To analyse whether BRCA1 has also an effect on the RNAPII chromatin occupancy upon the acute activation of MYCN, ChIP-sequencing for chromatin association of the transcription machinery was used. For these experiments, MYCN was just activated for few hours with the constitutive knockdown of BRCA1.

Antibodies against unphosphorylated RNAPII, all forms of RNAPII (total), whether phosphorylated or not, and RNAPII phosphorylated on Ser2 were used for the pulldown. The occupancy of different forms of RNAPII was visualised in metagene plots.

As previously shown for MYC (Rahl et al., 2010), also MYCN had an influence on the release of RNAPII into productive elongation (Herold et al., 2019). This could also be observed in the control conditions of this study: the activation of MYCN had no effect on unphosphorylated RNAPII (Figure 4.8 a), so the rate of initiation and recruitment of RNAPII to promoters was unaffected when looking at all expressed genes. When stratifying for activated and repressed genes, total RNAPII showed a drop at the start site after MYCN activation (Figure 4.8 b) indicating a release of RNAPII at the promoter. The analysis of the elongating form of RNAPII (pSer2-RNAPII) after activation of MYCN showed more productive elongation on activated and less on repressed genes (Figure 4.8 c).

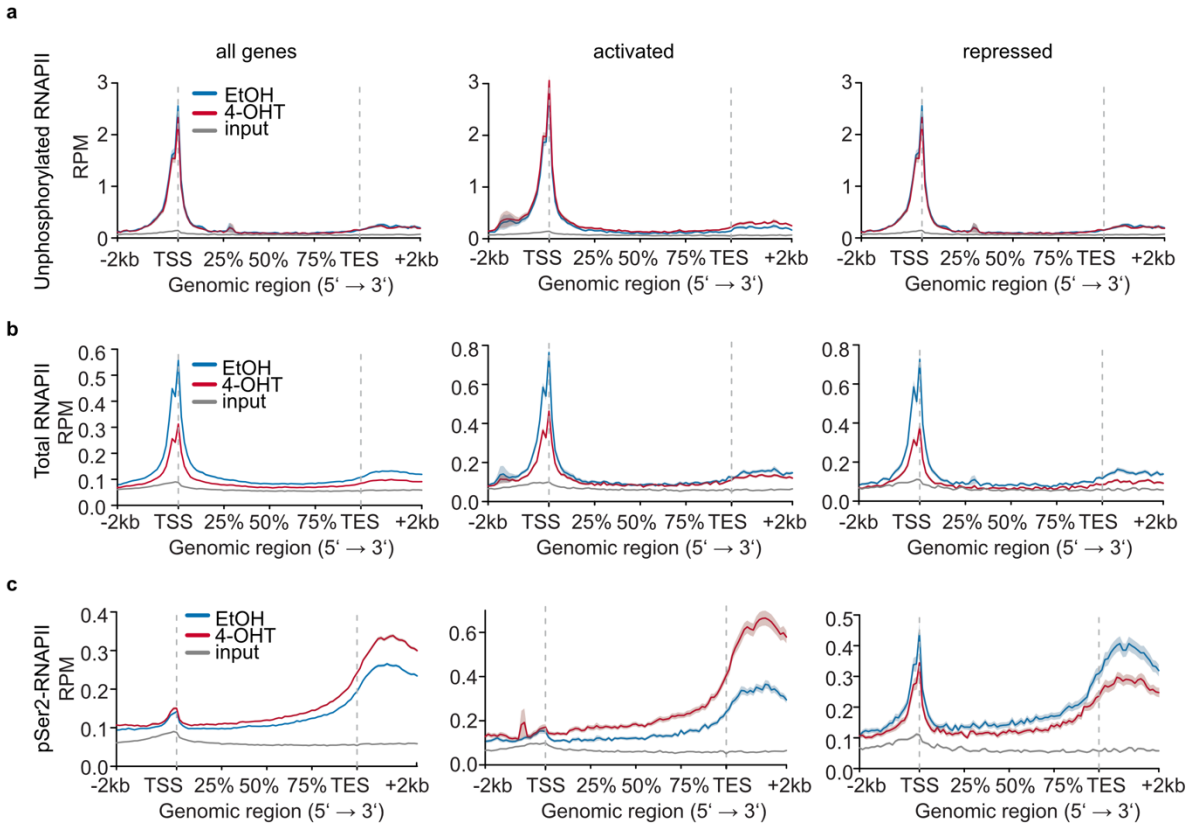

Figure 4.8 ChIP-sequencing experiments of RNAPII upon acute activation of MYCN
Metagene plots of unphosphorylated RNA Polymerase II (RNAPII) (**a**), total RNAPII (**b**) and pSer2-RNAPII (**c**) after 3 h 4-OHT or EtOH treatment for all expressed genes (14,488, left), the most strongly MYCN-activated (914, middle) and MYCN-repressed (615, right) genes (n=2). RPM: reads per million mapped reads.

On the other hand, when comparing the control and BRCA1 knockdown conditions, the knockdown of BRCA1 had mild effects on the initiation of transcription as seen for

unphosphorylated RNAPII (Figure 4.9 a). A drop of unphosphorylated RNAPII that is recruited to the promoter could be observed when MYCN is getting activated upon BRCA1 loss. As said, MYCN activation in control conditions resulted in a drop of total RNAPII at promoters, whereas the knockdown of BRCA1 led to an accumulation of RNAPII at the TSS and all over the gene body when MYCN is activated (Figure 4.9 b). The elongating form, pSer2-RNAPII, showed not only a peak around the TSS that was higher than in control conditions, indicating paused or stalled RNAPII even though it is Ser2 phosphorylated, but also a decrease within the genomic region upon BRCA1 knockdown (Figure 4.9 c). This would also explain the drop of unphosphorylated RNAPII at the TSS since paused RNAPII that does not go into productive elongation inhibits new transcription initiation (Shao and Zeitlinger, 2017).

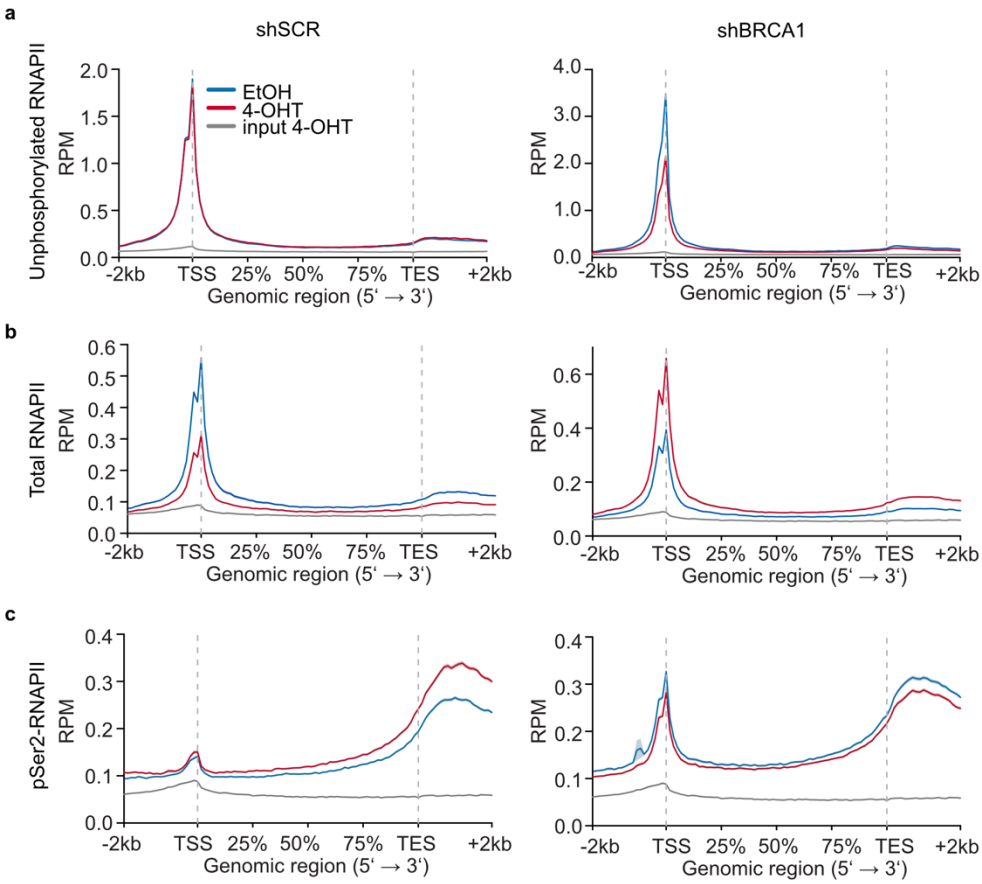

Figure 4.9 Behaviour of the transcription machinery upon BRCA1 loss
Metagene plots of unphosphorylated (**a**, n=1), total (**b**, n=2) and pSer2-RNAPII (**c**, n=2) in SH-EP MYCN-ER control (left) and BRCA1-deficient (right, shBRCA1#2) cells treated for 3 h with 4-OHT for 14,488 expressed genes.

In summary, MYCN promoted the release of RNAPII into productive elongation as seen before, especially on activated genes. BRCA1, as a partner protein of MYCN, seemed to be involved

in the decision making whether RNAPII goes into productive elongation or not, since its loss resulted in massive accumulation of RNAPII.

To inquire whether BRCA1 has not only an effect on chromatin association of RNAPII but also on gene expression, total mRNA-sequencing was performed. As described previously (Herold et al., 2019), the activation of MYCN in control cells led to an up- and downregulation of well-defined MYC gene sets, such as upregulation of MYC targets or the downregulation of immune genes in the TNF signalling via NFκB pathway (Figure 4.10 a). Depletion of BRCA1 showed for both shRNAs an upregulation of immune genes, which are repressed gene sets in control conditions (Figure 4.10 b). The majority of genes was not affected by BRCA1 loss and showed similar regulation as in control conditions (red and blue dots in Figure 4.10 c) with just some genes showing an inverted regulation upon BRCA1 knockdown (Figure 4.10 c upper left and lower right quarter).

a

gene set	NES	FDR
MYC targets V1	3.00	0.000
KIM: MYCN amplification targets up	2.02	0.005
IL6 JAK STAT3 Signaling	-1.80	0.003
TIAN: TNF signaling via NFκB	-2.25	0.001

b

gene set	NES	FDR	
Inflammatory response	1.64	0.022	**shBRCA1#1**
TIAN: TNF signaling via NFκB	2.14	0.001	
IL6 JAK STAT3 Signaling	1.38	0.198	**shBRCA1#2**
TIAN: TNF signaling via NFκB	1.95	0.007	

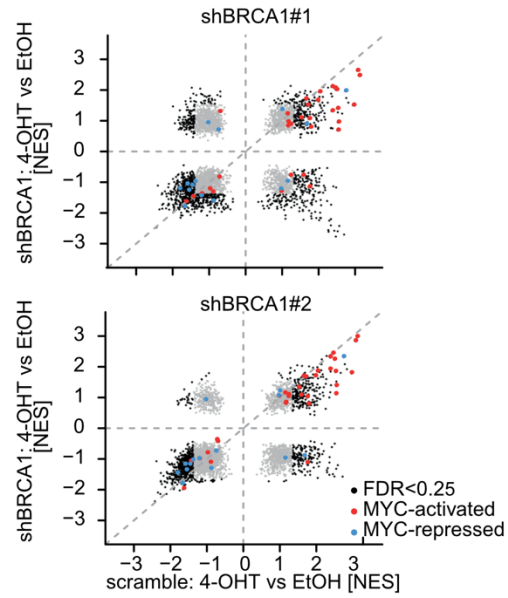

Figure 4.10 Effects of BRCA1 loss on global transcription
a Expression of selected gene sets from gene set enrichment analysis in SH-EP MYCN-ER cells after 5 h of 4-OHT vs ethanol treatment (n=3).
b Expression of selected gene sets from gene set enrichment analysis in SH-EP MYCN-ER comparing the treatment of 4-OHT (5 h, 200 nM) in control and BRCA1-deficient condition (n=3).
c Gene set enrichment analysis upon activation of MYCN (5 h) in control and BRCA1-deficient cells (n=3). Black dots indicate significantly enriched gene sets (FDR $q < 0.25$), red marked dots are MYC-activated gene sets and blue dots MYC-repressed gene sets. FDR was calculated using a Kolmogorov-Smirnov test with 1,000 permutations using a Benjamini-Hochberg correction for multiple testing.

Therefore, BRCA1's role in gene regulation was only moderate as compared to its strong impact on the chromatin association of RNAPII (Figure 4.9). For the MYCN-driven gene regulation, BRCA1 was not in this sense essential, since the majority of genes stayed up- or

downregulated as in control conditions. However, the former repression of the shown immune gene sets was reversed upon the knockdown of BRCA1. Whether this was a direct effect, or secondary, remains open.

4.2.3 The inhibition of ATM leads to hyperactivation of MYCN-activated genes

Since the recruitment of BRCA1 happens probably already at the step of promoter opening and before CDK7 mediated phosphorylation of the CTD and because transcriptional activity *per se* does not influence BRCA1 recruitment (Figure 4.7), it might be that BRCA1 recruitment depends on an already described upstream pathway. BRCA1 is one downstream target of the serine/threonine kinase ATM (Gatei et al., 2000). To investigate the role of the ATM pathway in the observed gene regulation profile, neuroblastoma cells were treated with the specific ATM inhibitor KU-60019 (Golding et al., 2009). Immunoblots showed that the treatment of cells with KU-60019, additionally exposed to etoposide as positive control, led to a reduction of CHK2-Thr68 phosphorylation, a specific phosphorylation site of the ATM kinase (Figure 4.11 a). This was independent of MYCN activation. To further see whether the inhibition of ATM had an impact on MYCN-mediated nascent transcription, 4sU-sequencing was performed. The activation of MYCN led to an up- and downregulation of certain genes in control conditions as described earlier (Figure 4.11 b). The inhibition of ATM upon MYCN activation boosted gene expression, inducing a further increase of activated genes, and downregulated genes were not as repressed as seen before (Figure 4.11 b, c).

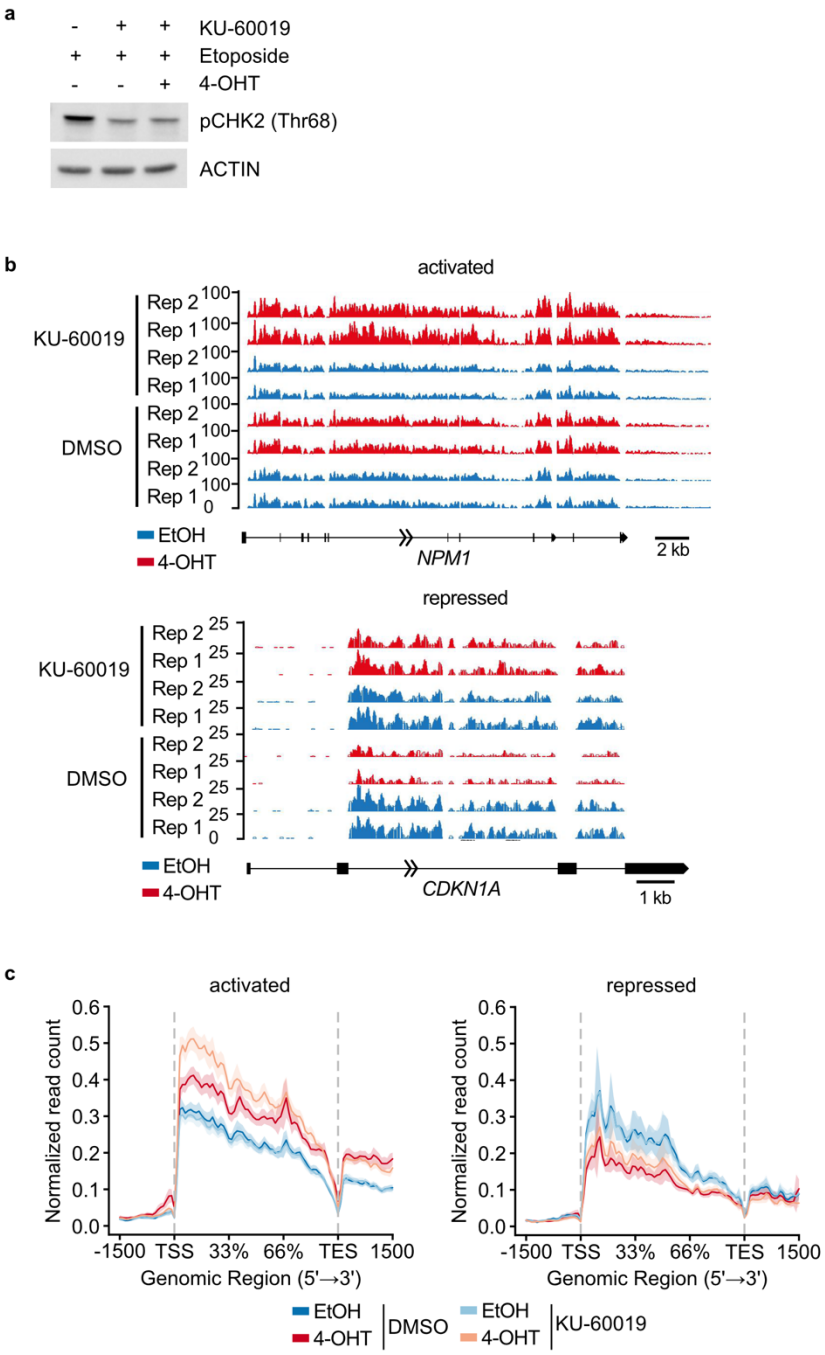

Figure 4.11 Effect on transcription upon ATM inhibition
a Immunoblot of SH-EP MYCN-ER cells treated with ATM inhibitor KU-60019 (100 nM, 4 h), etoposide (20 µM, 2h) or 4-OHT (200 nM, 4 h) where indicated showing the phosphorylation of CHK2 as an ATM target. Actin was used as loading control (n=2).
b Genome browser tracks of 4sU-sequencing experiment of SH-EP MYCN-ER cells treated with KU-60019 or DMSO (100 nM, 4 h) and 4-OHT or EtOH (200 nM, 4 h). TAF4B is an example of a MYCN-activated gene, CDKN1A is an example of a MYCN-repressed gene. Shown are both duplicates, y-axis represents 4sU density (reads), normalised to sequencing depth.
c Metagene plots of merged duplicates from c for MYCN-activated (914) and MYCN-repressed (615) genes.

As seen before for the gene regulation upon BRCA1 knockdown (Figure 4.10), also ATM and its inhibition had an effect on MYCN-driven gene regulation but also not in a genome wide manner. Most of the genes showed the same regulation as in control condition, but upon the

inhibition of ATM about a third of genes showed an upregulation. The 15% most downregulated genes in the control condition showed, as seen in the metagene plots before (Figure 4.11 c), a rescue in the sense of lesser repression (Figure 4.12).

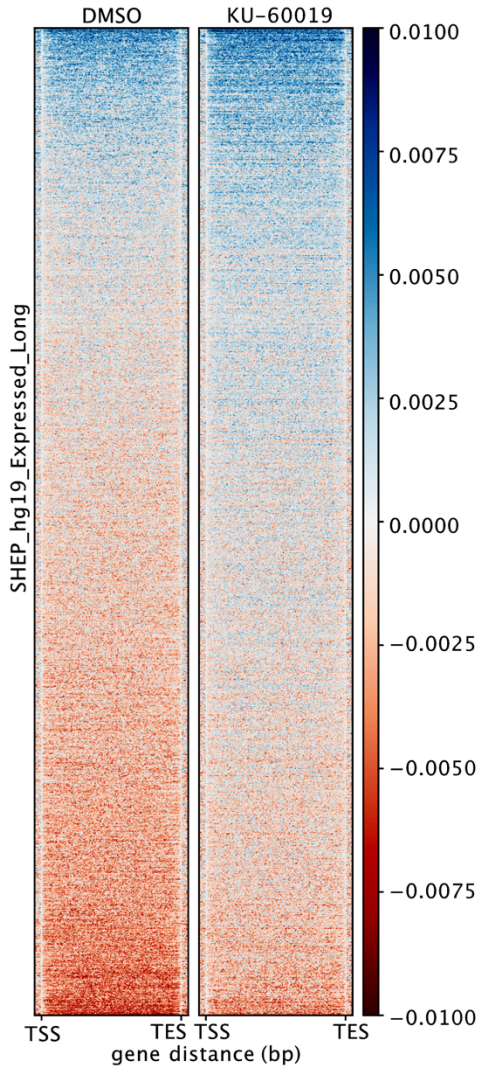

Figure 4.12 Heatmap showing gene expression upon ATM inhibition
Heat map of all expressed genes longer than 8 kb (8,622). Genes are sorted for the log_2FC of the control condition. Shown is the log_2FC +/- 4-OHT in control (left) and KU-60019 (right) treated SH-EP MYCN-ER cells. 0.5 kb flanking regions up- and downstream of the transcription start site (TSS) and transcription end site (TES) are also reported.

4.3 BRCA1 uses decapping factor DCP1A to resolve promoter-proximal R-loops

4.3.1 BRCA1 recruitment is necessary for the resolution of promoter proximal R-loops

The knockdown of BRCA1 resulted in a strong accumulation of RNAPII at promoter proximal sites, even though neither BRCA1 nor ATM inhibition had a strong effect on the overall gene expression profile (Chapter 4.2). The accumulation of RNAPII upon BRCA1 loss can have

different causes: First, the CTD phosphorylation of RNAPII - a signal for productive elongation - could be hindered by the negative elongation factor (NELF), since BRCA1 and NELF interact(Ye et al., 2001). Second, the elongation of RNAPII could be sterically hindered through the formation of DNA/RNA-hybrids - called R-loops - built upon the pausing or stalling of RNAPII at the promoter proximal site resulting in DNA damage as seen before (Figure 4.5) Interestingly, BRCA1 resolves R-loops via the DNA/RNA helicase Senataxin (SETX) (Hatchi et al., 2015). To investigate how BRCA1 prevents the accumulation of RNAPII, NELF and SETX were further examined.

For the hypothesis of the interplay between BRCA1 and NELF, the chromatin recruitment of NELF was investigated. The NELF subunit E (NELF-E), a key component of the NELF-complex, was analysed by ChIP. The activation of MYCN led to a decrease of NELF-E chromatin binding compared to the EtOH condition (Figure 4.13 a). The knockdown of BRCA1 itself did not alter the recruitment of NELF-E, but the additional activation of MYCN increased NELF recruitment to promoter proximal sites (Figure 4.13 a). These results indicated that NELF-E rather parallels the chromatin occupancy of RNAPII (Figure 4.8 and 4.9), suggesting that the decision whether RNAPII proceeds into productive elongation is not dependent on the BRCA1-NELF interplay directly, but the signal for NELF's dissociation from RNAPII is missing if BRCA1 is knocked down.

To investigate the second hypothesis, the accumulation of R-loops, DNA-RNA-immunoprecipitation (DRIP) was performed. Similar to ChIP, the S9.6 antibody was used for pulldown to detect chromatin associated R-loops (Boguslawski et al., 1986). As a proof of principle, the enrichment of R-loops on the well described *ACTB* locus was investigated (Hatchi et al., 2015). The enrichment increased towards the TES as described previously, and RNaseH (i.e. selectively digesting R-loops) was used as positive control and showed no enrichment (Figure 4.13 b). The loss of BRCA1 and the activation of MYCN resulted in an accumulation of promoter proximal R-loops on several tested loci in a pre-experiment (Figure 4.13 c). This could have been seen on even more promoter proximal sites in the hands of Gabriele Büchel where the activation of MYCN in general decreased R-loop levels, but the knockdown of BRCA1 upon MYCN activation led to R-loop accumulation (Figure 4.13 d, Herold et al., 2019). The differences of R-loop enrichment upon different treatments within these experiments can be explained by the highly dynamic structure of R-loops. The presented data suggested that BRCA1 was necessary for the prevention of promoter proximal R-loops.

BRCA1 is described for the resolution of R-loops at TES via its interplay with SETX (Hatchi et al., 2015). To test whether this is the mechanism how BRCA1 controls R-loop formation at promoter proximal pause sites, the enrichment for SETX was measured by ChIP. MYCN activation did not alter the chromatin recruitment of SETX in control conditions, while it increased SETX recruitment upon BRCA1 knockdown (Figure 4.13 e). These results indicated either that SETX got recruited independently of BRCA1 and is not the helicase resolving R-loops in a BRCA1 dependent manner or it cannot act as a DNA/RNA helicase to resolve R-loops upon BRCA1 loss.

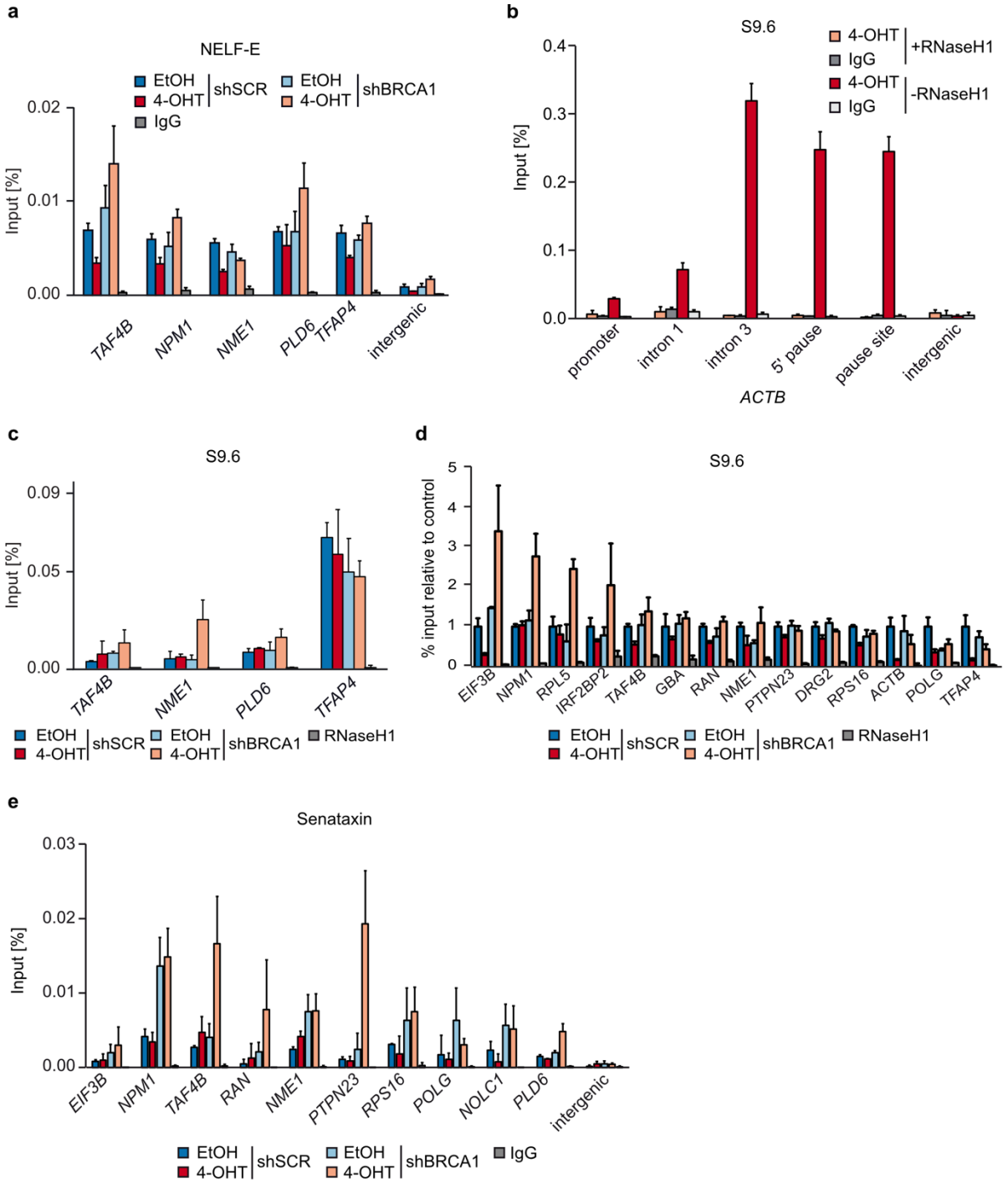

Figure 4.13 BRCA1 prevents promoter-proximal R-loop accumulation

a ChIP of NELF subunit NELF-E at the indicated loci in SH-EP MYCN-ER control and BRCA1 deficient cells treated for 3 h with 200 nM 4-OHT. Data show mean with SD of technical triplicates from one representative experiment (n=3 using two different shRNAs against BRCA1).

b DNA-RNA immunoprecipitation (DRIP) with the S9.6 antibody. Enrichment indicates R-loops at known loci within *ACTB*. RNaseH1 digestion was used as control for antibody specificity and IgG was used as control for unspecific chromatin binding. Data are mean with SD of technical triplicates. Shown is one representative experiment (n=2).

c DRIP indicating R-loops at indicated loci in SH-EP MYCN-ER control and BRCA1-deficient cells after 4 h of MYCN-activation (200 nM 4-OHT). Data represent mean and SD of technical triplicates (n=1).

d DRIP performed as described in c and done by Gabriele Büchel published in Herold et al., 2019. Data represent mean and SD of technical triplicates from one representative experiment normalised to the EtOH condition in control cells (n=4).

e ChIP of senataxin at the indicated loci in SH-EP MYCN-ER control and BRCA1-deficient cells with MYCN activation (3 h, 200 nM). Data show mean with SD of technical triplicates of one representative experiment (n=2 with 2 different antibodies).

4.3.2 Premature termination through decapping factors is BRCA1 mediated

The finding that the knockdown of BRCA1 results in a promoter proximal accumulation of RNAPII (Figure 4.9) suggested that BRCA1 was necessary for premature termination of RNAPII unable to proceed into productive elongation. Different pathways are described for premature termination. One relies on the standard termination machinery, that can be recruited to an alternative polyadenylation signal (PAS) positioned promoter proximally. This leads to the exonuclease digestion of the nascent RNA by different exonuclease, such as XRN2 or the exosome (Chiu et al., 2018) and the dissociation of RNAPII from chromatin. However, when looking at the exact position of the RNAPII that is accumulating upon BRCA1 knockdown, it pauses at a position about 1 kb upstream of the PAS site (Figure 4.14). The standard termination pathway via PAS cannot formally be ruled out since splicing factors, which are mediating this, were not investigated in this study, but since RNAPII accumulates before the PAS the focus was on alternative termination pathway which will be discussed as follows.

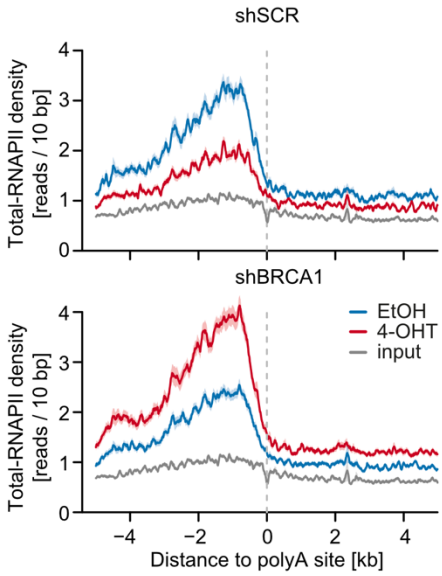

Figure 4.14 Accumulation of RNAPII before the polyA site
RNAPII density of 1,713 genes around the first polyA site downstream of the promoter. SH-EP MYCN-ER cells were treated for 3h with 200 nM 4-OHT for MYCN activation upon BRCA1 depletion (shBRCA1#2). Data show mean and SEM of one representative experiment (n=2).

The second mechanism of premature termination involves the recruitment of decapping factors to remove the 5'CAP of nascent RNA and the exonuclease activity of XRN2 to restrict bidirectional RNAPII from promoters (Brannan et al., 2012). Besides their role in P-bodies, decapping factors have also nuclear functions (Brannan et al., 2012; Hernandez et al., 2018). To see whether the loss of BRCA1 had an influence on the direct chromatin binding of decapping factors, ChIP-sequencing experiments upon BRCA1 knockdown and activation of

MYCN were performed for EDC4 and DCP1A, two substantial proteins of the decapping complex.

The activation of MYCN slightly decreased the chromatin binding of EDC4 in control conditions, and the knockdown of BRCA1 showed similar recruitment of EDC4 to the pausing site (Figure 4.15 a). Even though EDC4 recruitment to promoters was still intact upon BRCA1 knockdown, the vast majority of peaks for EDC4 was detected in intronic and intergenic sites (Figure 4.15 b). Upon the loss of BRCA1, EDC4 could potentially serve for BRCA1 at those loci in the DNA repair complex described previously (Hernandez et al., 2018) and is therefore not involved in promoter proximal decapping. EDC4's major function is decapping independent in neuroblastoma.

The recruitment of DCP1A was also slightly decreased upon the activation of MYCN (Figure 4.15 c). Strikingly, the loss of BRCA1 upon MYCN activation completely abolished the chromatin recruitment of DCP1A to promoter proximal pause sites (Figure 4.15 c).

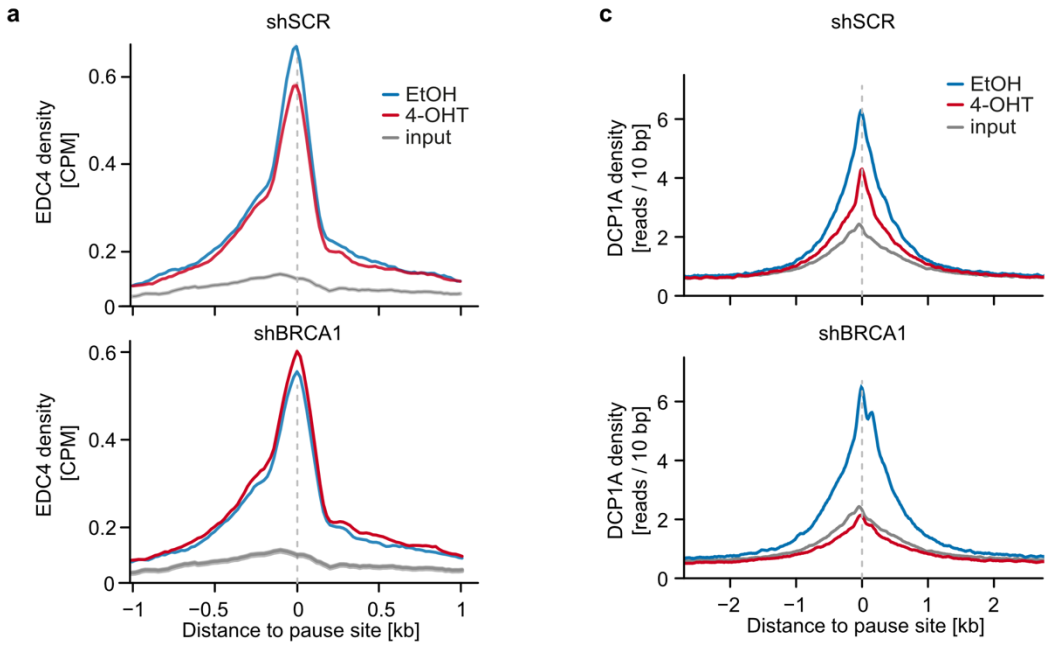

b EDC4 peaks

condition	promoter	intron	intergenic
shSCR EtOH	613	7,756	9,038
shSCR 4-OHT	386	5,689	6,758
shBRCA1 EtOH	615	9,544	10,524
shBRCA1 4-OHT	745	10,292	11,486

Figure 4.15 BRCA1 knockdown abolished DCP1A recruitment to pause sites
a Density plots of EDC4 occupancy after MYCN-activation (3 h, 200 nM 4-OHT) in control and BRCA1-deficient SH-EP MYCN-ER cells (shBRCA1#2) centered to the pause site. Data are mean ± SEM, CPM: counts per million mapped reads.
Figure legend continues on next page.

b Table of EDC4 peaks from cells described in a that fall into promoter, intron and distal intergenic region upon the indicated treatments.
c Density plots of DCP1A occupancy after MYCN-activation (5 h, 200 nM 4-OHT) in control and BRCA1-deficient SH-EP MYCN-ER cells (shBRCA1#2) centered to the pause site. Data are mean ± SEM. This experiment was performed by Steffi Herold.

The decapping factors EDC4 and DCP1A had different roles in neuroblastoma cells: EDC4 probably mimicked BRCA1 on intronic and intergenic sites in a DNA repair pathway because of BRCA1 loss in the complexes, whereas DCP1A was used for decapping and promoter proximal termination in a BRCA1- and MYCN-dependent manner.

4.3.3 ATM and BRCA1 recruit DCP1A to RNAPII

To investigate whether not only BRCA1 but also the upstream kinase ATM mediated the recruitment of decapping factors to the RNAPII, PLA assays upon BRCA1 knockdown and ATM inhibition with KU-60019 were performed. DCP1A increased its proximity to RNAPII upon MYCN activation (Figure 4.16 a, b). Conversely, the knockdown of BRCA1 and the inhibition of ATM led to a significant decrease of PLA foci of DCP1A and RNAPII (Figure 4.16 a, b). Strikingly, MYCN activation further decreased this proximity, probably because DCP1A is not recruited to chromatin anymore as seen before (Figure 4.15 c).

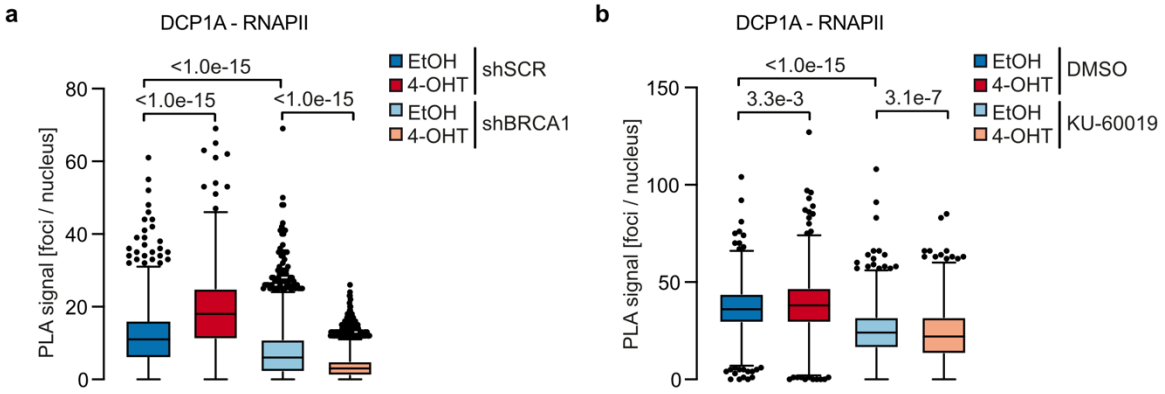

Figure 4.16 BRCA1 and ATM mediate the recruitment of decapping factors to RNAPII
a PLA quantification in single cells showing the proximity of DCP1A with RNAPII within the nucleus in SH-EP MYCN-ER control or BRCA1-deficient cells treated for 4 h with 4-OHT. *P* values were calculated using a two-tailed Wilcoxon rank-sum test (n=4). In the box plot, the central line represents the median, and the borders of the boxes show the interquartile range of the plotted data. The whiskers extend to 1.5 x the interquartile range. Shown is one representative experiment.
b PLA quantification in single cells showing the proximity of DCP1A with RNAPII within the nucleus in SH-EP MYCN-ER treated for 4 h with 200 nM 4-OHT or the ATM inhibitor KU60019 (100 nM) where indicated. *P* values were calculated using a two-tailed Wilcoxon rank-sum test (n=4). In the box plot, the central line represents the median, and the borders of the boxes show the interquartile range of the plotted data. The whiskers extend to 1.5 x the interquartile range. Shown is one representative experiment.

Collectively, MYCN increased the recruitment of DCP1A to RNAPII in control conditions. This suggested that both, BRCA1 and ATM, were necessary for the proximity – likely, the recruitment - of DCP1A to RNAPII.

4.3.4 MYCN recruits DCP1A to phosphorylated RNAPII

Results showed so far indicated that MYCN induced BRCA1 recruitment to promoters in S- and G2/M-phase (Figure 4.6 c) and BRCA1 mediated the proximity of decapping factors to RNAPII to perform premature termination (Figure 4.16). Furthermore, BRCA1 showed a higher proximity to Ser5-phosphorylated RNAPII (Herold et al., 2019). To test whether DCP1A has also a preference for a specific form of RNAPII and whether this is also cell cycle-dependent, PLA assays of DCP1A with unphosphorylated, Ser5- and Ser2-phosphorylated RNAPII were performed. They showed that MYCN increased the proximity of paused and elongating RNAPII with DCP1A, whereas there was no significant difference with the unphosphorylated form (Figure 4.17 a). This suggested that DCP1A played not only a role in premature termination of paused RNAPII but also of elongating RNAPII.

To inquire whether this recruitment played a major role in a specific cell cycle phase, cells tested for PLAs were labelled with EdU and Hoechst to identify cells in G1-, S- and G2/M-phase. It could be shown that the exonuclease XRN2 and DCP1A showed a higher proximity to RNAPII in cells of S- and G2/M-phase (Figure 4.17 b).

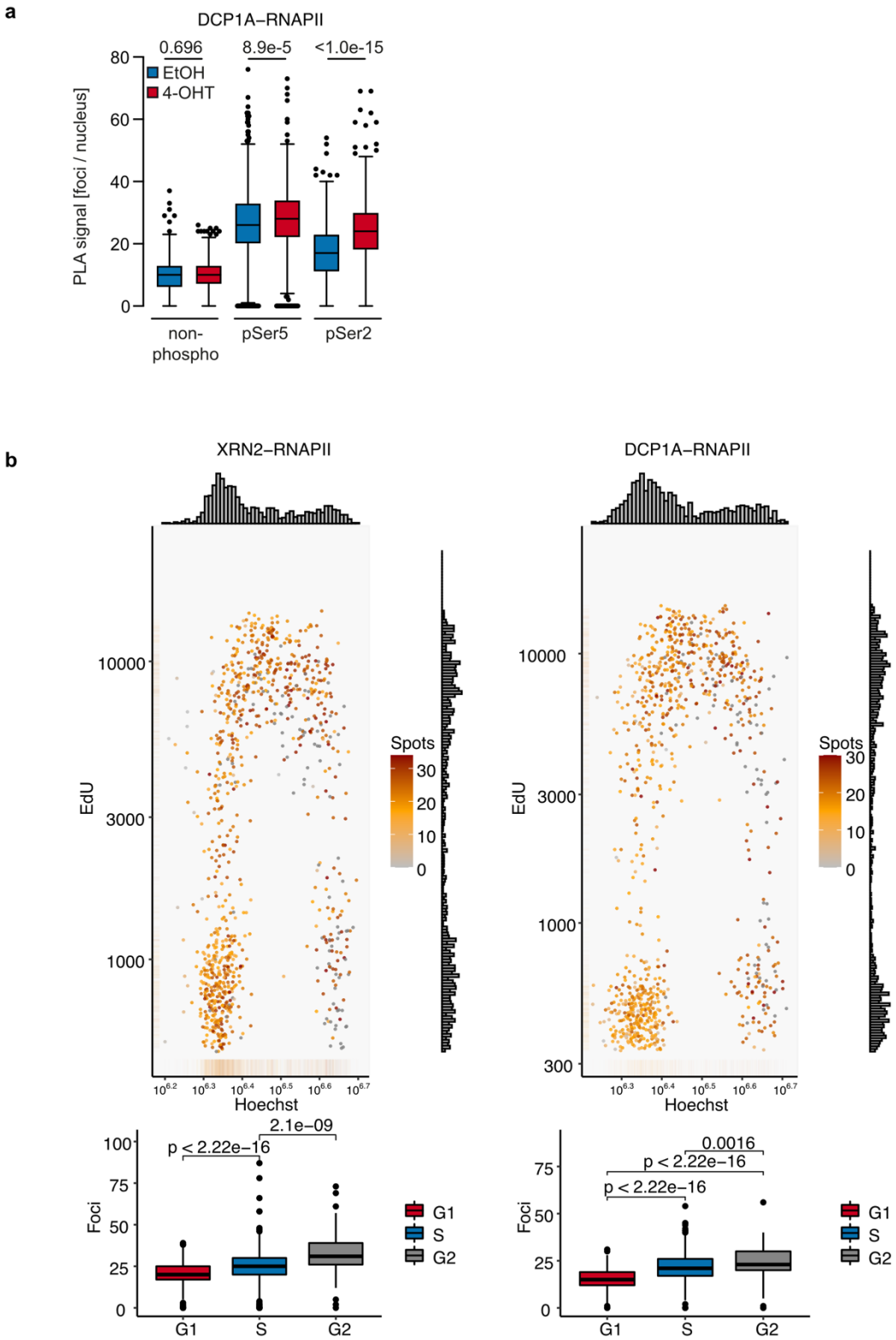

Figure 4.17 MYCN recruits DCP1A and XRN2 in a cell cycle dependent manner
a Box plots showing the single cell quantification of PLA foci documenting the proximity of DCP1A with unphosphorylated, Ser5-phosphorylated and Ser2-phoshorylated RNAPII within the nucleus upon activation of MYCN-ER (4h, 200 nM 4-OHT). *P* values were calculated using a two-tailed Wilcoxon rank-sum test (n=5). In the box plot, the central line represents the median, and the borders of the boxes show the interquartile range of the plotted data. The whiskers extend to 1.5 x the interquartile range. Shown is one representative experiment.
Figure legend continues on next page.

b Single cell quantification of PLA foci of XRN2 (left) and DCP1A (right) with RNAPII in SH-EP MYCN-ER cells in the condition when MYCN is activated (4 h, 200 nM 4-OHT). Cells were pulsed for 30 min with 10 μM 5-ethynyl-2-deoxyuridine (EdU) prior to fixation and nuclei were counterstained with Hoechst to determine cell cycle phase. 1,000 cells were quantified. *P* values were calculated using two-tailed Wilcoxon rank-sum test (n=5).

Interestingly, both BRCA1 recruitment to promoters and DCP1A recruitment to RNAPII happened in S- and G2/M-phase, with a higher prevalence of DCP1A for phosphorylated RNAPII.

Collectively, the promoter proximal termination mediated by BRCA1 was influenced by decapping through DCP1A and torpedo removal of RNAPII by XRN2. Whether alternative polyadenylation was also involved as second premature termination pathway (described in 1.1.1, Figure 1.4) cannot be fully excluded, but was not addressed within this study.

4.4 DCP1A loss leads to conflicts of transcription and replication machinery

4.4.1 Characterisation of decapping in neuroblastoma

To identify whether neuroblastoma cells show – as for BRCA1 – higher expression levels of decapping factors and if so whether this correlates with the *MYCN* status, immunoblots of DCP1A in *MYCN* non-amplified and *MYCN*-amplified neuroblastoma cells were performed. The expression of DCP1A was slightly increased in the *MYCN* non-amplified NB69 cells and in three *MYCN*-amplified cell lines (Figure 4.18 a). To investigate the role of DCP1A in neuroblastoma, an shRNA against DCP1A was cloned into the tetracycline inducible LT3-GEPIR vector system. The knockdown efficiency was determined for mRNA levels via RT-qPCR (Figure 4.18 b) and for protein levels by immunoblotting (Figure 4.18 c). The loss of DCP1A was also synthetic lethal for SH-EP MYCN-ER cells treated additionally with 4-OHT as colony formation assay (Figure 4.18 d) and AnnexinV/PI FACS analysis showed (Figure 4.18 e). These findings are a proof-of-principle suggesting that acute activation of MYCN lead to DCP1A dependency in cells, similarly to its upstream effector BRCA1.

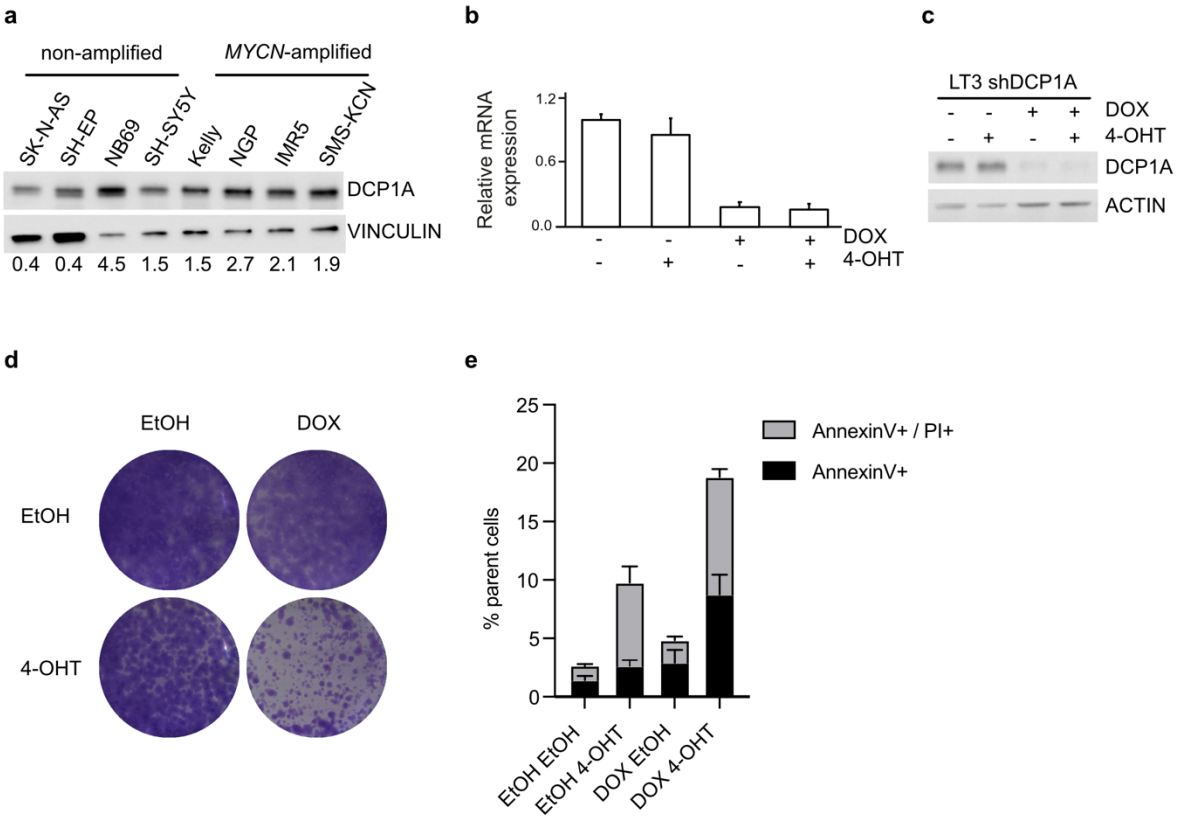

Figure 4.18 Synthetic lethality of DCP1A knockdown and MYCN activation
a Top: Immunoblot of DCP1A in *MYCN* non-amplified and *MYCN*-amplified neuroblastoma cell lines. Vinculin was used as loading control (n=2). Bottom: Quantification of the signal normalised to the Vinculin loading control of the indicated lane.
b qRT-PCR data of DCP1A mRNA levels in control or DCP1A-depleted (1 µg/ml DOX) of SH-EP MYCN-ER cells expressing an tetracycline (DOX) inducible shRNA against DCP1A upon MYCN-activation (200 nM 4-OHT, 4 h) where indicated. Data are mean and SD of technical triplicates, normalized to B2M expression (n=3).
c Immunoblot of SH-EP MYCN-ER cells expressing doxycycline inducible shRNA against DCP1A. Cells were treated for 6 d with 100 nM 4-OHT and 1 µg/ml DOX. Actin was used as loading control (n=3).
d Colony formation assays in SH-EP MYCN-ER cells expressing doxycycline inducible shDCP1A. Cells were treated for 10 d with 100 nM 4-OHT and 1 µg/ml DOX. Colonies were stained with crystal violet (n=4).
e Quantification of pre apoptotic (AnnexinV +) and apoptotic cells (AnnexinV/PI +) measured in a FACS analysis in SH-EP MYCN-ER cells expressing an inducible shRNA targeting DCP1A. Cells were treated for 6 d with 100 nM 4-OHT and 1 µg/ml DOX. Data represents mean with SD of biological triplicates.

With the aim of testing *MYCN*-amplified cells for their putative dependency on DCP1A, the same construct was infected in a panel of neuroblastoma cells. Unexpectedly, no obvious lethality and no preferentiality between differential *MYCN* status could be observed by colony formation assay (Figure 4.19).

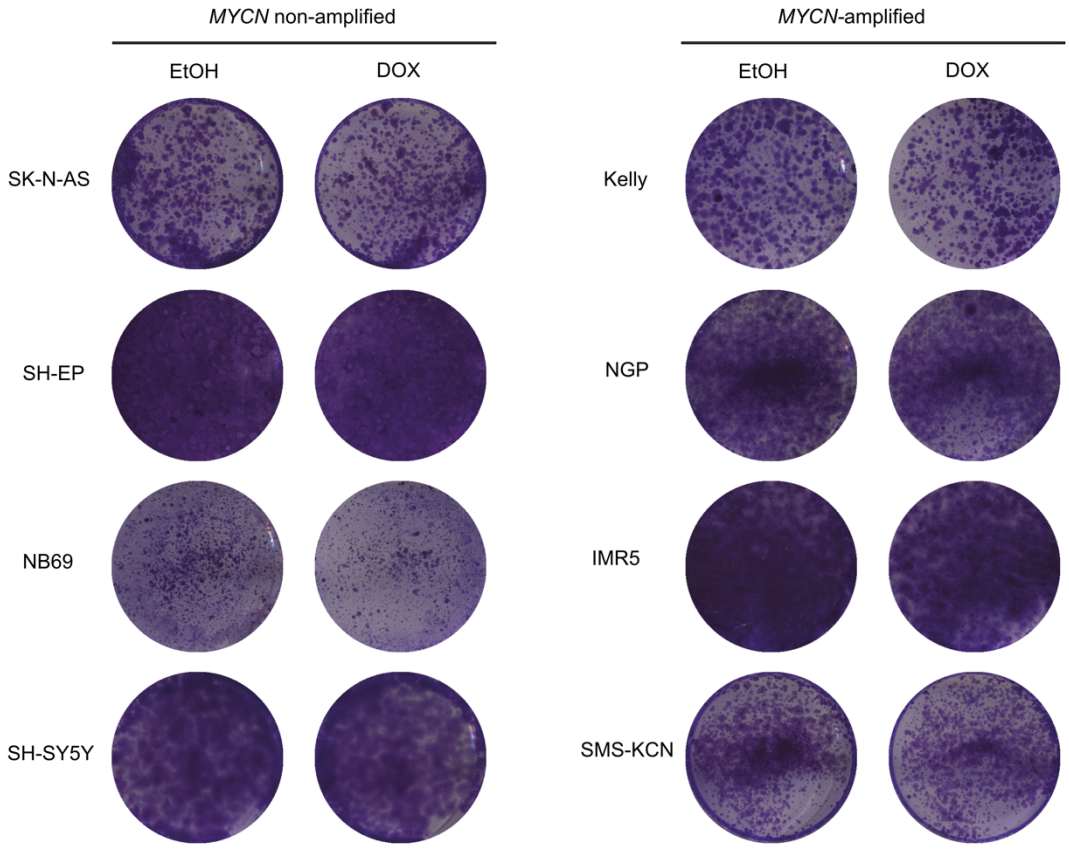

Figure 4.19 DCP1A knockdown in neuroblastoma cell lines
Knockdown of DCP1A (DOX, 1 µg/ml) for *MYCN* non-amplified (left) and *MYCN*-amplified (right) neuroblastoma cell lines.

Collectively, also the decapping factor DCP1A was essential to neuroblastoma cells, although only in the proof-of-principle SH-EP MYCN-ER system and upon acute activation of MYCN.

4.4.2 Loss of DCP1A leads to RNAPII accumulation within the gene body and after transcriptional end site

Presented results showed that both MYCN and BRCA1 can mediate the recruitment of DCP1A to RNAPII. Previous work indicated that a number of termination factors can influence the chromatin occupancy of RNAPII. For example, the knockdown of EDC3, DCP1A, DCP2 and TTF2 led to a decrease of RNAPII at the TSS and an increase further into the genomic region (Brannan et al., 2012). To better investigate the effect of DCP1A on the transcriptional machinery, ChIP-sequencing for total and Ser2-phosphorylated RNAPII was performed. As evidence before, the activation of MYCN induced an increase of RNAPII occupancy, especially the elongating form, on activated genes and a decrease on repressed ones (Figure 4.20 a, b). Interestingly, upon DCP1A knockdown, total RNAPII showed a general increased occupancy independently of the gene expression (Figure 4.20 a), similar to the RNAPII distribution upon

BRCA1 knockdown (Figure 4.9). DCP1A knockdown increased also the pSer2-RNAPII levels on activated genes and the difference to the EtOH condition on repressed genes was slightly damped (Figure 4.20 b).

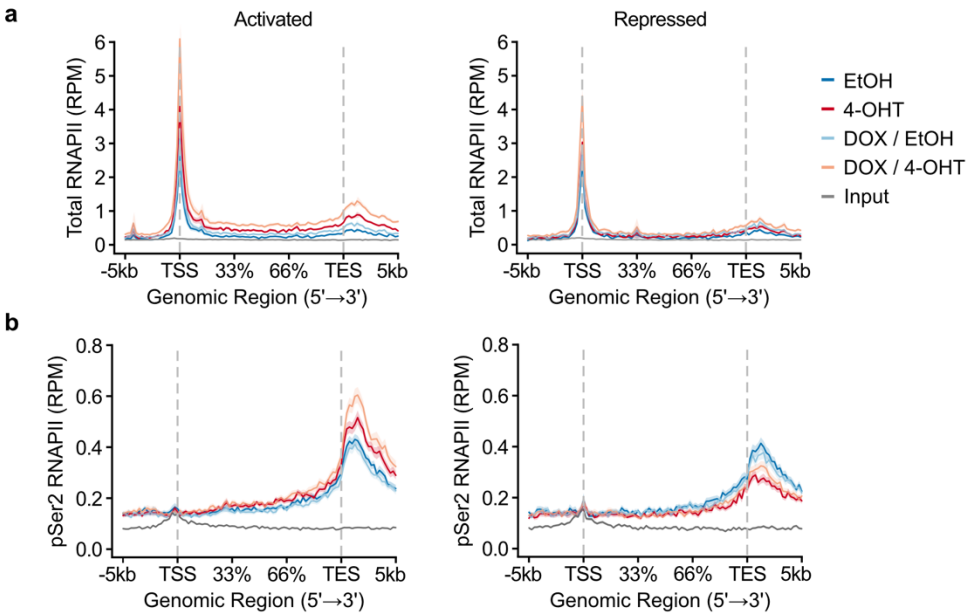

Figure 4.20 RNAPII occupancy upon DCP1A loss and MYCN activation
Metagene plots for total RNAPII (**a**) and pSer2-phosphorylated (**b**) RNAPII for 914 MYCN-activated (left) and 615 MYCN-repressed (right) genes in SH-EP MYCN-ER cells expressing an inducible shRNA against DCP1A (3 d 1 µg/ml DOX, 4 h 200 nM 4-OHT), n=2 for total RNAPII and pSer2-RNAPII.

The increased occupancy of RNAPII upon DCP1A loss could argue either for boost of transcription – as seen for the inhibition of ATM (Figure 4.11 and 4.12) – or for accumulation of RNAPII because of an obstacle. Whether transcription is upregulated could not be answered yet, whereas accumulation of RNAPII due to an obstacle will be investigated subsequently.

4.4.3 Recruitment of DCP1A prevents conflicts of transcription and replication

Since transcription and replication use both DNA as a template and are upregulated in highly proliferating cells, the replication machinery could potentially serve as an obstacle in this context that leads to increased RNAPII occupancy within gene bodies. Transcription-replication conflicts and DNA damage could be the consequences. Therefore, immunoblots of different DNA damage markers were performed to investigate, whether this scenario holds true upon DCP1A loss and MYCN activation. An increase of the pCHK1 and pS33-RPA32, targets of the ATR kinase (Blackford and Jackson, 2017; Olson et al., 2006), could be observed, indicating stalled replication forks upon the knockdown of DCP1A and the activation of MYCN (Figure 4.21 a). Downstream targets of ATM, such as pKAP1 and pCHK2, or pS4/8-RPA32 as

a target of DNA-PK, all sensing DSB, showed mild changes compared to MYCN activation alone (Figure 4.21 a). γH2A.x as a marker for DNA damage was also increased but already upon the sole MYCN activation (Figure 4.21 a). Additional immunofluorescence experiments confirmed these findings: both pS33-RPA32 and γH2A.x stainings were augmented in the double treated condition, with the latter moderately upregulation already in MYCN-activated cells (Figure 4.21 b).

γH2A.x can be a target of both DNA repair kinases, ATM and ATR (McManus and Hendzel, 2005; Ward and Chen, 2001). To test whether the damage that occurred during DCP1A knockdown and MYCN activation was mediated by DNA DSB, and therefore ATM, BLISS8 was performed to map DNA DSB. Interestingly, no major changes in DSB were visible throughout all conditions (Figure 4.21 c), suggesting that the damage was rather ATR-mediated and therefore resulted from stalled replication forks.

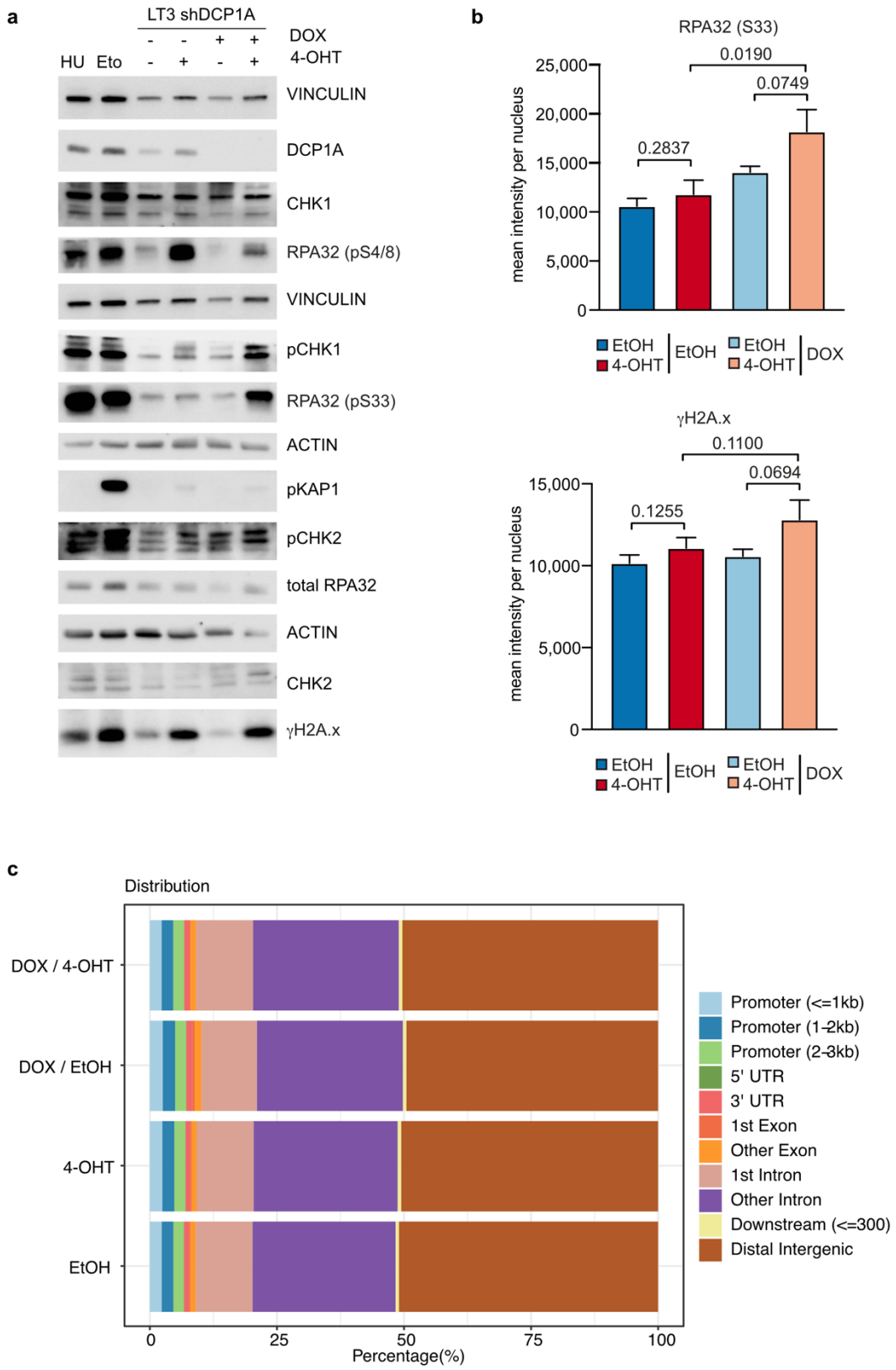

Figure 4.21 Knockdown of DCP1A and activation of MYCN lead to DNA damage
a Immunoblot of DNA damage markers in SH-EP MYCN-ER cells expressing an inducible shRNA against DCP1A. Cells were treated for 6 d with 100 nM 4-OHT and 1 µg/ml DOX where indicated. Vinculin and actin were used as loading controls. 0.5 mM Hydroxyurea (HU) and 20 µM Etoposide (Eto) were used as positive controls (n=3).
Figure legend continues on next page.

b Quantitative immunofluorescence of pRPA32-S33 and γH2A.x in SH-EP MYCN-ER cells expressing doxycycline inducible shDCP1A. Cells were treated for 6d with 100 nM 4-OHT, EtOH or 1 µg/ml DOX where indicated. Nuclei were counterstained with Hoechst. Shown is the mean and SD of biological triplicates. *P* values were calculated using a two-tailed, unpaired *t*-test with additional Welch's correlation.
c Relative genomic distribution of DSBs identified in BLISS8 of SH-EP MYCN-ER cells treated as described in **a**.

The knockdown of DCP1A and activation of MYCN resulted in accumulation of RNAPII within gene bodies and after TES and led to the activation of ATR resulting from stalled replication forks. To inquire whether this caused transcription-replication conflicts, PLAs were performed. The proximity of RNAPII with the sliding clamp of the replication machinery, PCNA, as well as the components RAD9 and RAD1 of the 9-1-1 complex were assessed as an indication of transcription-replication conflicts. Strikingly, the number of collisions were rather constant in all tested conditions but consistently increased upon DCP1A knockdown and MYCN activation, where an increase of PLA foci could be measured for RNAPII with PCNA as well as with RAD9 and RAD1 (Figure 4.22).

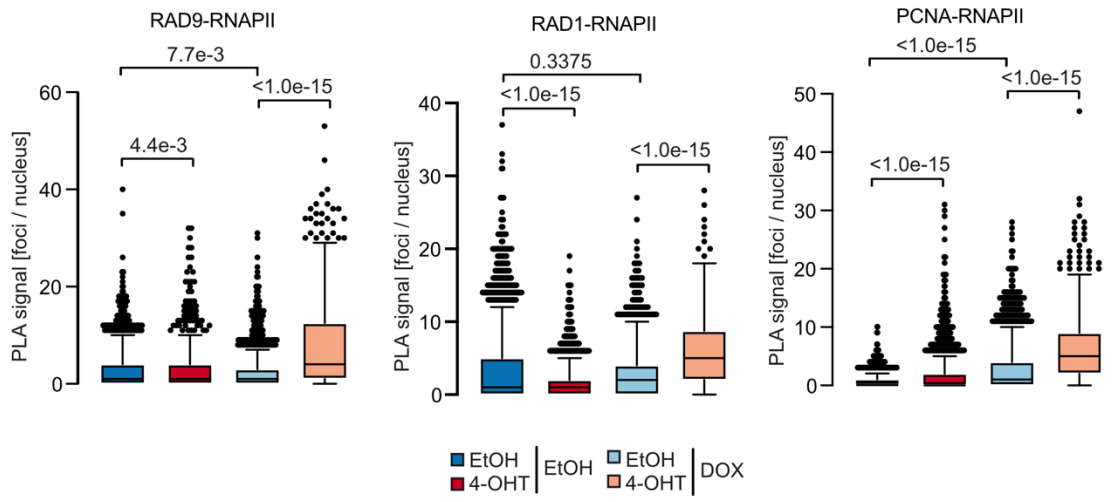

Figure 4.22 Transcription Replication conflicts occur upon DCP1A loss and MYCN activation
Quantification of Proximity ligation assay (PLA) showing the proximity of RNAPII with RAD9 (left, n=2), RAD1 (middle, n=3) and PCNA (right, n=3) in SH-EP MYCN-ER cells expressing inducible shRNA against DCP1A (6d, 100 nM 4-OHT, 1 µg/ml DOX). *P* values were calculated using a two-tailed Wilcoxon rank-sum test. In the box plot, the central line represents the median, and the borders of the boxes show the interquartile range of the plotted data. The whiskers extend to 1.5 x the interquartile range. Shown is one representative experiment.

In this view, DCP1A is able to protect the cell from DNA damage, resulting from transcription-replication conflicts and stalled replication machineries rescued by the activation of the ATR pathway.

4.4.4 Activation of ATR prevents early apoptosis

The knockdown of DCP1A and the acute activation of MYCN resulted in a synthetic lethal and apoptotic phenotype (Figure 4.18). To test whether the proliferation of those cells was connected to the collisions of transcription and replication machineries, DNA synthesis was measured by EdU incorporation and visualised by Click-IT reaction. The assay showed that loss of DCP1A together with acute MYCN activation led to a striking decrease of EdU incorporation (Figure 4.23 a). Proliferation defects and replication fork progression can be visualised by DNA fiber assays (Figure 4.23 b), which was performed as introduced earlier (Figure 4.5). The replication fork progression in cells that were treated for three days showed a marked decrease in fork progression upon concomitant DCP1A knockdown and MYCN activation as compared to the other tested conditions (Figure 4.23 c). Interestingly, cells treated for six days - thus the condition where ATR was activated and transcription-replication conflicts occurred - the reduction in fork progression was not visible anymore (Figure 4.23 d).

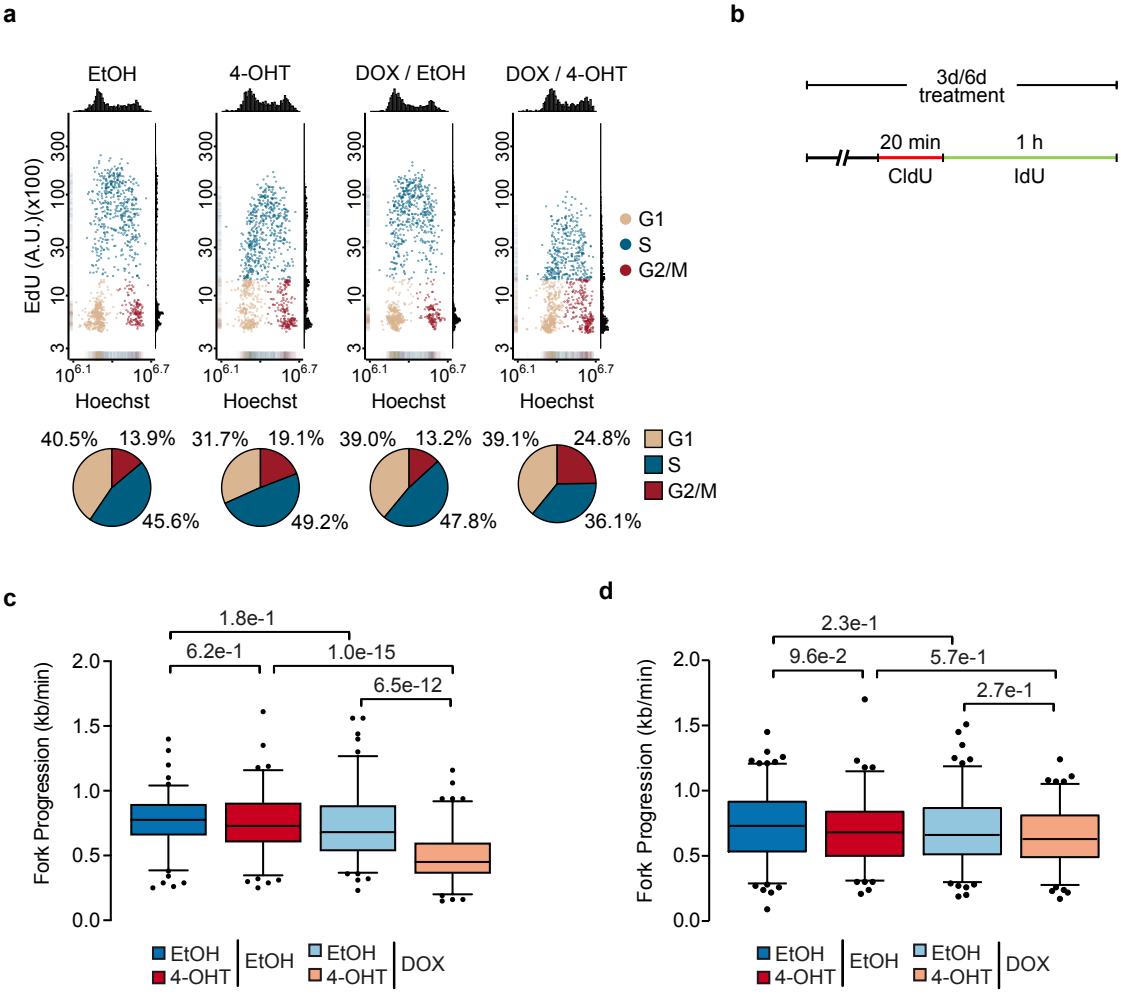

Figure legend on next page.

Figure 4.23 Proliferation defects upon DCP1A loss and MYCN activation
a Two dimensional quantitative single cell immunoflurorescence of SH-EP MYCN-ER cells expressing doxycycline (DOX) inducible shRNA against DCP1A. Cells were treated for 6d with 100 nM 4-OHT, EtOH or DOX where indicated and pulsed for 30 min with 10 µM 5-ethynyl-2-deoxyuridin (EdU) prior to fixation. Nuclei were counterstained with Hoechst to determine cell cycle phase. y-axis shows EdU incorporation, x-axis shows Hoechst content (n=3).
b Scheme of experimental setup for the DNA fiber assays that were carried out by Celeste Giansanti, Laboratory of Prof. Dobbelstein, Göttingen.
c, d Box plots showing the fork progression measured during both labels in SH-EP MYCN-ER cells, expressing an inducible shRNA against DCP1A. Cells were treated either for 3 d with 100 nM 4-OHT, EtOH and 1 µg/ml DOX where indicated for 3 d (**c**) or 6 d (**d**). Shown is one representative experiment (n=2 for 3 d, n=2 for 6 d). *P* values were calculated using a two-tailed, unpaired *t*-test with additional Welch's correlation. The central line within the boxes reflects the median, the borders show the lower and upper quartile of the plotted data, with 10th-90th-percentile whiskers and outliers are shown as dots. Number of analysed fibers, 3 d: EtOH EtOH (n = 124), EtOH 4-OHT (n = 105), DOX EtOH (n = 107), DOX 4-OHT (n = 106). 6 d: EtOH EtOH (n = 121), EtOH 4-OHT (n = 111), DOX EtOH (n = 128), DOX 4-OHT (n = 111).

This indicated that ATR prevented replication fork collapse and apoptosis in these cells. To prove this hypothesis, cells were treated together with the ATR inhibitor AZD6738 upon concomitant DCP1A knockdown and MYCN activation. Tellingly, while single treatments of AZD6738 or doxycycline / 4-OHT alone did not affect colony formation within six days, their combination reduced colony formation remarkably (Figure 4.24). The activation of ATR upon DCP1A knockdown and MYCN activation (Figure 4.20) prevents apoptosis in the first place.

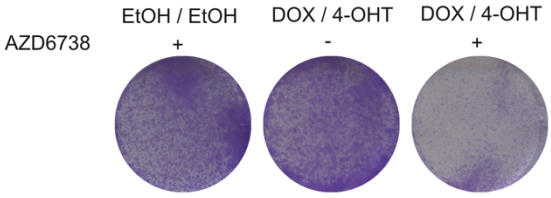

Figure 4.24 ATR activation prevents cells from early apoptosis
Colony formation assays in SH-EP MYCN-ER cells expressing doxycycline inducible shRNA against DCP1A. Cells were pre-treated for 3 d with 100 nM 4-OHT and 1 µg/ml DOX or EtOH where indicated, followed by 3 d of 1 µM AZD6738 treatment where indicated. Colonies were stained with crystal violet (n=4).

To summarise, the data showed that DCP1A was necessary for premature termination. Loss of DCP1A resulted in accumulation of RNAPII, transcription-replication conflicts, genomic instability, proliferation defects and made those cells more vulnerable to the inhibition of ATR.

5 Discussion

MYCN, whose amplification in neuroblastoma is considered a driving event of tumorigenesis and a poor prognostic marker for patient outcome, has been studied together with its partner proteins. The further characterisation of MYCN as oncogene and the involvement of partner proteins might lead to potential new therapeutic targets. One hit for synthetic lethality in a MYCN-dependent context was the tumour suppressor protein BRCA1 which showed higher expression levels in *MYCN*-amplified neuroblastoma and correlates with the *MYCN* status for worse overall survival (Herold et al., 2019). Therefore, the aim of this study was to elucidate the role of BRCA1 in neuroblastoma and especially in MYCN-driven transcription.

5.1 BRCA1 affects the DNA damage response in neuroblastoma

BRCA1 is described as a tumour suppressor in several tumour entities and is one of the key players for DNA damage response, amongst other things responsible for homologous recombination (HR) that takes place in S- and G2-phase (Venkitaraman, 2014). HR together with non-homologous end-joining (NHEJ) are the two pathways involved in DSB repair (Brandsma and Gent, 2012). MYCN activation induced BRCA1 recruitment to promoters, mainly in S and G2/M-phase (Figure 4.6). This suggests that BRCA1 is required to keep the 'fragile' promoter region, reflected by increased DSB incidence (Endres et al., 2021; Madabhushi et al., 2015), stable. The results in this study showed that BRCA1 recruitment occurs before the CTD phosphorylation by CDK7 happens and is independent of the transcriptional activity itself (Figure 4.7). This could imply that binding of MYCN to chromatin itself is sufficient to sensitise the DNA damage response followed by the recruitment of BRCA1 to prevent DNA damage at promoters. Since transcription initiation happens as a two-step process (Aibara et al., 2021; Holstege et al., 1996) and THZ1 is a specific CDK7 inhibitor, the XBP activity beforehand could remain unperturbed and the promoter stays open. The usage of THZ1 in other studies shows decreased RNAPII occupancy at promoters as expected, but still some RNAPII molecules remaining bound to promoters (Chipumuro et al., 2014). In this context, the remaining RNAPII would need to be cleared off for ongoing replication and would result otherwise in transcription-replication conflicts which makes BRCA1 recruitment necessary independent of transcription *per se*. Promoters bound by MYCN could therefore be defined as early replication fragile sites, zones that are difficult to replicate, with increased occupancy of RNAPII and replication fork subunits (Sanchez et al., 2020) which break more easily upon elevated MYC expression (Barlow et al., 2013).

53BP1 is the key component of NHEJ throughout all cell cycle phases and inhibits BRCA1 accumulation at DSBs (Escribano-Diaz et al., 2013). The increased 53BP1 foci upon BRCA1 knockdown and MYCN activation (Figure 4.5) could result from cells trying to repair their DSBs via NHEJ since HR via BRCA1 is not available. 53BP1 foci are also an indicator for the persistence of damage though the cell cycle (Lezaja and Altmeyer, 2018). In this view, cells accumulated in G1-phase upon BRCA1 knockdown (Figure 4.4), probably because of increased DNA damage, are forced by MYCN into S-phase, which would then lead to problems in replication. Recent work showed that MYC together with the PAF complex leads to the coordination of transcription with the chromatin accessibility for DNA repair factors around the +1 nucleosome (Endres et al., 2021). This would mean that in the context of MYCN, DSB repair via BRCA1 plays a major role in *MYCN*-driven neuroblastoma and is necessary to keep the promoter region repaired and transcription ongoing.

5.2 MYCN mediates its transcriptional profile with the help of the DNA damage response

The knockdown of BRCA1 resulted in a massive accumulation of RNAPII at promoter regions and all over the gene body but a decrease of elongating RNAPII (Ser2-phosphorylated) within the gene body (Figure 4.9). The contradictory metagene profile of total and Ser2-phosphorylated RNAPII could mean that RNAPII is not elongating properly and is stuck because of an obstacle such as DSB or R-loops. This could lead to ubiquitination of the hyperphosphorylated RNAPII, turnover and dissociation from chromatin as described previously (Tufegdzic Vidakovic et al., 2020). The ubiquitination of the largest RNAPII subunit, RPB1, could also prohibit the recognition of the elongating RNAPII by the Ser2-phosphorylation of CTD antibody. The usage of the phosphorylation independent antibody (‘total’, raised against the N-terminus of RNAPII) would therefore provide an objective image of RNAPII within the gene body and showed increased occupancy of RNAPII which would argue for stalled transcription machineries. Interestingly, BRCA1 itself, in a complex with BARD1, acts as E3 ligase (Hashizume et al., 2001) that marks stalled RNAPII at damage sites (Kleiman et al., 2005). The ubiquitin marking of the RNAPII in the pre-initiation complex (PIC) results in transcriptional repression since transcription factors cannot bind (Horwitz et al., 2007). Generally speaking, cells developed different mechanisms to deal with stalled RNAPII, which usually result in R-loop formation or conflicts of transcription and replication which need to be cleared off the chromatin (Noe Gonzalez et al., 2021). In this view, the ubiquitination and the subsequent turnover of RNAPII plays a major role (Wilson et al., 2013). Recent studies

showed, that the ubiquitination of RNAPII is essential for the DNA damage response (Tufegdzic Vidakovic et al., 2020) since the 'recycling' of RNAPII and the pool of available RNAPII is necessary for a transcriptional restart after DNA damage. Furthermore, the ubiquitination of stalled RNAPII upon DNA damage promotes another repair mechanism involved in DNA damage within transcribed regions, the transcription coupled nucleotide excision repair (TC-NER) (Nakazawa et al., 2020). Whether BRCA1 is necessary for the ubiquitination of RNAPII upon acute overexpression of MYCN and dictates transcriptional regulation through its E3 Ligase function cannot formally be ruled out, but was not addressed within this study.

Although the knockdown of BRCA1 showed a massive accumulation of RNAPII (Figure 4.9), only mild effects could be noticed on gene expression (Figure 4.10). As seen before (Herold et al., 2019), the activation of MYCN led to an up- or downregulation of MYC targets up and immune genes down, respectively (both well-known MYC regulated gene sets). Interestingly, BRCA1 knockdown induced an upregulation of former repressed immune gene sets (Figure 4.10). This could be explained either by a direct gene regulation or an intrinsic signalling, such as cGAS. The cytosolic cGAS is a component and activator of the innate immune response that detects cytosolic DNA (Sun et al., 2013; Wu et al., 2013). Interestingly, micronuclei can form by cell cycle progression upon DSB and serve as a depot for cGAS (Harding et al., 2017), which links the cGAS pathway to DNA damage.

Consistently, the inhibition of ATM, the upstream kinase of BRCA1, showed similar results. The inhibition of ATM upon MYC activation had mild effects on transcriptional regulation genome-wide (Figure 4.11, 4.12), but both activated and repressed genes showed an increase of nascent transcription visible in metagene plots (Figure 4.11). The transcriptional repression in *MYC*-driven cells is mediated through the interaction of MYC and MIZ1, that leads to resistance to antimitotic signalling (Wiese et al., 2013). Since the interaction of MYCN with the zinc finger protein and repressor MIZ-1 is weaker than for MYC (Vo et al., 2016), there might be a different mechanism involved in gene repression in *MYCN*-driven cells, thus explaining the behaviour of repressed genes upon BRCA1 depletion or ATM inhibition. Furthermore, ATM and BRCA1 can act as transcriptional repressors via H2A ubiquitination through PRC1 (Kalb et al., 2014b; Ui et al., 2015), or H2B ubiquitination (Moyal et al., 2011) or via the downstream target KAP1 (TRIM28), whose contribution to gene regulation is a matter of debate (Goodarzi et al., 2011; Ziv et al., 2006). In this context, ATM through BRCA1 and decapping proteins might be the reason for transcriptional downregulation of genes in a

MYCN dependent context. However, the involvement of any of these mediators in the described phenotype needs further investigation.

The increased levels of nascent transcripts when ATM is inhibited and also the increased levels of total RNAPII in the situation where BRCA1 is lost, could also be explained by both proteins being involved in the spliceosomal process because nascent transcripts are not further processed and this leads to stalled RNAPII. Interestingly, ATM mediates the assembly of the core spliceosome in a non-canonical signalling pathway: If RNAPII stalls upon a DNA lesion, the spliceosome gets removed to make the chromatin accessible for DNA repair factors and R-loops accumulate which initiates a positive feedback loop through ATM that ends in alternative splicing genome-wide (Tresini et al., 2016; Tresini et al., 2015). Also BRCA1, the downstream target of ATM, builds a complex with the spliceosomal proteins upon DNA damage to regulate the mRNA stability of different DNA damage repair proteins (Savage et al., 2014). It was already shown that *MYC*-driven cells are highly dependent on a functional spliceosome (Cossa et al., 2020). But even though there is evidence for the involvement of ATM and BRCA1 in the splicing process, further analyses are warranted, preferentially using techniques (e.g. NET-sequencing) which are the standard for the investigation of splicing events (Churchman and Weissman, 2011).

5.3 BRCA1 prevents R-loop accumulation through premature termination

ChIP-sequencing experiments upon BRCA1 loss showed an accumulation of total RNAPII and the Ser2-phosphorylated form at promoters of all expressed genes (Figure 4.9). Paused and therefore stalled RNA polymerase occur naturally during a transcription cycle, either at the promoter proximal pausing or the +1 nucleosome (Noe Gonzalez et al., 2021). The pausing and release of RNAPII is mediated by NELF (Adelman and Lis, 2012) and the +1 nucleosome plays a major role for a second pausing step of RNAPII that is dependent on the negative elongation factor NELF and rather on the recruitment of the 5'capping machinery (Aoi et al., 2020). BRCA1 is known for its interaction with NELF (Ye et al., 2001). However, the activation of MYCN led to a decrease of NELF-E chromatin recruitment and the knockdown of BRCA1 increased – and not decreased, as expected – NELF binding to chromatin (Figure 4.13). This simply mirrored the chromatin occupancy of RNAPII rather than explained its gene regulatory function, even though NELF is also described for transcriptional repression at DSB (Awwad et al., 2017). So to say, the presented data show either a BRCA1 independent function of NELF

or the dissociation of NELF from RNAPII is perturbed upon BRCA1 knockdown which leads to RNAPII stalling.

The knockdown of BRCA1 and the activation of MYCN not only led to accumulation of RNAPII, but also the formation of R-loops: the activation of MYCN decreased the formation of R-loops (Figure 4.13), correlating with its pause release effect (Herold et al., 2019). However, the knockdown of BRCA1 upon MYCN activation led to an increase of R-loops (Figure 4.13) at promoter proximal sites of either MYCN target genes, or sites were R-loops were detected in other datasets (Chen et al., 2017). BRCA1 can suppress the formation of R-loops both at promoter proximal sites (Zhang et al., 2017) and at TES (Hatchi et al., 2015). In particular, the resolution of R-loops at the TES involves the DNA/RNA-helicase SETX (Hatchi et al., 2015). The ChIP of SETX, however, showed similar recruitment to chromatin when MYCN was activated, but also an increase where BRCA1 was knocked down (Figure 4.13). Therefore, neither NELF nor SETX were involved in the BRCA1 dependent resolution of R-loops. Whether the R-loops were the cause or the consequence of the accumulation of RNAPII remains elusive. The formation of R-loops leads also subsequently to the activation of the cGAS pathway and interferon response (Crow and Manel, 2015), which could explain the upregulation of immune genes in mRNA-sequencing upon BRCA1 knockdown.

A further emerging interpretation of BRCA1's role upon MYCN activation postulates its direct involvement in the chromatin occupancy of RNAPII and in particular RNAPII premature termination. Since paused RNAPII inhibits new initiation of transcription (Shao and Zeitlinger, 2017), it is fascinating to hypothesise that MYCN – a transcription factor – can promote the eviction of stalled RNAPII to 'free' genes to be transcribed. In this view, the increased chromatin recruitment of BRCA1 upon CDK9 inhibition and BRCA1's higher proximity to paused RNAPII (Herold et al., 2019) suggest that BRCA1 is not only involved in the repair of DNA damage, but also fulfils further tasks connected to transcription.

Strikingly, the presented results indicate that BRCA1 promotes the recruitment of decapping factors to stalled RNAPII. Two decapping factors, EDC4 and DCP1A, were investigated. Importantly, DCP1A chromatin recruitment was abolished upon the knockdown of BRCA1 (Figure 4.15) while EDC4 displayed an increase of intergenic peaks (Figure 4.15), probably reflecting EDC4's role independent of decapping in the TOPBP1/BRIP1 complex to mimic BRCA1 for the DNA damage response as described previously (Hernandez et al., 2018). Consistently, the proximity of DCP1A to RNAPII was strongly reduced upon BRCA1 knockdown and inhibition of ATM (Figure 4.16). This suggests the existence of a novel

mechanism where ATM and BRCA1 are necessary for the recruitment of DCP1A to the pausing site and RNAPII to promote premature transcription termination to prevent the cell from DNA damage. Interestingly, EDC4 seems to have an additional role in neuroblastoma and works independent of the promoter proximal termination and decapping pathway.

5.4 DCP1A is involved in termination of RNAPII

Similarly to BRCA1, the knockdown of DCP1A was synthetic lethal with the activation of MYCN (Figure 4.18). Interestingly, the results indicate that this holds true only upon acute activation of MYCN and not in cell lines with stable *MYCN*-amplification (Figure 4.19). The only *MYCN* non-amplified cell line that reacted to the knockdown of DCP1A was NB69 which had also the highest DCP1A protein levels (Figure 4.18). This indicates that decapping is necessary in a cell type specific context and – additionally – upon acute activation of the oncoprotein.

Importantly, the recruitment of DCP1A to RNAPII increased in S- and further in G2/M-phase (Figure 4.17), as seen also for BRCA1. This argues for DCP1A as a downstream acting protein of BRCA1. However, DCP1A had the highest tendency towards RNAPII that is Ser2 phosphorylated (Figure 4.17). This suggest that the BRCA1-mediated mechanism involved in premature termination is necessary especially for cells in S- and G2/M-phase and polymerases that are elongating.

Comparable to the data seen for the RNAPII chromatin occupancy upon BRCA1 loss, the knockdown of DCP1A upon MYCN activation led to an accumulation of RNAPII all over the gene (Figure 4.20) and a read through effect of Ser2-phosphorylated RNAPII. It was especially increased after the TES on activated genes and decreased to a lesser extent on repressed ones (Figure 4.20). This was already shown for DCP1A and other decapping factors (Brannan et al., 2012). It indicates that decapping might be necessary for an intragenic premature termination pathway if obstacles like DNA breaks or a replication forks occur. This would block productive elongation or lead to the removal of the transcriptional machinery, also when transcription-replication conflicts occur (Hamperl and Cimprich, 2016). Decapping could prevent DNA damage and R-loops to keep transcription elongation ongoing, since also XRN2 prevents the accumulation of R-loops and is necessary for transcription termination upon DNA damage to make chromatin accessible for repair factors (Morales et al., 2016).

Since MYCN bound only to promoters and not within gene bodies, it is difficult to say whether it also affects the shuttling of decapping factors to the nucleus which leads to termination of elongating RNAPII within the gene body. However, the mRNA abundance in general can favour the shuttling of different RNA binding proteins (Gilbertson et al., 2018). Decapping factors are typically cytoplasmic-resident, indicating a MYCN-driven and BRCA1-mediated signal that increased the shuttling of DCP1A to the nucleus and led to premature termination in case of a stalled RNAPII.

The backtracking of RNAPII at the pausing site, its reinitiation or premature termination are regulating gene expression (Sheridan et al., 2019). The rapid degradation of XRN2 via an AID system leads to inhibition of premature termination (Eaton et al., 2020), and the elongation rate of RNAPII influences the kinetics between XRN2 and RNAPII since termination either happens through XRN2 or translocation of RNAPII by the elongation complex. This dictates where and how termination happens (Fong et al., 2015). These evidences indicate that a balance between transcription termination and productive elongation regulates gene expression and might be responsible for the MYCN-induced up- or downregulation of certain genes. However, what the exact signal for termination factors is, where and how to stop, and how MYCN influences this in detail, needs further investigation.

The cap binding complex controls the promoter proximal pause release step in a gene specific manner (Rambout and Maquat, 2020) and serves as a quality control mechanism (Jiao et al., 2013). A previous publication indicated that MYC influences transcript stability via capping of nascent transcripts (Lombardi et al., 2016). The presented results showed furthermore that MYCN together with BRCA1 is involved in the decapping mechanism of nascent transcripts followed by premature termination of stalled RNAPII.

5.5 DCP1A as decapping factor is involved in the coordination of transcription and replication

Premature transcription termination regulates gene expression (Kamieniarz-Gdula and Proudfoot, 2019) and just a minority of RNA polymerases are going into productive elongation while the rest is prematurely terminated (Steurer et al., 2018). As discussed earlier, this process can happen either via ubiquitination and degradation of RNAPII or through the exonuclease XRN2 as a ‘torpedo’. This mechanism is needed to prevent stalled polymerases, transcription-replication conflicts and ultimately to avoid DNA damage (Noe Gonzalez et al., 2021). It coordinates also pre-mRNA processing (Davidson et al., 2012). Indeed, the knockdown of

DCP1A upon acute activation of MYCN led to the accumulation of DNA damage and the activation of the DNA damage response via ATR by phosphorylation of RPA32-S33 and CHK1-S345 (Figure 4.21). The DNA damage that occurred was not due to increased DSB because BLISS8 showed similar results in all tested conditions (Figure 4.21), so the damage signalling was likely mediated by ATR and stalled replication forks. The sliding clamp of the replication fork, PCNA, and the structurally similar 9-1-1 complex, which gets loaded on DNA upon DNA damage (Eichinger and Jentsch, 2011) and is necessary for the activation and phosphorylation of CHK1 via TOPBP1 (Delacroix et al., 2007), showed increased proximity with RNAPII upon loss of DCP1A and MYCN activation (Figure 4.22). Interestingly, under these conditions cells showed defects in proliferation, as indicated by the reduced EdU incorporation and a decrease of fork progression after three days (Figure 4.23). DNA damage measured as γH2A.x chromatin marks lead to transcriptionally inactive genomic regions, eventually to prevent collisions between replication and transcription (Blackford & Jackson, 2017). In this view, DCP1A and ATR are needed for the regulation of these processes in a MYCN-dependent context, which result otherwise in stalled and maybe collapsed replication forks leading to damaged DNA, perturbed cell progression or even cell death.

The orientation of the collision dictates which DNA damage pathway gets activated. Co-directional collisions lead to ATM kinase activation and decrease of R-loops, since transcription is getting downregulated. Whereas, head-on conflicts lead to the activation of the ATR dependent DNA damage response and R-loop levels increase (Hamperl et al., 2017). The premature termination via DCP1A prevents head-on conflicts of the RNAPII with the replication fork. This prevention would lead otherwise to transcription read through, DNA damage and decreased EdU incorporation, as seen with the loss of pre-mRNA cleavage factors before (Teloni et al., 2019). Whether this conflict occurs at promoters, where BRCA1 binds, or at TES, where the pS33-RPA32 signal increased as previously shown (Promonet et al., 2020), needs further investigation also because of the increased proximity of DCP1A and Ser2-phosphorylated RNAPII (Figure 4.17) and the massive accumulation of pSer2-RNAPII upon DCP1A loss and MYCN activation around the TES (Figure 4.20). However, it is not only the ATR kinase that protects stalled replication forks: Also the dimer of BRCA1 and BARD1 that promotes replication fork protection (Daza-Martin et al., 2019), arguing that BRCA1 is not only involved in the DNA damage repair in neuroblastoma (Chapter 5.1) but can also prevent – at the promoter but also within the gene body – fork collapses by recruiting the decapping machinery and terminate transcription.

5.6 Conflict of transcription and replication could serve as a therapeutic target

As described earlier, it might be that ATR rescues the stalled replication forks from a collapse which would result in DNA breaks (Chapter 5.5). Interestingly, if the ATR activation rescued the stalled forks at first place, cells should be more sensitive to ATR inhibition. Indeed, the cells with DCP1A knockdown upon MYCN activation together with the ATR inhibition showed drastic reduction in colony formation assays within a few days compared to the single treatment of ATR inhibition or the knockdown of DCP1A and MYCN activation alone (Figure 4.24). Head-on conflicts of transcription and replication, observed upon DCP1A loss and MYCN activation, seem to be rescued by ATR and RPA32. ATR blocks the origin of replication (ORI) firing and prevents the cells from replication catastrophe (Toledo et al., 2013). The uncontrolled firing of ORIs leads to exhaustion of the single stranded binding protein RPA32 and subsequently to apoptosis. Strikingly, cells showed increased apoptosis upon DCP1A loss and MYCN activation over several days even with proficient ATR (i.e., which rescued the stalled replication forks): This is likely due to progressive RPA32 exhaustion after several rounds of cell division or the collapse of stalled replication forks and increased DNA damage.

Overall, the stabilisation of replication forks appears to have a pivotal role in the metabolism of proliferative cells. Mechanistically, highly proliferating cells driven by acute activation of MYCN appear to have a small tolerance range in dealing with deregulation of these processes. Deregulated transcription though the inhibition of BRD4 showed an accumulation of R-loops and transcription replication conflicts (Lam et al., 2020). Furthermore, the inhibition of Aurora-A results in transcription-replication conflicts, ATR activation and shows a redistribution of RNAPII upon MYCN activation (Buchel et al., 2017) as described here with the knockdown of DCP1A. Importantly, this could be harnessed therapeutically as recently shown for the proposed combinatorial therapy of Aurora-A inhibitors with ATR inhibitors in neuroblastoma mouse models (Roeschert et al., 2021).

5.7 Conclusions

There is an ongoing debate about the oncogenic potential of the MYC proto-oncogene family. Through their genome wide binding to thousands of promoters, they can be discussed as global amplifiers. However, as transcription factors, they are also defined as regulators of specific gene expression profiles, resulting in up- and downregulation of certain genes (Baluapuri et al., 2020). Recent studies postulate a transcription factor and gene regulatory independent function

of MYC proteins, p.e. the interplay of MYC together with the transcription elongation factor PAF1 which makes chromatin accessible for repair factors to coordinate transcription and DNA repair (Endres et al., 2021). This mechanism can hold the promoter region stable, which has an increased capability of DSB (Madabhushi et al., 2015).

Collectively, these findings suggest a major change in perspective concerning the MYC family as 'transcription factors', rather suggesting they are 'transcription coordination factors'. The data presented in this study would also argue for a transcription factor independent function of MYCN together with its partner proteins involved in DNA damage, like BRCA1, and premature termination, like DCP1A. These factors seem to be needed to start transcription in general or keep transcription levels high while the cancer cell is proliferating extensively. BRCA1 gets recruited by MYCN to promoters at a step when the CTD residue of RNAPII is not yet phosphorylated by CDK7 but the promoter region is potentially already open through the action of XBP. BRCA1 is necessary for the recruitment of decapping factors in case a replication fork is entering the promoter region, to promote premature termination of RNAPII to continue replication and prevent transcription-replication conflicts (Figure 5.1).

Defining the MYC proteins more as 'coordinators of transcription' with essential processes as DNA damage repair or replication could lead to more effective therapeutic strategies. The combinational treatment of ATR and Aurora-A inhibition showed positive effects on the survival of mice suffering from neuroblastoma (Roeschert et al., 2021). This combinational treatment led to the activation of the immune system and the infiltration of immune cells into tumour mass. Since such immune genes are generally repressed by MYC (e.g. Kortlever et al., 2017; Muthalagu et al., 2020) and MYCN (Herold et al., 2019; Layer et al., 2017), the interaction with the host immune system is downregulated. But already other studies showed that especially this interplay has an important role in targeting *MYC*-driven cancer cells (Topper et al., 2017). However, any therapeutic approach including direct targeting of DCP1A warrants further investigation. An hypothetical drug targeting DCP1A, for example, should discriminate between its nuclear and cytoplasmic functions. To this extent, further knowledge concerning the mechanism of MYCN-mediated DCP1A recruitment would be advantageous, as well as whether and how MYCN and BRCA1 influence the shuttling of decapping factors to the nucleus.

Collectively, this study showed an unknown function of tumour suppressor protein BRCA1 in neuroblastoma, where it rather acts as a 'tumour promoting protein' while supporting MYCN. In the mechanism presented here, MYCN uses BRCA1 to coordinate transcription with

replication though the interplay with the decapping factor DCP1A to prevent RNAPII accumulation by premature termination.

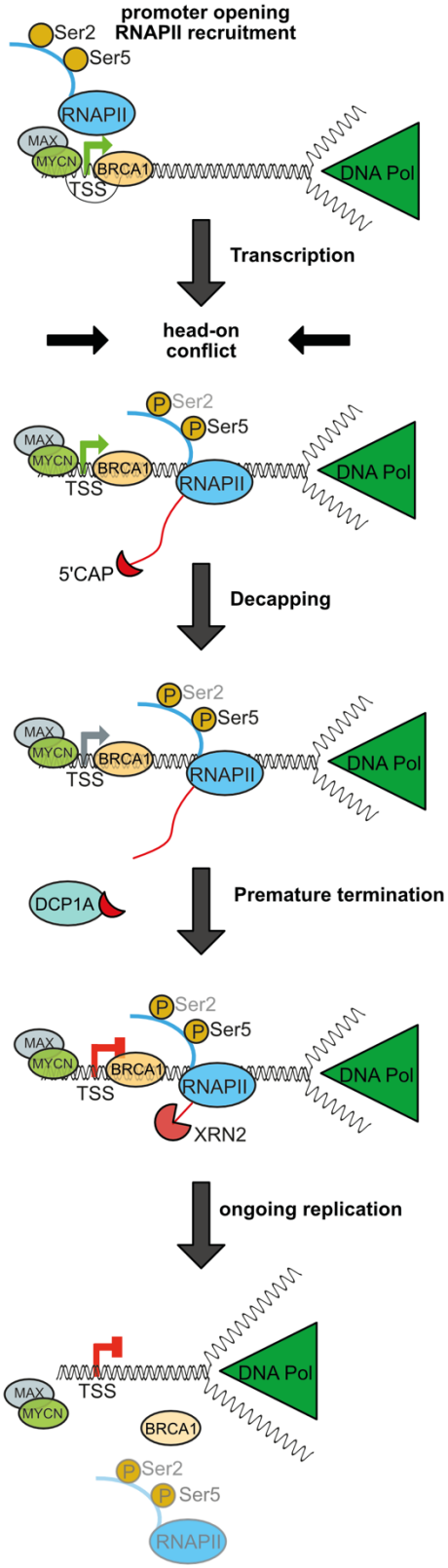

Figure 5.1 Model summarising the findings of this study.

6 Bibliography

Adelman, K., and Lis, J.T. (2012). Promoter-proximal pausing of RNA polymerase II: emerging roles in metazoans. Nat Rev Genet *13*, 720-731.

Adhikari, B., Bozilovic, J., Diebold, M., Schwarz, J.D., Hofstetter, J., Schroder, M., Wanior, M., Narain, A., Vogt, M., Dudvarski Stankovic, N.*, et al.* (2020). PROTAC-mediated degradation reveals a non-catalytic function of AURORA-A kinase. Nat Chem Biol *16*, 1179-1188.

Aguilera, A., and Garcia-Muse, T. (2012). R loops: from transcription byproducts to threats to genome stability. Mol Cell *46*, 115-124.

Ahn, J.Y., Schwarz, J.K., Piwnica-Worms, H., and Canman, C.E. (2000). Threonine 68 phosphorylation by ataxia telangiectasia mutated is required for efficient activation of Chk2 in response to ionizing radiation. Cancer Res *60*, 5934-5936.

Ahnesorg, P., Smith, P., and Jackson, S.P. (2006). XLF interacts with the XRCC4-DNA ligase IV complex to promote DNA nonhomologous end-joining. Cell *124*, 301-313.

Aibara, S., Schilbach, S., and Cramer, P. (2021). Structures of mammalian RNA polymerase II pre-initiation complexes. Nature.

Akhtar, M.S., Heidemann, M., Tietjen, J.R., Zhang, D.W., Chapman, R.D., Eick, D., and Ansari, A.Z. (2009). TFIIH kinase places bivalent marks on the carboxy-terminal domain of RNA polymerase II. Mol Cell *34*, 387-393.

Alt, F.W., Zhang, Y., Meng, F.L., Guo, C., and Schwer, B. (2013). Mechanisms of programmed DNA lesions and genomic instability in the immune system. Cell *152*, 417-429.

Anderson, S.F., Schlegel, B.P., Nakajima, T., Wolpin, E.S., and Parvin, J.D. (1998). BRCA1 protein is linked to the RNA polymerase II holoenzyme complex via RNA helicase A. Nat Genet *19*, 254-256.

Aoi, Y., Smith, E.R., Shah, A.P., Rendleman, E.J., Marshall, S.A., Woodfin, A.R., Chen, F.X., Shiekhattar, R., and Shilatifard, A. (2020). NELF Regulates a Promoter-Proximal Step Distinct from RNA Pol II Pause-Release. Mol Cell *78*, 261-274 e265.

Awwad, S.W., Abu-Zhayia, E.R., Guttmann-Raviv, N., and Ayoub, N. (2017). NELF-E is recruited to DNA double-strand break sites to promote transcriptional repression and repair. EMBO Rep *18*, 745-764.

Bacon, C.W., Challa, A., Hyder, U., Shukla, A., Borkar, A.N., Bayo, J., Liu, J., Wu, S.Y., Chiang, C.M., Kutateladze, T.G.*, et al.* (2020). KAP1 Is a Chromatin Reader that Couples Steps of RNA Polymerase II Transcription to Sustain Oncogenic Programs. Mol Cell *78*, 1133-1151 e1114.

Bai, R.Y., Koester, C., Ouyang, T., Hahn, S.A., Hammerschmidt, M., Peschel, C., and Duyster, J. (2002). SMIF, a Smad4-interacting protein that functions as a co-activator in TGFbeta signalling. Nat Cell Biol *4*, 181-190.

Baluapuri, A., Hofstetter, J., Dudvarski Stankovic, N., Endres, T., Bhandare, P., Vos, S.M., Adhikari, B., Schwarz, J.D., Narain, A., Vogt, M.*, et al.* (2019). MYC Recruits SPT5 to RNA Polymerase II to Promote Processive Transcription Elongation. Mol Cell *74*, 674-687 e611.

Baluapuri, A., Wolf, E., and Eilers, M. (2020). Target gene-independent functions of MYC oncoproteins. Nat Rev Mol Cell Biol *21*, 255-267.

Barlow, J.H., Faryabi, R.B., Callen, E., Wong, N., Malhowski, A., Chen, H.T., Gutierrez-Cruz, G., Sun, H.W., McKinnon, P., Wright, G.*, et al.* (2013). Identification of early replicating fragile sites that contribute to genome instability. Cell *152*, 620-632.

Barroso, S., Herrera-Moyano, E., Munoz, S., Garcia-Rubio, M., Gomez-Gonzalez, B., and Aguilera, A. (2019). The DNA damage response acts as a safeguard against harmful DNA-RNA hybrids of different origins. EMBO Rep *20*, e47250.

Bentley, D.L. (2014). Coupling mRNA processing with transcription in time and space. Nat Rev Genet *15*, 163-175.

Blackford, A.N., and Jackson, S.P. (2017). ATM, ATR, and DNA-PK: The Trinity at the Heart of the DNA Damage Response. Mol Cell *66*, 801-817.

Blumenthal, J., Behar, L., Elliott, E., and Ginzburg, I. (2009). Dcp1a phosphorylation along neuronal development and stress. FEBS Lett *583*, 197-201.

Boguslawski, S.J., Smith, D.E., Michalak, M.A., Mickelson, K.E., Yehle, C.O., Patterson, W.L., and Carrico, R.J. (1986). Characterization of monoclonal antibody to DNA.RNA and its application to immunodetection of hybrids. J Immunol Methods *89*, 123-130.

Boros-Olah, B., Dobos, N., Hornyak, L., Szabo, Z., Karanyi, Z., Halmos, G., Roszik, J., and Szekvolgyi, L. (2019). Drugging the R-loop interactome: RNA-DNA hybrid binding proteins as targets for cancer therapy. DNA Repair (Amst) *84*, 102642.

Bradford, M.M. (1976). A rapid and sensitive method for the quantitation of microgram quantities of protein utilizing the principle of protein-dye binding. Anal Biochem *72*, 248-254.

Brandsma, I., and Gent, D.C. (2012). Pathway choice in DNA double strand break repair: observations of a balancing act. Genome Integr *3*, 9.

Brannan, K., Kim, H., Erickson, B., Glover-Cutter, K., Kim, S., Fong, N., Kiemele, L., Hansen, K., Davis, R., Lykke-Andersen, J.*, et al.* (2012). mRNA decapping factors and the exonuclease Xrn2 function in widespread premature termination of RNA polymerase II transcription. Mol Cell *46*, 311-324.

Brockmann, M., Poon, E., Berry, T., Carstensen, A., Deubzer, H.E., Rycak, L., Jamin, Y., Thway, K., Robinson, S.P., Roels, F.*, et al.* (2013). Small molecule inhibitors of aurora-a induce proteasomal degradation of N-myc in childhood neuroblastoma. Cancer Cell *24*, 75-89.

Buchel, G., Carstensen, A., Mak, K.Y., Roeschert, I., Leen, E., Sumara, O., Hofstetter, J., Herold, S., Kalb, J., Baluapuri, A.*, et al.* (2017). Association with Aurora-A Controls N-MYC-Dependent Promoter Escape and Pause Release of RNA Polymerase II during the Cell Cycle. Cell Rep *21*, 3483-3497.

Bunch, H., Lawney, B.P., Lin, Y.F., Asaithamby, A., Murshid, A., Wang, Y.E., Chen, B.P., and Calderwood, S.K. (2015). Transcriptional elongation requires DNA break-induced signalling. Nat Commun *6*, 10191.

Burger, K., Ketley, R.F., and Gullerova, M. (2019). Beyond the Trinity of ATM, ATR, and DNA-PK: Multiple Kinases Shape the DNA Damage Response in Concert With RNA Metabolism. Front Mol Biosci *6*, 61.

Byun, T.S., Pacek, M., Yee, M.C., Walter, J.C., and Cimprich, K.A. (2005). Functional uncoupling of MCM helicase and DNA polymerase activities activates the ATR-dependent checkpoint. Genes Dev *19*, 1040-1052.

Carter, D.R., Murray, J., Cheung, B.B., Gamble, L., Koach, J., Tsang, J., Sutton, S., Kalla, H., Syed, S., Gifford, A.J.*, et al.* (2015). Therapeutic targeting of the MYC signal by inhibition of histone chaperone FACT in neuroblastoma. Sci Transl Med *7*, 312ra176.

Chan, S., Choi, E.A., and Shi, Y. (2011). Pre-mRNA 3'-end processing complex assembly and function. Wiley Interdiscip Rev RNA *2*, 321-335.

Chang, C.T., Bercovich, N., Loh, B., Jonas, S., and Izaurralde, E. (2014). The activation of the decapping enzyme DCP2 by DCP1 occurs on the EDC4 scaffold and involves a conserved loop in DCP1. Nucleic Acids Res *42*, 5217-5233.

Chen, G., and Deng, X. (2018). Cell Synchronization by Double Thymidine Block. Bio Protoc *8*.

Chen, L., Chen, J.Y., Huang, Y.J., Gu, Y., Qiu, J., Qian, H., Shao, C., Zhang, X., Hu, J., Li, H.*, et al.* (2018). The Augmented R-Loop Is a Unifying Mechanism for Myelodysplastic Syndromes Induced by High-Risk Splicing Factor Mutations. Mol Cell *69*, 412-425 e416.

Chen, L., Chen, J.Y., Zhang, X., Gu, Y., Xiao, R., Shao, C., Tang, P., Qian, H., Luo, D., Li, H.*, et al.* (2017). R-ChIP Using Inactive RNase H Reveals Dynamic Coupling of R-loops with Transcriptional Pausing at Gene Promoters. Mol Cell *68*, 745-757 e745.

Chipumuro, E., Marco, E., Christensen, C.L., Kwiatkowski, N., Zhang, T., Hatheway, C.M., Abraham, B.J., Sharma, B., Yeung, C., Altabef, A.*, et al.* (2014). CDK7 inhibition suppresses super-enhancer-linked oncogenic transcription in MYCN-driven cancer. Cell *159*, 1126-1139.

Churchman, L.S., and Weissman, J.S. (2011). Nascent transcript sequencing visualizes transcription at nucleotide resolution. Nature *469*, 368-373.

Cohen, S., Puget, N., Lin, Y.L., Clouaire, T., Aguirrebengoa, M., Rocher, V., Pasero, P., Canitrot, Y., and Legube, G. (2018). Senataxin resolves RNA:DNA hybrids forming at DNA double-strand breaks to prevent translocations. Nat Commun *9*, 533.

Core, L., and Adelman, K. (2019). Promoter-proximal pausing of RNA polymerase II: a nexus of gene regulation. Genes Dev *33*, 960-982.

Core, L.J., Waterfall, J.J., and Lis, J.T. (2008). Nascent RNA sequencing reveals widespread pausing and divergent initiation at human promoters. Science *322*, 1845-1848.

Cossa, G., Roeschert, I., Prinz, F., Baluapuri, A., Silveira Vidal, R., Schulein-Volk, C., Chang, Y.C., Ade, C.P., Mastrobuoni, G., Girard, C.*, et al.* (2020). Localized Inhibition of Protein Phosphatase 1 by NUAK1 Promotes Spliceosome Activity and Reveals a MYC-Sensitive Feedback Control of Transcription. Mol Cell *77*, 1322-1339 e1311.

Cramer, P. (2019). Organization and regulation of gene transcription. Nature *573*, 45-54.

Cristini, A., Groh, M., Kristiansen, M.S., and Gromak, N. (2018). RNA/DNA Hybrid Interactome Identifies DXH9 as a Molecular Player in Transcriptional Termination and R-Loop-Associated DNA Damage. Cell Rep *23*, 1891-1905.

Critchlow, S.E., Bowater, R.P., and Jackson, S.P. (1997). Mammalian DNA double-strand break repair protein XRCC4 interacts with DNA ligase IV. Curr Biol *7*, 588-598.

Crow, Y.J., and Manel, N. (2015). Aicardi-Goutieres syndrome and the type I interferonopathies. Nat Rev Immunol *15*, 429-440.

Daley, J.M., and Sung, P. (2014). 53BP1, BRCA1, and the choice between recombination and end joining at DNA double-strand breaks. Mol Cell Biol *34*, 1380-1388.

Dang, C.V. (2012). MYC on the path to cancer. Cell *149*, 22-35.

Dang, T.T., and Morales, J.C. (2020). XRN2 Links RNA:DNA Hybrid Resolution to Double Strand Break Repair Pathway Choice. Cancers (Basel) *12*.

Davidson, L., Kerr, A., and West, S. (2012). Co-transcriptional degradation of aberrant pre-mRNA by Xrn2. EMBO J *31*, 2566-2578.

Day, D.S., Zhang, B., Stevens, S.M., Ferrari, F., Larschan, E.N., Park, P.J., and Pu, W.T. (2016). Comprehensive analysis of promoter-proximal RNA polymerase II pausing across mammalian cell types. Genome Biol *17*, 120.

Daza-Martin, M., Starowicz, K., Jamshad, M., Tye, S., Ronson, G.E., MacKay, H.L., Chauhan, A.S., Walker, A.K., Stone, H.R., Beesley, J.F.J.*, et al.* (2019). Isomerization of BRCA1-BARD1 promotes replication fork protection. Nature *571*, 521-527.

de Pretis, S., Kress, T.R., Morelli, M.J., Sabo, A., Locarno, C., Verrecchia, A., Doni, M., Campaner, S., Amati, B., and Pelizzola, M. (2017). Integrative analysis of RNA polymerase II and transcriptional dynamics upon MYC activation. Genome Res *27*, 1658-1664.

Dejure, F.R., Royla, N., Herold, S., Kalb, J., Walz, S., Ade, C.P., Mastrobuoni, G., Vanselow, J.T., Schlosser, A., Wolf, E.*, et al.* (2017). The MYC mRNA 3'-UTR couples RNA polymerase II function to glutamine and ribonucleotide levels. EMBO J *36*, 1854-1868.

Delacroix, S., Wagner, J.M., Kobayashi, M., Yamamoto, K., and Karnitz, L.M. (2007). The Rad9-Hus1-Rad1 (9-1-1) clamp activates checkpoint signaling via TopBP1. Genes Dev *21*, 1472-1477.

Dutta, D., Shatalin, K., Epshtein, V., Gottesman, M.E., and Nudler, E. (2011). Linking RNA polymerase backtracking to genome instability in E. coli. Cell *146*, 533-543.

Eaton, J.D., Francis, L., Davidson, L., and West, S. (2020). A unified allosteric/torpedo mechanism for transcriptional termination on human protein-coding genes. Genes Dev *34*, 132-145.

Eaton, J.D., and West, S. (2020). Termination of Transcription by RNA Polymerase II: BOOM! Trends Genet *36*, 664-675.

Egly, J.M., and Coin, F. (2011). A history of TFIIH: two decades of molecular biology on a pivotal transcription/repair factor. DNA Repair (Amst) *10*, 714-721.

Eichinger, C.S., and Jentsch, S. (2011). 9-1-1: PCNA's specialized cousin. Trends Biochem Sci *36*, 563-568.

Elia, A.E., Boardman, A.P., Wang, D.C., Huttlin, E.L., Everley, R.A., Dephoure, N., Zhou, C., Koren, I., Gygi, S.P., and Elledge, S.J. (2015). Quantitative Proteomic Atlas of Ubiquitination and Acetylation in the DNA Damage Response. Mol Cell *59*, 867-881.

Endres, T., Solvie, D., Heidelberger, J.B., Andrioletti, V., Baluapuri, A., Ade, C.P., Muhar, M., Eilers, U., Vos, S.M., Cramer, P.*, et al.* (2021). Ubiquitylation of MYC couples transcription elongation with double-strand break repair at active promoters. Mol Cell *81*, 830-844 e813.

Erickson, B., Sheridan, R.M., Cortazar, M., and Bentley, D.L. (2018). Dynamic turnover of paused Pol II complexes at human promoters. Genes Dev *32*, 1215-1225.

Escribano-Diaz, C., Orthwein, A., Fradet-Turcotte, A., Xing, M., Young, J.T., Tkac, J., Cook, M.A., Rosebrock, A.P., Munro, M., Canny, M.D.*, et al.* (2013). A cell cycle-dependent regulatory circuit composed of 53BP1-RIF1 and BRCA1-CtIP controls DNA repair pathway choice. Mol Cell *49*, 872-883.

Falck, J., Coates, J., and Jackson, S.P. (2005). Conserved modes of recruitment of ATM, ATR and DNA-PKcs to sites of DNA damage. Nature *434*, 605-611.

Fellmann, C., Hoffmann, T., Sridhar, V., Hopfgartner, B., Muhar, M., Roth, M., Lai, D.Y., Barbosa, I.A., Kwon, J.S., Guan, Y.*, et al.* (2013). An optimized microRNA backbone for effective single-copy RNAi. Cell Rep *5*, 1704-1713.

Fong, N., Brannan, K., Erickson, B., Kim, H., Cortazar, M.A., Sheridan, R.M., Nguyen, T., Karp, S., and Bentley, D.L. (2015). Effects of Transcription Elongation Rate and Xrn2 Exonuclease Activity on RNA Polymerase II Termination Suggest Widespread Kinetic Competition. Mol Cell *60*, 256-267.

Fuchs, G., Hollander, D., Voichek, Y., Ast, G., and Oren, M. (2014). Cotranscriptional histone H2B monoubiquitylation is tightly coupled with RNA polymerase II elongation rate. Genome Res *24*, 1572-1583.

Fuchs, G., Voichek, Y., Rabani, M., Benjamin, S., Gilad, S., Amit, I., and Oren, M. (2015). Simultaneous measurement of genome-wide transcription elongation speeds and rates of RNA polymerase II transition into active elongation with 4sUDRB-seq. Nat Protoc *10*, 605-618.

Garcia-Muse, T., and Aguilera, A. (2016). Transcription-replication conflicts: how they occur and how they are resolved. Nat Rev Mol Cell Biol *17*, 553-563.

Gatei, M., Scott, S.P., Filippovitch, I., Soronika, N., Lavin, M.F., Weber, B., and Khanna, K.K. (2000). Role for ATM in DNA damage-induced phosphorylation of BRCA1. Cancer Res *60*, 3299-3304.

Gell, D., and Jackson, S.P. (1999). Mapping of protein-protein interactions within the DNA-dependent protein kinase complex. Nucleic Acids Res *27*, 3494-3502.

Gilbertson, S., Federspiel, J.D., Hartenian, E., Cristea, I.M., and Glaunsinger, B. (2018). Changes in mRNA abundance drive shuttling of RNA binding proteins, linking cytoplasmic RNA degradation to transcription. Elife *7*.

Ginno, P.A., Lim, Y.W., Lott, P.L., Korf, I., and Chedin, F. (2013). GC skew at the 5' and 3' ends of human genes links R-loop formation to epigenetic regulation and transcription termination. Genome Res *23*, 1590-1600.

Ginno, P.A., Lott, P.L., Christensen, H.C., Korf, I., and Chedin, F. (2012). R-loop formation is a distinctive characteristic of unmethylated human CpG island promoters. Mol Cell *45*, 814-825.

Golding, S.E., Rosenberg, E., Valerie, N., Hussaini, I., Frigerio, M., Cockcroft, X.F., Chong, W.Y., Hummersone, M., Rigoreau, L., Menear, K.A.*, et al.* (2009). Improved ATM kinase inhibitor KU-60019 radiosensitizes glioma cells, compromises insulin, AKT and ERK prosurvival signaling, and inhibits migration and invasion. Mol Cancer Ther *8*, 2894-2902.

Goodarzi, A.A., Kurka, T., and Jeggo, P.A. (2011). KAP-1 phosphorylation regulates CHD3 nucleosome remodeling during the DNA double-strand break response. Nat Struct Mol Biol *18*, 831-839.

Guo, Z., Kumagai, A., Wang, S.X., and Dunphy, W.G. (2000). Requirement for Atr in phosphorylation of Chk1 and cell cycle regulation in response to DNA replication blocks and UV-damaged DNA in Xenopus egg extracts. Genes Dev *14*, 2745-2756.

Haffner, M.C., Aryee, M.J., Toubaji, A., Esopi, D.M., Albadine, R., Gurel, B., Isaacs, W.B., Bova, G.S., Liu, W., Xu, J.*, et al.* (2010). Androgen-induced TOP2B-mediated double-strand breaks and prostate cancer gene rearrangements. Nat Genet *42*, 668-675.

Hamperl, S., Bocek, M.J., Saldivar, J.C., Swigut, T., and Cimprich, K.A. (2017). Transcription-Replication Conflict Orientation Modulates R-Loop Levels and Activates Distinct DNA Damage Responses. Cell *170*, 774-786 e719.

Hamperl, S., and Cimprich, K.A. (2016). Conflict Resolution in the Genome: How Transcription and Replication Make It Work. Cell *167*, 1455-1467.

Harding, S.M., Benci, J.L., Irianto, J., Discher, D.E., Minn, A.J., and Greenberg, R.A. (2017). Mitotic progression following DNA damage enables pattern recognition within micronuclei. Nature *548*, 466-470.

Harlen, K.M., and Churchman, L.S. (2017). The code and beyond: transcription regulation by the RNA polymerase II carboxy-terminal domain. Nat Rev Mol Cell Biol *18*, 263-273.

Hashizume, R., Fukuda, M., Maeda, I., Nishikawa, H., Oyake, D., Yabuki, Y., Ogata, H., and Ohta, T. (2001). The RING heterodimer BRCA1-BARD1 is a ubiquitin ligase inactivated by a breast cancer-derived mutation. J Biol Chem *276*, 14537-14540.

Hatchi, E., Skourti-Stathaki, K., Ventz, S., Pinello, L., Yen, A., Kamieniarz-Gdula, K., Dimitrov, S., Pathania, S., McKinney, K.M., Eaton, M.L.*, et al.* (2015). BRCA1 recruitment to transcriptional pause sites is required for R-loop-driven DNA damage repair. Mol Cell *57*, 636-647.

Henssen, A., Althoff, K., Odersky, A., Beckers, A., Koche, R., Speleman, F., Schafers, S., Bell, E., Nortmeyer, M., Westermann, F.*, et al.* (2016). Targeting MYCN-Driven Transcription By BET-Bromodomain Inhibition. Clin Cancer Res *22*, 2470-2481.

Hernandez, G., Ramirez, M.J., Minguillon, J., Quiles, P., Ruiz de Garibay, G., Aza-Carmona, M., Bogliolo, M., Pujol, R., Prados-Carvajal, R., Fernandez, J.*, et al.* (2018). Decapping protein EDC4 regulates DNA repair and phenocopies BRCA1. Nat Commun *9*, 967.

Herold, S., Kalb, J., Buchel, G., Ade, C.P., Baluapuri, A., Xu, J., Koster, J., Solvie, D., Carstensen, A., Klotz, C.*, et al.* (2019). Recruitment of BRCA1 limits MYCN-driven accumulation of stalled RNA polymerase. Nature *567*, 545-549.

Holstege, F.C., van der Vliet, P.C., and Timmers, H.T. (1996). Opening of an RNA polymerase II promoter occurs in two distinct steps and requires the basal transcription factors IIE and IIH. EMBO J *15*, 1666-1677.

Horwitz, A.A., Affar el, B., Heine, G.F., Shi, Y., and Parvin, J.D. (2007). A mechanism for transcriptional repression dependent on the BRCA1 E3 ubiquitin ligase. Proc Natl Acad Sci U S A *104*, 6614-6619.

Huang, M., and Weiss, W.A. (2013). Neuroblastoma and MYCN. Cold Spring Harb Perspect Med *3*, a014415.

Huertas, P., and Aguilera, A. (2003). Cotranscriptionally formed DNA:RNA hybrids mediate transcription elongation impairment and transcription-associated recombination. Mol Cell *12*, 711-721.

Hustedt, N., and Durocher, D. (2017). The control of DNA repair by the cell cycle. Nature Cell Biology *19*, 1-9.

Iannelli, F., Galbiati, A., Capozzo, I., Nguyen, Q., Magnuson, B., Michelini, F., D'Alessandro, G., Cabrini, M., Roncador, M., Francia, S.*, et al.* (2017). A damaged genome's transcriptional landscape through multilayered expression profiling around in situ-mapped DNA double-strand breaks. Nat Commun *8*, 15656.

Jaenicke, L.A., von Eyss, B., Carstensen, A., Wolf, E., Xu, W., Greifenberg, A.K., Geyer, M., Eilers, M., and Popov, N. (2016). Ubiquitin-Dependent Turnover of MYC Antagonizes MYC/PAF1C Complex Accumulation to Drive Transcriptional Elongation. Mol Cell *61*, 54-67.

Jeronimo, C., and Robert, F. (2014). Kin28 regulates the transient association of Mediator with core promoters. Nat Struct Mol Biol *21*, 449-455.

Jette, N., and Lees-Miller, S.P. (2015). The DNA-dependent protein kinase: A multifunctional protein kinase with roles in DNA double strand break repair and mitosis. Prog Biophys Mol Biol *117*, 194-205.

Jiao, X., Chang, J.H., Kilic, T., Tong, L., and Kiledjian, M. (2013). A mammalian pre-mRNA 5' end capping quality control mechanism and an unexpected link of capping to pre-mRNA processing. Mol Cell *50*, 104-115.

Jimeno-Gonzalez, S., Ceballos-Chavez, M., and Reyes, J.C. (2015). A positioned +1 nucleosome enhances promoter-proximal pausing. Nucleic Acids Res *43*, 3068-3078.

Jung, L.A., Gebhardt, A., Koelmel, W., Ade, C.P., Walz, S., Kuper, J., von Eyss, B., Letschert, S., Redel, C., d'Artista, L.*, et al.* (2017). OmoMYC blunts promoter invasion by oncogenic MYC to inhibit gene expression characteristic of MYC-dependent tumors. Oncogene *36*, 1911-1924.

Kalb, R., Latwiel, S., Baymaz, H.I., Jansen, P.W., Muller, C.W., Vermeulen, M., and Muller, J. (2014a). Histone H2A monoubiquitination promotes histone H3 methylation in Polycomb repression. Nat Struct Mol Biol *21*, 569-571.

Kalb, R., Mallery, D.L., Larkin, C., Huang, J.T., and Hiom, K. (2014b). BRCA1 is a histone-H2A-specific ubiquitin ligase. Cell Rep *8*, 999-1005.

Kamieniarz-Gdula, K., Gdula, M.R., Panser, K., Nojima, T., Monks, J., Wisniewski, J.R., Riepsaame, J., Brockdorff, N., Pauli, A., and Proudfoot, N.J. (2019). Selective Roles of Vertebrate PCF11 in Premature and Full-Length Transcript Termination. Mol Cell *74*, 158-172 e159.

Kamieniarz-Gdula, K., and Proudfoot, N.J. (2019). Transcriptional Control by Premature Termination: A Forgotten Mechanism. Trends Genet *35*, 553-564.

Kim, T.K., Ebright, R.H., and Reinberg, D. (2000). Mechanism of ATP-dependent promoter melting by transcription factor IIH. Science *288*, 1418-1422.

Kireeva, M.L., Hancock, B., Cremona, G.H., Walter, W., Studitsky, V.M., and Kashlev, M. (2005). Nature of the nucleosomal barrier to RNA polymerase II. Mol Cell *18*, 97-108.

Kleiman, F.E., Wu-Baer, F., Fonseca, D., Kaneko, S., Baer, R., and Manley, J.L. (2005). BRCA1/BARD1 inhibition of mRNA 3' processing involves targeted degradation of RNA polymerase II. Genes Dev *19*, 1227-1237.

Klusmann, I., Rodewald, S., Muller, L., Friedrich, M., Wienken, M., Li, Y., Schulz-Heddergott, R., and Dobbelstein, M. (2016). p53 Activity Results in DNA Replication Fork Processivity. Cell Rep *17*, 1845-1857.

Kortlever, R.M., Sodir, N.M., Wilson, C.H., Burkhart, D.L., Pellegrinet, L., Brown Swigart, L., Littlewood, T.D., and Evan, G.I. (2017). Myc Cooperates with Ras by Programming Inflammation and Immune Suppression. Cell *171*, 1301-1315 e1314.

Kouzine, F., Gupta, A., Baranello, L., Wojtowicz, D., Ben-Aissa, K., Liu, J., Przytycka, T.M., and Levens, D. (2013). Transcription-dependent dynamic supercoiling is a short-range genomic force. Nat Struct Mol Biol *20*, 396-403.

Kowalczykowski, S.C. (2015). An Overview of the Molecular Mechanisms of Recombinational DNA Repair. Cold Spring Harb Perspect Biol *7*.

Krum, S.A., Miranda, G.A., Lin, C., and Lane, T.F. (2003). BRCA1 associates with processive RNA polymerase II. J Biol Chem *278*, 52012-52020.

Kuo, L.J., and Yang, L.X. (2008). Gamma-H2AX - a novel biomarker for DNA double-strand breaks. In Vivo *22*, 305-309.

Lai, W.K.M., and Pugh, B.F. (2017). Understanding nucleosome dynamics and their links to gene expression and DNA replication. Nat Rev Mol Cell Biol *18*, 548-562.

Lam, F.C., Kong, Y.W., Huang, Q., Vu Han, T.L., Maffa, A.D., Kasper, E.M., and Yaffe, M.B. (2020). BRD4 prevents the accumulation of R-loops and protects against transcription-replication collision events and DNA damage. Nat Commun *11*, 4083.

Layer, J.P., Kronmuller, M.T., Quast, T., van den Boorn-Konijnenberg, D., Effern, M., Hinze, D., Althoff, K., Schramm, A., Westermann, F., Peifer, M.*, et al.* (2017). Amplification of N-Myc is associated with a T-cell-poor microenvironment in metastatic neuroblastoma restraining interferon pathway activity and chemokine expression. Oncoimmunology *6*, e1320626.

Lee, J.S., and Mendell, J.T. (2020). Antisense-Mediated Transcript Knockdown Triggers Premature Transcription Termination. Mol Cell *77*, 1044-1054 e1043.

Lesnik, E.A., and Freier, S.M. (1995). Relative thermodynamic stability of DNA, RNA, and DNA:RNA hybrid duplexes: relationship with base composition and structure. Biochemistry *34*, 10807-10815.

Lezaja, A., and Altmeyer, M. (2018). Inherited DNA lesions determine G1 duration in the next cell cycle. Cell Cycle *17*, 24-32.

Li, Z., Otevrel, T., Gao, Y., Cheng, H.L., Seed, B., Stamato, T.D., Taccioli, G.E., and Alt, F.W. (1995). The XRCC4 gene encodes a novel protein involved in DNA double-strand break repair and V(D)J recombination. Cell *83*, 1079-1089.

Lin, C.Y., Loven, J., Rahl, P.B., Paranal, R.M., Burge, C.B., Bradner, J.E., Lee, T.I., and Young, R.A. (2012). Transcriptional amplification in tumor cells with elevated c-Myc. Cell *151*, 56-67.

Livak, K.J., and Schmittgen, T.D. (2001). Analysis of relative gene expression data using real-time quantitative PCR and the 2(-Delta Delta C(T)) Method. Methods *25*, 402-408.

Lombardi, O., Varshney, D., Phillips, N.M., and Cowling, V.H. (2016). c-Myc deregulation induces mRNA capping enzyme dependency. Oncotarget *7*, 82273-82288.

Lorenzin, F., Benary, U., Baluapuri, A., Walz, S., Jung, L.A., von Eyss, B., Kisker, C., Wolf, J., Eilers, M., and Wolf, E. (2016). Different promoter affinities account for specificity in MYC-dependent gene regulation. Elife *5*.

Lu, H., Flores, O., Weinmann, R., and Reinberg, D. (1991). The nonphosphorylated form of RNA polymerase II preferentially associates with the preinitiation complex. Proc Natl Acad Sci U S A *88*, 10004-10008.

Luo, Y., Na, Z., and Slavoff, S.A. (2018). P-Bodies: Composition, Properties, and Functions. Biochemistry *57*, 2424-2431.

Madabhushi, R., Gao, F., Pfenning, A.R., Pan, L., Yamakawa, S., Seo, J., Rueda, R., Phan, T.X., Yamakawa, H., Pao, P.C.*, et al.* (2015). Activity-Induced DNA Breaks Govern the Expression of Neuronal Early-Response Genes. Cell *161*, 1592-1605.

Marchal, C., Sima, J., and Gilbert, D.M. (2019). Control of DNA replication timing in the 3D genome. Nat Rev Mol Cell Biol *20*, 721-737.

Marshall, N.F., Peng, J., Xie, Z., and Price, D.H. (1996). Control of RNA polymerase II elongation potential by a novel carboxyl-terminal domain kinase. J Biol Chem *271*, 27176-27183.

Matsuoka, S., Ballif, B.A., Smogorzewska, A., McDonald, E.R., 3rd, Hurov, K.E., Luo, J., Bakalarski, C.E., Zhao, Z., Solimini, N., Lerenthal, Y.*, et al.* (2007). ATM and ATR substrate analysis reveals extensive protein networks responsive to DNA damage. Science *316*, 1160-1166.

McManus, K.J., and Hendzel, M.J. (2005). ATM-dependent DNA damage-independent mitotic phosphorylation of H2AX in normally growing mammalian cells. Mol Biol Cell *16*, 5013-5025.

Mikuda, N., Kolesnichenko, M., Beaudette, P., Popp, O., Uyar, B., Sun, W., Tufan, A.B., Perder, B., Akalin, A., Chen, W.*, et al.* (2018). The IkappaB kinase complex is a regulator of mRNA stability. EMBO J *37*.

Monteiro, A.N. (2000). BRCA1: exploring the links to transcription. Trends Biochem Sci *25*, 469-474.

Morales, J.C., Richard, P., Patidar, P.L., Motea, E.A., Dang, T.T., Manley, J.L., and Boothman, D.A. (2016). XRN2 Links Transcription Termination to DNA Damage and Replication Stress. PLoS Genet *12*, e1006107.

Mordes, D.A., Glick, G.G., Zhao, R., and Cortez, D. (2008). TopBP1 activates ATR through ATRIP and a PIKK regulatory domain. Genes Dev *22*, 1478-1489.

Mosse, Y.P., Fox, E., Teachey, D.T., Reid, J.M., Safgren, S.L., Carol, H., Lock, R.B., Houghton, P.J., Smith, M.A., Hall, D.*, et al.* (2019). A Phase II Study of Alisertib in Children with Recurrent/Refractory Solid Tumors or Leukemia: Children's Oncology Group Phase I and Pilot Consortium (ADVL0921). Clin Cancer Res *25*, 3229-3238.

Moyal, L., Lerenthal, Y., Gana-Weisz, M., Mass, G., So, S., Wang, S.Y., Eppink, B., Chung, Y.M., Shalev, G., Shema, E.*, et al.* (2011). Requirement of ATM-dependent monoubiquitylation of histone H2B for timely repair of DNA double-strand breaks. Mol Cell *41*, 529-542.

Muthalagu, N., Monteverde, T., Raffo-Iraolagoitia, X., Wiesheu, R., Whyte, D., Hedley, A., Laing, S., Kruspig, B., Upstill-Goddard, R., Shaw, R.*, et al.* (2020). Repression of the Type I Interferon Pathway Underlies MYC- and KRAS-Dependent Evasion of NK and B Cells in Pancreatic Ductal Adenocarcinoma. Cancer Discov *10*, 872-887.

Nakazawa, Y., Hara, Y., Oka, Y., Komine, O., van den Heuvel, D., Guo, C., Daigaku, Y., Isono, M., He, Y., Shimada, M.*, et al.* (2020). Ubiquitination of DNA Damage-Stalled RNAPII Promotes Transcription-Coupled Repair. Cell *180*, 1228-1244 e1224.

Ni, Z., Saunders, A., Fuda, N.J., Yao, J., Suarez, J.R., Webb, W.W., and Lis, J.T. (2008). P-TEFb is critical for the maturation of RNA polymerase II into productive elongation in vivo. Mol Cell Biol *28*, 1161-1170.

Nie, Z., Hu, G., Wei, G., Cui, K., Yamane, A., Resch, W., Wang, R., Green, D.R., Tessarollo, L., Casellas, R.*, et al.* (2012). c-Myc is a universal amplifier of expressed genes in lymphocytes and embryonic stem cells. Cell *151*, 68-79.

Niehrs, C., and Luke, B. (2020). Regulatory R-loops as facilitators of gene expression and genome stability. Nat Rev Mol Cell Biol *21*, 167-178.

Noe Gonzalez, M., Blears, D., and Svejstrup, J.Q. (2021). Causes and consequences of RNA polymerase II stalling during transcript elongation. Nat Rev Mol Cell Biol *22*, 3-21.

Olson, E., Nievera, C.J., Klimovich, V., Fanning, E., and Wu, X. (2006). RPA2 is a direct downstream target for ATR to regulate the S-phase checkpoint. J Biol Chem *281*, 39517-39533.

Otto, T., Horn, S., Brockmann, M., Eilers, U., Schuttrumpf, L., Popov, N., Kenney, A.M., Schulte, J.H., Beijersbergen, R., Christiansen, H.*, et al.* (2009). Stabilization of N-Myc is a critical function of Aurora A in human neuroblastoma. Cancer Cell *15*, 67-78.

Peterlin, B.M., and Price, D.H. (2006). Controlling the elongation phase of transcription with P-TEFb. Mol Cell *23*, 297-305.

Phoenix, P., Raymond, M.A., Masse, E., and Drolet, M. (1997). Roles of DNA topoisomerases in the regulation of R-loop formation in vitro. J Biol Chem *272*, 1473-1479.

Promonet, A., Padioleau, I., Liu, Y., Sanz, L., Biernacka, A., Schmitz, A.L., Skrzypczak, M., Sarrazin, A., Mettling, C., Rowicka, M.*, et al.* (2020). Topoisomerase 1 prevents replication stress at R-loop-enriched transcription termination sites. Nat Commun *11*, 3940.

Rahl, P.B., Lin, C.Y., Seila, A.C., Flynn, R.A., McCuine, S., Burge, C.B., Sharp, P.A., and Young, R.A. (2010). c-Myc regulates transcriptional pause release. Cell *141*, 432-445.

Rambout, X., and Maquat, L.E. (2020). The nuclear cap-binding complex as choreographer of gene transcription and pre-mRNA processing. Genes Dev *34*, 1113-1127.

Rickman, D.S., Schulte, J.H., and Eilers, M. (2018). The Expanding World of N-MYC-Driven Tumors. Cancer Discov *8*, 150-163.

Rivera-Mulia, J.C., and Gilbert, D.M. (2016). Replication timing and transcriptional control: beyond cause and effect-part III. Curr Opin Cell Biol *40*, 168-178.

Roeschert, I., Poon, E., Henssen, A.G., Dorado Garcia, H., Gatti, M., Giansanti, C., Jamin, Y., Ade, C.P., Gallant, P., Schülein-Völk, C.*, et al.* (2021). Combined inhibition of Aurora-A and ATR kinases results in regression of MYCN-amplified neuroblastoma. Nature Cancer *2*, 312-326.

Roy, D., Yu, K., and Lieber, M.R. (2008). Mechanism of R-Loop Formation at Immunoglobulin Class Switch Sequences. Molecular and Cellular Biology *28*, 50-60.

Sanchez, A., de Vivo, A., Tonzi, P., Kim, J., Huang, T.T., and Kee, Y. (2020). Transcription-replication conflicts as a source of common fragile site instability caused by BMI1-RNF2 deficiency. PLoS Genet *16*, e1008524.

Sanz, L.A., Hartono, S.R., Lim, Y.W., Steyaert, S., Rajpurkar, A., Ginno, P.A., Xu, X., and Chedin, F. (2016). Prevalent, Dynamic, and Conserved R-Loop Structures Associate with Specific Epigenomic Signatures in Mammals. Mol Cell *63*, 167-178.

Savage, K.I., Gorski, J.J., Barros, E.M., Irwin, G.W., Manti, L., Powell, A.J., Pellagatti, A., Lukashchuk, N., McCance, D.J., McCluggage, W.G.*, et al.* (2014). Identification of a BRCA1-mRNA splicing complex required for efficient DNA repair and maintenance of genomic stability. Mol Cell *54*, 445-459.

Schroeder, S.C., Schwer, B., Shuman, S., and Bentley, D. (2000). Dynamic association of capping enzymes with transcribing RNA polymerase II. Genes Dev *14*, 2435-2440.

Sclafani, R.A., and Holzen, T.M. (2007). Cell Cycle Regulation of DNA Replication. Annual Review of Genetics *41*, 237-280.

Scully, R., Anderson, S.F., Chao, D.M., Wei, W., Ye, L., Young, R.A., Livingston, D.M., and Parvin, J.D. (1997). BRCA1 is a component of the RNA polymerase II holoenzyme. Proc Natl Acad Sci U S A *94*, 5605-5610.

Seto, E., Yoshida-Sugitani, R., Kobayashi, T., and Toyama-Sorimachi, N. (2015). The Assembly of EDC4 and Dcp1a into Processing Bodies Is Critical for the Translational Regulation of IL-6. PLoS One *10*, e0123223.

Shanbhag, N.M., Rafalska-Metcalf, I.U., Balane-Bolivar, C., Janicki, S.M., and Greenberg, R.A. (2010). ATM-dependent chromatin changes silence transcription in cis to DNA double-strand breaks. Cell *141*, 970-981.

Shao, W., and Zeitlinger, J. (2017). Paused RNA polymerase II inhibits new transcriptional initiation. Nat Genet *49*, 1045-1051.

Sheridan, R.M., Fong, N., D'Alessandro, A., and Bentley, D.L. (2019). Widespread Backtracking by RNA Pol II Is a Major Effector of Gene Activation, 5' Pause Release, Termination, and Transcription Elongation Rate. Mol Cell *73*, 107-118 e104.

Shivji, M.K.K., Renaudin, X., Williams, C.H., and Venkitaraman, A.R. (2018). BRCA2 Regulates Transcription Elongation by RNA Polymerase II to Prevent R-Loop Accumulation. Cell Rep *22*, 1031-1039.

Singleton, B.K., Torres-Arzayus, M.I., Rottinghaus, S.T., Taccioli, G.E., and Jeggo, P.A. (1999). The C terminus of Ku80 activates the DNA-dependent protein kinase catalytic subunit. Mol Cell Biol *19*, 3267-3277.

Skourti-Stathaki, K., Proudfoot, N.J., and Gromak, N. (2011). Human senataxin resolves RNA/DNA hybrids formed at transcriptional pause sites to promote Xrn2-dependent termination. Mol Cell *42*, 794-805.

Smith, T., Heger, A., and Sudbery, I. (2017). UMI-tools: modeling sequencing errors in Unique Molecular Identifiers to improve quantification accuracy. Genome Res *27*, 491-499.

Song, C., Hotz-Wagenblatt, A., Voit, R., and Grummt, I. (2017). SIRT7 and the DEAD-box helicase DDX21 cooperate to resolve genomic R loops and safeguard genome stability. Genes Dev *31*, 1370-1381.

Soucek, L., Jucker, R., Panacchia, L., Ricordy, R., Tato, F., and Nasi, S. (2002). Omomyc, a potential Myc dominant negative, enhances Myc-induced apoptosis. Cancer Res *62*, 3507-3510.

Steurer, B., Janssens, R.C., Geverts, B., Geijer, M.E., Wienholz, F., Theil, A.F., Chang, J., Dealy, S., Pothof, J., van Cappellen, W.A.*, et al.* (2018). Live-cell analysis of endogenous GFP-RPB1 uncovers rapid turnover of initiating and promoter-paused RNA Polymerase II. Proc Natl Acad Sci U S A *115*, E4368-E4376.

Stolz, A., Ertych, N., Kienitz, A., Vogel, C., Schneider, V., Fritz, B., Jacob, R., Dittmar, G., Weichert, W., Petersen, I.*, et al.* (2010). The CHK2-BRCA1 tumour suppressor pathway ensures chromosomal stability in human somatic cells. Nat Cell Biol *12*, 492-499.

Sun, L., Wu, J., Du, F., Chen, X., and Chen, Z.J. (2013). Cyclic GMP-AMP synthase is a cytosolic DNA sensor that activates the type I interferon pathway. Science *339*, 786-791.

Teloni, F., Michelena, J., Lezaja, A., Kilic, S., Ambrosi, C., Menon, S., Dobrovolna, J., Imhof, R., Janscak, P., Baubec, T.*, et al.* (2019). Efficient Pre-mRNA Cleavage Prevents Replication-Stress-Associated Genome Instability. Mol Cell *73*, 670-683 e612.

Thomas, M., White, R.L., and Davis, R.W. (1976). Hybridization of RNA to double-stranded DNA: formation of R-loops. Proceedings of the National Academy of Sciences *73*, 2294-2298.

Tian, F., Sharma, S., Zou, J., Lin, S.Y., Wang, B., Rezvani, K., Wang, H., Parvin, J.D., Ludwig, T., Canman, C.E.*, et al.* (2013). BRCA1 promotes the ubiquitination of PCNA and recruitment of translesion polymerases in response to replication blockade. Proc Natl Acad Sci U S A *110*, 13558-13563.

Tibbetts, R.S., Cortez, D., Brumbaugh, K.M., Scully, R., Livingston, D., Elledge, S.J., and Abraham, R.T. (2000). Functional interactions between BRCA1 and the checkpoint kinase ATR during genotoxic stress. Genes Dev *14*, 2989-3002.

Toledo, L.I., Altmeyer, M., Rask, M.B., Lukas, C., Larsen, D.H., Povlsen, L.K., Bekker-Jensen, S., Mailand, N., Bartek, J., and Lukas, J. (2013). ATR prohibits replication catastrophe by preventing global exhaustion of RPA. Cell *155*, 1088-1103.

Topper, M.J., Vaz, M., Chiappinelli, K.B., DeStefano Shields, C.E., Niknafs, N., Yen, R.C., Wenzel, A., Hicks, J., Ballew, M., Stone, M.*, et al.* (2017). Epigenetic Therapy Ties MYC Depletion to Reversing Immune Evasion and Treating Lung Cancer. Cell *171*, 1284-1300 e1221.

Tresini, M., Marteijn, J.A., and Vermeulen, W. (2016). Bidirectional coupling of splicing and ATM signaling in response to transcription-blocking DNA damage. RNA Biol *13*, 272-278.

Tresini, M., Warmerdam, D.O., Kolovos, P., Snijder, L., Vrouwe, M.G., Demmers, J.A., van, I.W.F., Grosveld, F.G., Medema, R.H., Hoeijmakers, J.H.*, et al.* (2015). The core spliceosome as target and effector of non-canonical ATM signalling. Nature *523*, 53-58.

Tritschler, F., Braun, J.E., Motz, C., Igreja, C., Haas, G., Truffault, V., Izaurralde, E., and Weichenrieder, O. (2009). DCP1 forms asymmetric trimers to assemble into active mRNA decapping complexes in metazoa. Proc Natl Acad Sci U S A *106*, 21591-21596.

Tritschler, F., Eulalio, A., Truffault, V., Hartmann, M.D., Helms, S., Schmidt, S., Coles, M., Izaurralde, E., and Weichenrieder, O. (2007). A divergent Sm fold in EDC3 proteins mediates DCP1 binding and P-body targeting. Mol Cell Biol *27*, 8600-8611.

Tubbs, A., and Nussenzweig, A. (2017). Endogenous DNA Damage as a Source of Genomic Instability in Cancer. Cell *168*, 644-656.

Tufegdzic Vidakovic, A., Mitter, R., Kelly, G.P., Neumann, M., Harreman, M., Rodriguez-Martinez, M., Herlihy, A., Weems, J.C., Boeing, S., Encheva, V.*, et al.* (2020). Regulation of the RNAPII Pool Is Integral to the DNA Damage Response. Cell *180*, 1245-1261 e1221.

Ui, A., Nagaura, Y., and Yasui, A. (2015). Transcriptional elongation factor ENL phosphorylated by ATM recruits polycomb and switches off transcription for DSB repair. Mol Cell *58*, 468-482.

Venkitaraman, A.R. (2014). Cancer suppression by the chromosome custodians, BRCA1 and BRCA2. Science *343*, 1470-1475.

Vo, B.T., Wolf, E., Kawauchi, D., Gebhardt, A., Rehg, J.E., Finkelstein, D., Walz, S., Murphy, B.L., Youn, Y.H., Han, Y.G.*, et al.* (2016). The Interaction of Myc with Miz1 Defines Medulloblastoma Subgroup Identity. Cancer Cell *29*, 5-16.

Vos, S.M., Farnung, L., Boehning, M., Wigge, C., Linden, A., Urlaub, H., and Cramer, P. (2018a). Structure of activated transcription complex Pol II-DSIF-PAF-SPT6. Nature *560*, 607-612.

Vos, S.M., Farnung, L., Urlaub, H., and Cramer, P. (2018b). Structure of paused transcription complex Pol II-DSIF-NELF. Nature *560*, 601-606.

Walz, S., Lorenzin, F., Morton, J., Wiese, K.E., von Eyss, B., Herold, S., Rycak, L., Dumay-Odelot, H., Karim, S., Bartkuhn, M.*, et al.* (2014). Activation and repression by oncogenic MYC shape tumour-specific gene expression profiles. Nature *511*, 483-487.

Wang, H., Wang, M., Wang, H., Bocker, W., and Iliakis, G. (2005). Complex H2AX phosphorylation patterns by multiple kinases including ATM and DNA-PK in human cells exposed to ionizing radiation and treated with kinase inhibitors. J Cell Physiol *202*, 492-502.

Ward, I.M., and Chen, J. (2001). Histone H2AX is phosphorylated in an ATR-dependent manner in response to replicational stress. J Biol Chem *276*, 47759-47762.

Wei, X., Samarabandu, J., Devdhar, R.S., Siegel, A.J., Acharya, R., and Berezney, R. (1998). Segregation of transcription and replication sites into higher order domains. Science *281*, 1502-1506.

West, S., Gromak, N., and Proudfoot, N.J. (2004). Human 5' --> 3' exonuclease Xrn2 promotes transcription termination at co-transcriptional cleavage sites. Nature *432*, 522-525.

Westover, K.D., Bushnell, D.A., and Kornberg, R.D. (2004). Structural basis of transcription: separation of RNA from DNA by RNA polymerase II. Science *303*, 1014-1016.

Wiese, K.E., Walz, S., von Eyss, B., Wolf, E., Athineos, D., Sansom, O., and Eilers, M. (2013). The role of MIZ-1 in MYC-dependent tumorigenesis. Cold Spring Harb Perspect Med *3*, a014290.

Wilson, M.D., Harreman, M., Taschner, M., Reid, J., Walker, J., Erdjument-Bromage, H., Tempst, P., and Svejstrup, J.Q. (2013). Proteasome-mediated processing of Def1, a critical step in the cellular response to transcription stress. Cell *154*, 983-995.

Wolf, E., and Eilers, M. (2020). Targeting MYC Proteins for Tumor Therapy. Annual Review of Cancer Biology *4*, 61-75.

Wolf, E., Gebhardt, A., Kawauchi, D., Walz, S., von Eyss, B., Wagner, N., Renninger, C., Krohne, G., Asan, E., Roussel, M.F.*, et al.* (2013). Miz1 is required to maintain autophagic flux. Nat Commun *4*, 2535.

Wong, K.H., Jin, Y., and Struhl, K. (2014). TFIIH phosphorylation of the Pol II CTD stimulates mediator dissociation from the preinitiation complex and promoter escape. Mol Cell *54*, 601-612.

Wu, C.H., Yamaguchi, Y., Benjamin, L.R., Horvat-Gordon, M., Washinsky, J., Enerly, E., Larsson, J., Lambertsson, A., Handa, H., and Gilmour, D. (2003). NELF and DSIF cause promoter proximal pausing on the hsp70 promoter in Drosophila. Genes Dev *17*, 1402-1414.

Wu, J., Sun, L., Chen, X., Du, F., Shi, H., Chen, C., and Chen, Z.J. (2013). Cyclic GMP-AMP is an endogenous second messenger in innate immune signaling by cytosolic DNA. Science *339*, 826-830.

Yan, W.X., Mirzazadeh, R., Garnerone, S., Scott, D., Schneider, M.W., Kallas, T., Custodio, J., Wernersson, E., Li, Y., Gao, L.*, et al.* (2017). BLISS is a versatile and quantitative method for genome-wide profiling of DNA double-strand breaks. Nat Commun *8*, 15058.

Ye, Q., Hu, Y.F., Zhong, H., Nye, A.C., Belmont, A.S., and Li, R. (2001). BRCA1-induced large-scale chromatin unfolding and allele-specific effects of cancer-predisposing mutations. J Cell Biol *155*, 911-921.

Yu, Z., Mersaoui, S.Y., Guitton-Sert, L., Coulombe, Y., Song, J., Masson, J.Y., and Richard, S. (2020). DDX5 resolves R-loops at DNA double-strand breaks to promote DNA repair and avoid chromosomal deletions. NAR Cancer *2*, zcaa028.

Zhang, X., Chiang, H.C., Wang, Y., Zhang, C., Smith, S., Zhao, X., Nair, S.J., Michalek, J., Jatoi, I., Lautner, M.*, et al.* (2017). Attenuation of RNA polymerase II pausing mitigates BRCA1-associated R-loop accumulation and tumorigenesis. Nat Commun *8*, 15908.

Ziv, Y., Bielopolski, D., Galanty, Y., Lukas, C., Taya, Y., Schultz, D.C., Lukas, J., Bekker-Jensen, S., Bartek, J., and Shiloh, Y. (2006). Chromatin relaxation in response to DNA double-

strand breaks is modulated by a novel ATM- and KAP-1 dependent pathway. Nat Cell Biol *8*, 870-876.

Zou, L., and Elledge, S.J. (2003). Sensing DNA damage through ATRIP recognition of RPA-ssDNA complexes. Science *300*, 1542-1548.

7 Appendix

7.1 Abbreviations

Prefixes

p	pico
n	nano
µ	micro
m	milli
c	centi
k	kilo

Units

°C	degree celsius
A	ampere
Da	dalton
g	gram
h	hour
l	liter
m	meter
min	minute
M	mol/l
OD	optical density
s	second
U	unit
v/v	volume per volume
w/v	weight per volume

Further abbreviations

α	anti
A	adenine
A	alanine, Ala
aa	amino acid
APS	ammoniumpersulfate
ATCC	American type culture collection
ATP	adenosin-5'-triphosphate
B2M	β2-microglobulin
BET	bromodomain and extra-terminal
bp	basepairs
BR	basic region
BrdU	5-bromo-2-deoxyuridine
BSA	bovine serum albumin
C	cytosine
cDNA	complementary DNA
CDK	cycline-dependent kinase
CDS	coding sequence

ChIP	chromatin immunoprecipitation
ChIP-Seq	chromatin immunoprecipitation followed by deep-sequencing
CMV	cytomegalovirus
CPM	counts per million mapped reads
CTD	C-terminal domain
Ctrl	control
ddH_2O	bidestilled water
DMSO	dimethylsulfoxide
DNA	deoxyribonucleic acid
dNTPs	deoxyribolnucleoside-5'-triphosphate (dATP, dCTP, dGTP, dTTP)
DSB	double strand break
DTT	dithiothreitol
DUB	deubiquitinating enzyme
E3	ubiquitin ligase
EdU	5-ethynyl-2'deoxyuridine
E. coli	*Escherichia coli*
EDTA	ethylendiamintetraacetate
ECL	enhanced chemoluminescence
e.g.	exempli gratia, for example
EGF	epidermal growth factor
FBS	fetal bovine serum
FC	fold change
FDR	false discovery rate
Fig.	figure
g	rcf, relative centrifugal force
G	guanine
GFP	green fluorescent protein
GTP	guanosine-5'-triphosphate
HLH	helix-loop-helix
HECT	homologous to the E6-AP carboxyl terminus
HRP	horseradish peroxidase
hygro	hygromycine
IgG	immunoglobulin G
IF	immunofluorescence
IP	immunoprecipitation
IRES	internal ribosomal entry site
K	lysine, Lys
LB	lysogeny broth
LZ	leucine zipper
mRNA	messenger RNA
NEM	N-ethylmaleimide
NES	normalised enrichment score
NLS	nuclear localisation signal
NP-40	Nonidet P-40
NTA	nitrilotriacetic acid
p	phosphor
PAGE	polyacrylamide-gelelectrophoresis
PBS	phosphate-buffered saline
PCR	polymerase chain reaction

PEI	polyethylenimin
PEST	proline-, glutamate-, serine-, threonine-rich region
PI	propidiumiodide
PIC	preinitiation complex
PMSF	phenylmethylsulfonylfluoride
PVDF	polyvinylidene difluoride
qPCR	quantitative polymerase chain reaction
R	arginine, Arg
RING	really interesting new gene
RNA	ribonucleic acid
RNAPII	RNA polymerase II
RNase	riboluclease
RPM	reads per million mapped reads
rpm	revolutions per minute
RT	room temperature
Thr	threonine
$t_{1/2}$	half-life
TBE	Tris-borate EDTA buffer
TBS	Tris-buffered saline
TBS-T	Tris-buffered saline with tween-20
TE	Tris-EDTA buffer
TEMED	N,N,N',N'-tetramethylethylendiamine
TES	Transcriptional end site
TNT	Tris-NaCl-Triton X-100
Tris	Tris-(hydroxymethyl)-aminomethan
TRRAP	transactivation / transformation-associated protein
TSS	transcriptional start site
S	serine, Ser
SD	standard deviation
SDS	sodium dodecyl sulfate
SDS-PAGE	SDS polyacrylamide gelelectrophoresis
SEM	standard error of the mean
shSCR	shRNA scramble
shRNA	small hairpin RNA
S-phase	synthesis phase
U	uridine
Ub	ubiquitin
UTR	untranslated region
WB	Western Blot
WT	wild type

7.2 Acknowledgements

I would like to express my gratitude towards Prof. Martin Eilers who gave me the opportunity doing my PhD in his department and in doing so building a fundament for my scientific career. He was a great supervisor, showed me how the science world works, what passion means and had always an open door and open ear to discuss newest data and interpret it.

I thank my thesis committee members wholeheartedly, Prof. Matthias Dobbelstein and Prof. Stefan Gaubatz, who were always a great help in discussing my findings and mentoring me on my way.

I am deeply grateful to Steffi Herold for her guidance, supervision, wisdom, help and tips that supported me a lot in becoming the scientist that I am today.

My thank goes to all former and current members of the whole department of Biochemistry and Molecular Biology for the time I spent there, for the technical support I received and for the fruitful discussions and fun we had.

My dearest office members, Gabriele, Giacomo and Daniel, I have to thank you and Dimi for spending these times with me, the ups and downs, the laughs and tears and the critical and helpful reading of my thesis. Special thanks go to Carsten, Bastian and Lorenz, for always having an open ear and an open heart, for useful scientific and funny non-scientific conversations. I am honoured to have met such wonderful people.

The attendance of the Graduate School of Life Sciences helped me to become the scientist that I am today, and the SCIENTIA mentoring program inspired me in becoming the human being that I am today. Thank you!

From the bottom of my heart I would like to thank my beloved ones, the ones who went ahead, out of this world, and the ones who are still among us. They were there when there was just dark, always backed me up, never let me down, encouraged me continuously and helped me to end up with a smile on my face: My family, my dearest friend Annsophie, the Dresen family and Maximilian.

7.3 Publications

Dejure*, Royla*, Herold, **Kalb**, Walz, Ade, Mastrobuoni, Vanselow, Schlosser, Wolf, Kempa, Eilers. *These authors contributed equally. (2017) **The *MYC* mRNA 3'UTR couples RNA polymerase II function to glutamine and ribonucleotide levels.** *EMBO Journal* 36, 1854-1868

Büchel*, Carstensen*, Mak*, Roeschert, Leen, Sumara, Hofstetter, Herold, **Kalb**, Baluapuri, Poon, Kwok, Chesler, Maric, Rickman, Wolf, Bayliss, Walz, Eilers. *These authors contributed equally. (2017) **Association with Aurora-A Controls N-MYC-Dependent Promoter Escape and Pause Release of RNA Polymerase II during the Cell Cycle**. *Cell Reports* 21, 3483-3497

Herold*, **Kalb***, Büchel*, Ade, Baluapuri, Xu, Koster, Solvie, Carstensen, Klotz, Rodewald, Schülein-Völk, Dobbelstein, Wolf, Molenaar, Versteeg, Walz, Eilers. *These authors contributed equally. (2019) **Recruitment of BRCA1 limits MYCN-driven accumulation of stalled RNA polymerase.** *Nature* 567, 545-549

Papadopoulos, **Kalb**, Solvie, Baluapuri, Herold, Endres, Giansanti, Schülein-Völk, Ade, Schneider, Fischer, Dobbelstein, Wolf, Eilers. **The MYCN oncoprotein resolves conflicts of stalling RNA Polymerase with the replication fork.** *In Revision.*

7.4 Curriculum vitae

7.5 Affidavit

I hereby confirm that my thesis entitled “The role of BRCA1 and DCP1A in the coordination of transcription and replication in neuroblastoma” is the result of my own work. I did not receive any help or support from commercial consultants. All Sources and/or materials applied are listed and specified in the thesis.

Furthermore, I confirm that this thesis has not yet been submitted as part of another examination process neither in identical nor in similar form.

_____ _____

Place, Date Signature